


SLBC_cci+

SEA LEVEL BUDGET CLOSURE - CLIMATE CHANGE INITIATIVE +

PRODUCT VALIDATION AND INTERCOMPARISON REPORT (PVIR)

	Name	Organisation	Date	Visa
Written by :	Martin Horwath	TU Dresden	31/03/2025	
	Thorben Döhne			
	Robin Fraudeau	Magellium		
	Marie Bouih			
	Ramiro Ferrari			
	Michael Ablain			
	Erwan Oulhen	LOPS		
	William Llovel			
	Nicolas Kolodziejczyk			
	Kevin Balem			

	Hugo Lecomte Benoit Meyssignac Anny Cazenave Alejandro Blazquez Sébastien Fourest Jonathan Bamber Anrijs Abele Xueqing Yin Giorgio Spada Stéphanie Leroux	LEGOS Univ. Bristol UNIBO Datlas		
Checked by :	Michaël Ablain	Magellium	31/03/2025	
Approved by :	Joël Dorandeu	Magellium	31/03/2025	
Accepted by :	Sarah Connors	ESA		

Document reference:	SLBC_CCI-DT-075-MAG_PVIR_D3-4
Edition.Revision:	1.0
Release date:	31/03/2025
Customer:	ESA

Ref. Market, consultation:	ESA AO/1-11340/22/I-NB
-----------------------------------	------------------------

Mailing list

	Name	organisation	Nb. copies
Recipients :	Sarah Connors	ESA	1 digital copy
Internal copy :			1 digital copy

Document evolution sheet

Ed.	Rev.	Date	Purpose of evolution	Observations
1	0	31/03/2025	First version of the document	

Contents

1. Introduction	12
1.1. Context and Objectives of the Document	12
1.2. Document structure	12
1.3. Related documents	12
1.3.1. Applicable documents	12
1.3.2. References	13
1.4. Acronyms	13
2. Scientific Context	15
3. Intercomparison of each SLBC components	16
3.1. Altimetric component	16
3.1.1. Description of the product	16
3.1.2. Validation Strategy	16
3.2. Steric component	19
3.3. Manometric and Barystatic component from GRACE	27
3.4. Individual mass contributions	30
3.4.1. Land Water Storage component	30
3.4.2. Atmosphere water vapour component	33
3.4.3. Ice Sheets component	34
3.4.4. Glaciers component	37
3.5. Glacial Isostatic Adjustment and Present Days Ice Melting component	40
4. Analysis of the unconstrained SLBC: Historical Approach	42
4.1. Overview	42
4.2. At global mean	44
4.2.1. Validation of the SLB product	44
4.2.1.1. Input data	44
4.2.1.2. Ocean mass budget and sea level budget	45
4.2.2. Comparison with other datasets	48
4.2.2.1. Comparison with Phase 1 SLBC CCI products	48
4.2.2.2. Complementary work using other datasets	54
4.3. At regional scale	57
4.3.1. Validation of the SLB product	57
4.3.2. Comparison with other datasets	61
4.4. Improvements	64
5. Analysis of the objectively constrained SLBC: Innovative Approach	65
5.1. At global mean	65

5.1.1. Sea level budget	66
5.1.2. Ocean mass budget	70
5.2. At regional scale	76
6. Conclusions and Recommendations	76

List of figures and tables

Figure 1 Comparison between the total sea level component of the SLBC_CCI Phase I project and the total sea level component of the SLBC_CCI+ Phase II project. Panel (a) presents the GMSL time series, and Panel (b) shows the difference between the time series.	17
Figure 2 Comparison between the total sea level component of the SLBC_CCI+ project (C3S) and alternative data such as GMSL from L4 CMEMS, from L2P DT 2021 and L2P DT 2024. Panel (a) presents the GMSL time series, and Panel (b) shows the difference between the time series.	18
Figure 3 Standard deviation of the monthly climatology estimated from JAMSTEC (a), EN4 (b), SCRIPPS (c) and ISAS (d).	21
Figure 4 Differences between the climatology standard deviations of JAMSTEC (a), EN4 (b) and SCRIPPS (c) with this of ISAS). (d) Interproduct standard deviation of the climatology standard deviations	21
Figure 5 (a) Globally average of anomalies of JAMSTEC, EN4, SCRIPPS and ISAS, following the removal of the monthly climatology, but with the linear trend still present. (b) Differences of the global averages of JAMSTEC, EN4 and SCRIPPS with ISAS'.	22
Figure 6 (a) Globally average of interannual anomalies of JAMSTEC, EN4, SCRIPPS and ISAS, following the removal of the monthly climatology and the linear trend. (b) Differences of the global averages of JAMSTEC, EN4 and SCRIPPS with ISAS'.	23
Figure 7 SSL linear trends for JAMSTEC (a), EN4 (b) SCRIPPS (c) and ISAS (d).	24
Figure 8 Differences of the linear trends of JAMSTEC (a), EN4 (b) SCRIPPS, SCRIPPS (c) with ISAS. (d) Inter-product standard deviations of the trends.	24

Figure 9 (a) Zonally averaged SSL linear trends for JAMSTEC, EN4, SCRIPPS and ISAS. (b) Differences of the zonally averages SSL linear trends of JAMSTEC, EN4 and SCRIPPS with ISAS'.	25
Figure 10 Standard deviations associated with SSL anomalies, following the removal of the monthly climatology and linear trend, for JAMSTEC (a), EN4 (b) SCRIPPS (c) and ISAS (d).	26
Figure 11 Differences of the interannual standard deviations of JAMSTEC (a), EN4 (b) SCRIPPS, SCRIPPS (c) with ISAS. (d) Inter-product standard deviations of the interannual standard deviations.	27
Figure 12 Comparison between (a) mass-change time series for the global ocean from the SLBC-1 ocean-mass change solutions (orange) and the current ocean-mass change solution (blue). For the current solution, different from its standard run, the GIA model by Caron et al. (2018) was applied for GIA correction, to be consistent with SLBC-1. Seasonal components are removed. (b) Difference between the two time series and the associated uncertainties assessed in SLBC-1 (light orange) and in the current project (light blue). (Note that the uncertainties for the current phase are clipped following 2020).	28
Figure 13 Comparison between time series of global ocean mass change from this project (blue) and derived from alternative mascon solutions.	29
Figure 14 Comparison between manometric sea level trends. (a): Trends derived in this project using the UNIBO SLBC_cci+ GIA correction. (b): Trends derived in this project using the ICE-6G_D GIA correction. (c): Trend from an ensemble of three alternative mascon solutions using the ICE-6G_D GIA model.	30
Figure 15 Comparison of the estimate of land water storage variation contribution to sea level change from various hydrological models: four estimates of the WaterGAP Hydrological Model (WGHM) version 22e, the ISBA-CTRIP hydrological model and six estimates of the GRACE_REC model. Plain lines indicate estimates including the human-induced contribution ("hum.") while dotted lines indicate estimates taking into consideration only the climate-driven contribution ("cli."). Only the GRACE-REC estimates include the land ice contribution.	31
Figure 16 Land water storage variations contribution to global mean sea level change, from the WaterGap Hydrological Model (WGHM) version 22e with ERA5 (light blue) and W5e5 (blue) climate forcing and including the anthropogenic contribution. The LWS time series obtained by averaging the WGHM 22e times series is in black. The LWS time series estimated with W5e5 climate forcing was completed by overlapping WGHM with ERA5 forcing data.	32

Figure 17 Land water storage variations contribution to global mean sea level change obtained by averaging the WGHM 22e with ERA5 and W5e5 climate forcing and including the anthropogenic contribution with its standard uncertainty.	33
Figure 18 Comparison of the global mean atmosphere mass change estimated from ERA5 (blue line), HOAPS (orange line) and AOD1B (black line) over the period 1993-2024	34
Figure 19 Comparison of the global mean atmosphere mass change estimated from ERA5 (blue line), HOAPS (orange line) and AOD1B (black line) over the period 2005-2016, trend has been removed from each dataset	34
Figure 20 Mass changes of the Greenland Ice Sheet according to the latest IMBIE assessment (red), the GIS_cci+ Gravimetric Mass Balance (GMB) RL4.1 assessment (dark green), the GRACE-based assessment used by the first SLBC_cci project (light green) and the altimetry-based assessment used by the first SLBC_cci project (blue). The curves are offset along the y-axis for better legibility. Error bars provided with the assessments refer to mass anomalies w.r.t. 1992 for the case of IMBIE and w.r.t. 2011.0 for the case of the other three assessments.	36
Figure 21 Mass changes of the Antarctic Ice Sheet according to the latest IMBIE assessment (red), the AIS_cci+ Gravimetric Mass Balance (GMB) RL5.0 assessment (dark green), the GRACE-based assessment used by the first SLBC_cci project (light green) and the altimetry-based assessment used by the first SLBC_cci project (blue). The curves are offset along the y-axis for better legibility. Error bars provided with the assessments refer to mass anomalies w.r.t. 1992 for the case of IMBIE and w.r.t. 2011.0 for the case of the other three assessments.	37
Figure 22 Comparison of spatially integrated GIC mass balance for the data set used here (black), the SLB P1 product and the community intercomparison ensemble for 2000-2023 (blue).	38
Figure 23 Comparison of different data sets undertaken in Zemp et al, 2025 for RGI region Central Asia. The GLAMBIE ensemble estimate is in black and the P2 product used here in green. Similar figures are provided for all 19 RGI regions and in all cases the P2 product is in close agreement with the GLAMBIE ensemble which currently must be considered as the benchmark data set for the post 2000 period. It does not, however, include a seasonal component and does not extend back before 2000.	40
Figure 24 GIA rate of present day absolute sea level change (mm/yr), according to the implementation of the nominal ICE-6G_C mode of Argus et al. (2014) and Peltier et al. (2015), obtained using SELEN ⁴ of Spada and Melini (2019).	41

Figure 25 GIA rate of present-day absolute sea level change (mm/yr) according to the ANU model. Same color table as in Figure 24. 41

Figure 26 (a) Global mean barystatic sea level time series for SLBC CCI+. Blue lines show the total barystatic component: solid for barystatic from GRACE/GRACE-FO data, and dashed for barystatic from the sum of individual mass components. Teal lines show land water storage, purple lines show glacier melt, green lines Greenland Ice Sheet mass loss, and yellow lines Antarctic Ice Sheet mass loss. (b) Difference between barystatic sea level estimates from GRACE/GRACE-FO and sum of individual mass components. Trends estimated over the period 06/2002 - 12/2022. 47

Figure 27 Sea level budget comparison using two different barystatic components. (a) Global mean sea level budget components using SLBC CCI+ data. The black curves represent altimetry-based sea level; the blue curves show the manometric (barystatic) component from GRACE; the orange curve shows the thermosteric contribution, respectively; and the red curves show the sum of all components. Solid lines indicate values based on GRACE-derived barystatic sea level; dashed lines indicate values based on the sum of individual mass contributions. (b) Residuals of the sea level budget, computed as the difference between the observed sea level (altimetry) and the sum of all components. Trends estimated over the period 06/2002 - 06/2016. 48

Figure 28 (a) Global mean barystatic sea level time series. Blue lines show the total barystatic component: solid for SLBC CCI+, and dashed for SLBC CCI Phase 1. Teal lines show land water storage, purple lines show glacier melt, green lines Greenland Ice Sheet mass loss, and yellow lines Antarctic Ice Sheet mass loss — with solid lines for SLBC CCI+ and dashed lines for SLBC CCI Phase 1. (b) Difference between barystatic sea level estimates from SLBC CCI+ and SLBC CCI Phase 1. 50

Figure 29 Sea level budget comparison (SLBC CCI vs. SLBC CCI+). (a) Global mean sea level budget components estimated using the sum of individual mass contributions. Black curves show the observed sea level from altimetry; orange curves represent the thermosteric component; blue curves show the barystatic component (from the sum of mass contributions); and red curves indicate the total sea level from the sum of all components. Solid lines correspond to SLBC CCI+ (Phase 2), while dashed lines represent SLBC CCI (Phase 1). (b) Residuals of the sea level budget, computed as the difference between the observed sea level (altimetry) and the sum of all components, for both SLBC CCI+ (solid line) and SLBC CCI Phase 1 (dashed line). Trends estimated over the period 01/1993 - 12/2016. 52

Figure 30 (a) Global mean sea level budget components using the GRACE-derived barystatic estimate, for SLBC CCI (Phase 1, dashed lines) and SLBC CCI+ (Phase 54

2, solid lines). The black curves represent altimetry-based sea level; the blue curves show the barystatic component from GRACE; the orange curves show the thermosteric contribution; and the red curves show the sum of all components. (b) Residuals of the sea level budget, computed as the difference between the observed sea level (altimetry) and the sum of thermosteric and GRACE-based barystatic components. Trends are estimated over 06/2002-06/2016 period.

Figure 31 Sea level budget over the January 2005–December 2019 period. The shaded areas correspond to the estimated 1-sigma uncertainties. (a) Budget with altimetry, Gravity Recovery and Climate Experiment and steric Argo contributions. (b) Residuals of the budget. (c) Variance of the residuals. The right three panels (d, e and f) are similar to the left, but with only Argo thermosteric effect considered. From Barnoud et al., 2021.

56

Figure 32 Upper panel: Altimetry-based GMSL with and without the Jason-3 radiometer correction (dashed and solid blue curves); Altimetry-based base GMSL minus steric component with and without the Jason-3 radiometer drift (dashed and solid red curves). Lower panel; residuals. From Barnoud et al., 2023.

56

Figure 33 Sea level trends over April 2002 to December 2019 in observed altimetry-based sea level (a), components (b, c, d: GRACE-based manometric, Argo-based thermosteric and Argo-based halosteric sea level) and budget residual trends (observed sea level minus sum of components) (e).

58

Figure 34 Sea level trends anomalies over April 2002 to December 2019 in observed altimetry-based sea level (a), components (b, c, d: GRACE-based manometric, Argo-based thermosteric and Argo-based halosteric sea level) and budget residual trends (observed sea level minus sum of components) (e).

59

Figure 35 Sea level trends over April 2002 to December 2019 in observed altimetry-based sea level corrected using ICE-5 GIA model (Peltier, 2004) and PDIM correction from Frederikse et al., 2017 (a), components (b, c, d: GRACE-based manometric corrected using ICE-6 GIA model (Peltier et al., 2015), Argo-based thermosteric and Argo-based halosteric sea level) and budget residual trends (observed sea level minus sum of components) (e).

60

Figure 36 Sea level trends anomalies over April 2002 to December 2019 in observed altimetry-based sea level corrected using ICE-5 GIA model (Peltier, 2004) and PDIM correction from Frederikse et al., 2017 (a), components (b, c, d: GRACE-based manometric corrected using ICE-6 GIA model (Peltier et al., 2015), Argo-based thermosteric and Argo-based halosteric sea level) and budget residual trends (observed sea level minus sum of components) (e).

61

Figure 37 Sea level trends anomalies over January 2004 to December 2022 in

63

observed altimetry-based sea level (a), components (b, c, d: GRACE-based manometric, Argo-based thermosteric and Argo-based halosteric sea level) and budget residual trends (observed sea level minus sum of components) (e). From Bouih et al., 2025.

Figure 38 Residual trends anomalies of the regional sea level budget computed with each of the six reanalyses-based manometric data sets, as well as with their mean (panels a to g) (with altimetry-based and steric components unchanged). GRACE-based residual trends for both mascons and spherical harmonic solutions are also shown (panels h and i). The period of analysis here is from January 2004 to December 2019. From Bouih et al., 2025.

64

Figure 39 Sea level budget over the period 2005-2019 (panel a) and the budget residual (panel b). The shaded areas correspond to the estimated 1-sigma uncertainties.

67

Figure 40 Sea level budget with objectively constrained components obtained by inversion over the period 2005-2019 (panel a) and the budget residual (panel b). The shaded areas correspond to the estimated 1-sigma uncertainties.

68

Figure 41 Sea level budget components before inversion (black curves) and after inversion (red curves) for relative sea level by altimetry (left top), barystaric sea level by gravimetry (right top), thermosteric sea level by in-situ profiles (lower left) and budget residuals (lower right). The shaded areas correspond to the estimated 1-sigma uncertainties.

70

Figure 42 Ocean mass budget over the period 2005-2019 (panel a) and the budget residual (panel b). The shaded areas correspond to the estimated 1-sigma uncertainties.

72

Figure 43 Ocean mass budget with objectively constrained components obtained by inversion over the period 2005-2019 (panel a) and the budget residual (panel b). The shaded areas correspond to the estimated 1-sigma uncertainties.

73

Figure 44 Simultaneous inversion of the sea level and ocean mass budget over the period 2005-2019 (panel a) and the budgets residuals (panel b). The shaded areas correspond to the estimated 1-sigma uncertainties.

75

Table 1 List of applicable documents.

12

Table 2 List of abbreviations and acronyms.

13

Table 3 Trends of global ocean mass change

29

Mean linear trends for the common period from 2003-01 to 2016-08 (Table 4) are between -98 Gt/a and -135 Gt/yr. This range reflects the well-known spread among results from different techniques (and even from different realisations of the same techniques). Uncertainties quoted for the gravimetric results are in line with this spread, while uncertainties quoted for IMBIE and SLBC-1 altimetry are smaller. A possible underestimation of the IMBIE uncertainties might arise from their methodology of uncertainty aggregation, which relies on the uncertainties per epoch stated by the individual contributors and has limited account for temporal error correlations.	36
Table 5 Mean linear trends of ice sheet mass over the period 2003-01 – 2016-08 for the Greenland Ice Sheet (GIS) and the Antarctic Ice Sheet (AIS) from the four assessments considered here. Uncertainties are quoted from the data sources. They exceed the formal uncertainties that would just result from the linear regression. In the case of the IMBIE assessment, uncertainties are calculated from the uncertainties quoted by Otosaka et al. (2023) for three consecutive 5-year intervals under the assumption of uncorrelated errors, in line with the uncertainty aggregation approach of IMBIE.	37
Table 6 Table describing the input data used in the sea level and ocean mass budget equations	44
Table 7 Sea level budget component trend (mm/yr) before and after inversion over the period 2005-2019	69
Table 8 Ocean mass budget component trend (mm/yr) before and after inversion over the period 2005-2019	74

1. Introduction

1.1. Context and Objectives of the Document

This document is the Product Validation and Intercomparison Report (PVIR) of the ESA Sea Level Budget Close of the Climate Change Initiative+ (SLBC_cci+) project. This PVIR is dedicated to the validation and intercomparison of each SLB component against other datasets. It also shows the results of the budget itself at global mean and regional scale and comparisons for the 2 approaches proposed within the project ([\[AD6\]](#)).

1.2. Document structure

In addition to this introduction, the document is organised as follows:

- Section 2 describes the scientific background of the SLBC activities and its objectives
- Section 3 show the validation and intercomparisons of each SLB component used
- Section 4 presents the results of the SLBC for the historical approach (unconstrained) as well as comparisons and analysis of the results
- Section 5 present the results of the SLBC for the innovative approach (objectively constrained) as well as preliminary analysis of the results

1.3. Related documents

1.3.1. Applicable documents

Table 1 *List of applicable documents.*

Id.	Ref.	Description
[AD1]	SLBC_CCI-DT-076-MAG_UCR	SEA LEVEL BUDGET CLOSURE_CCI+ Uncertainty Characterisation Report
[AD2]	SLBC_CCI-DT-074-MAG_PUG	SEA LEVEL BUDGET CLOSURE_CCI+ Product User Guide
[AD3]	SLBC_CCI-DT-041-MAG_ATBD	SEA LEVEL BUDGET CLOSURE_CCI+ Algorithm Theoretical Baseline Document
[AD4]	SLBC_CCI-DT-039-MAG_PSD	SEA LEVEL BUDGET CLOSURE_CCI+ Product Specification Document

[AD5]	SLBC_CCI-DT-040-MAG_DARD	SEA LEVEL BUDGET CLOSURE_CCI+ Data Access Requirements Document
[AD6]	MAG-22-PTF-060_DetailedProposal_V2	Detailed proposal in response to ESA/ESRIN Request for Quotation "SEA LEVEL BUDGET CLOSURE_CCI+ (SLBC_CCI+)" ESA AO/1-11340/22/I-NB

1.3.2. References

- Barnoud, A., Pfeffer, J., Guérou, A., Frery, M., Siméon, M., Cazenave, A., Chen, J., Llovel, W., Thierry, V., Legeais, J., and Ablain, M.: Contributions of Altimetry and Argo to Non-Closure of the Global Mean Sea Level Budget Since 2016, *Geophys. Res. Lett.*, 48, e2021GL092824, <https://doi.org/10.1029/2021GL092824>, 2021.
- Barnoud, A., Pfeffer, J., Cazenave, A., Fraudeau, R., Rousseau, V., and Ablain, M.: Revisiting the global mean ocean mass budget over 2005–2020, *Ocean Sci.*, 19, 321–334, <https://doi.org/10.5194/os-19-321-2023>, 2023.
- Bouih, M., Barnoud, A., Yang, C., Storto, A., Blazquez, A., Llovel, W., Fraudeau, R., Cazenave, A., Yang, C., Storto, A., Blazquez, A., Llovel, W., Fraudeau, R., and Cazenave, A.: Regional sea level budget over 2004–2022, *EGUsphere Ocean Sci.*, <https://doi.org/10.5194/egusphere-2024-3945>, 2025.
- Bouih et al., *Ocean Sciences*, in press (2025)
- Camargo, C. M. L., Riva, R. E. M., Hermans, T. H. J., Schütt, E. M., Marcos, M., Hernandez-Carrasco, I., and Slangen, A. B. A.: Regionalizing the sea-level budget with machine learning techniques, *Ocean Sci.*, 19, 17–41, <https://doi.org/10.5194/os-19-17-2023>, 2023.
- Caron, L., Ivins, E. R., Larour, E., Adhikari, S., Nilsson, J., and Blewitt, G.: GIA Model Statistics for GRACE Hydrology, Cryosphere, and Ocean Science, *Geophys. Res. Lett.*, 45, 2203–2212, <https://doi.org/10.1002/2017GL076644>, 2018.
- Cazenave, A., Meyssignac, B., Ablain, M., Balmaseda, M., Bamber, J., Barletta, V., Beckley, B., Benveniste, J., Berthier, E., Blazquez, A., Boyer, T., Cáceres, D., Chambers, D., Champollion, N., Chao, B., Chen, J., Cheng, L., Church, J. A., Chuter, S., Cogley, J. G., Dangendorf, S., Desbruyères, D., Döll, P., Domingues, C., Falk, U., Famiglietti, J., Fenoglio-Marc, L., Forsberg, R., Galassi, G., Gardner, A., Groh, A., Hamlington, B., Hogg, A., Horwath, M., Humphrey, V., Husson, L., Ishii, M., Jäggi, A., Jevrejeva, S., Johnson, G. C., Kolodziejczyk, N., Kusche, J., Lambeck, K., Landerer, F., Leclercq, P. W., Legresy, B., Leuliette, E., Llovel, W., Longuevergne, L., Loomis, B. D., Luthcke, S. B., Marcos, M., Marzeion, B., Merchant, C., Merrifield, M., Milne, G., Mitchum, G., Mohajerani, Y., Monier, M., Monselesan, D., Nerem, S., Palanisamy, H., Paul, F., Perez, B., Piecuch, C. G., Ponte, R. M., Purkey, S. G., Reager, J. T., Rietbroek, R., Rignot, E., Riva, R., Roemmich, D., Sørensen, L. S., Sasgen, I., Schrama, E. J. O., Seneviratne, S. I., Shum, C. K., Spada, G., Stammer, D., Velicogna, I., Von Schuckmann, K., Wada, Y., Wang, Y., Watson, C., Wiese, D., Wijffels, S., Westaway, R., Woppelmann, G., and Wouters, B.: Global sea-level budget 1993-present, <https://doi.org/10.3929/ETHZ-B-000287786>, 2018.
- Chen, J., Tapley, B., Save, H., Tamisiea, M. E., Bettadpur, S., and Ries, J.: Quantification of Ocean Mass Change Using Gravity Recovery and Climate Experiment, Satellite Altimeter,

- and Argo Floats Observations, *J. Geophys. Res. Solid Earth*, 123, 10,212-10,225, <https://doi.org/10.1029/2018JB016095>, 2018.
- Chen, J., Tapley, B., Wilson, C., Cazenave, A., Seo, K.-W., and Kim, J.-S.: Global Ocean Mass Change From GRACE and GRACE Follow-On and Altimeter and Argo Measurements, *Geophys. Res. Lett.*, 47, e2020GL090656, <https://doi.org/10.1029/2020GL090656>, 2020.
 - Chen, J., Cazenave, A., Dahle, C., Llovel, W., Panet, I., Pfeffer, J., and Moreira, L.: Applications and Challenges of GRACE and GRACE Follow-On Satellite Gravimetry, *Surv. Geophys.*, 43, 305–345, <https://doi.org/10.1007/s10712-021-09685-x>, 2022.
 - Dangendorf, S., Frederikse, T., Chafik, L., Klinck, J., Ezer, T., Hamlington, B., 2021. Data-driven reconstruction reveals large-scale ocean circulation control on coastal sea level, *Nature Climate Change*, 11(6), 514-520.
 - Dangendorf, S., Hendricks, N., Sun, Q., Klinck, J., Ezer, T., Frederikse, T., Calafat, F. M., Wahl, T., and Törnqvist, T. E.: Acceleration of U.S. Southeast and Gulf coast sea-level rise amplified by internal climate variability, *Nat. Commun.*, 14, 1935, <https://doi.org/10.1038/s41467-023-37649-9>, 2023.
 - Dieng, H. B., Cazenave, A., Meyssignac, B., and Ablain, M.: New estimate of the current rate of sea level rise from a sea level budget approach, *Geophys. Res. Lett.*, 44, 3744–3751, <https://doi.org/10.1002/2017gl073308>, 2017.
 - Dieng, H. B., Dadou, I., Léger, F., Morel, Y., Jouanno, J., Lyard, F., and Allain, D.: Sea level anomalies using altimetry, model and tide gauges along the African coasts in the Eastern Tropical Atlantic Ocean: Inter-comparison and temporal variability, *Adv. Space Res.*, 68, 534–552, <https://doi.org/10.1016/j.asr.2019.10.019>, 2021.
 - Dièye, A., Sow, B. A., Dieng, H. B., Marchesiello, P., and Descroix, L.: Impact of climate variability modes on trend and interannual variability of sea level near the West African coast, *Afr. J. Environ. Sci. Technol.*, 17, 157–166, <https://doi.org/10.5897/AJEST2022.3173>, 2023.
 - Frederikse, T., Riva, R., Kleinherenbrink, M., Wada, Y., van den Broeke, M., and Marzeion, B.: Closing the sea level budget on a regional scale: Trends and variability on the Northwestern European continental shelf, *Geophys. Res. Lett.*, 43, 10,864-10,872, <https://doi.org/10.1002/2016GL070750>, 2016.
 - Frederikse, T., Jevrejeva, S., Riva, R. E. M., and Dangendorf, S.: A Consistent Sea-Level Reconstruction and Its Budget on Basin and Global Scales over 1958–2014, *J. Clim.*, 31, 1267–1280, <https://doi.org/10.1175/jcli-d-17-0502.1>, 2018.
 - Frederikse, T., Landerer, F., Caron, L., Adhikari, S., Parkes, D., Humphrey, V. W., Dangendorf, S., Hogarth, P., Zanna, L., Cheng, L., and Wu, Y.-H.: The causes of sea-level rise since 1900, *Nature*, 584, 393–397, <https://doi.org/10.1038/s41586-020-2591-3>, 2020.
 - Gaillard, F., Reynaud, T., Thierry, V., Kolodziejczyk, N., and Schuckmann, K. von: In Situ–Based Reanalysis of the Global Ocean Temperature and Salinity with ISAS: Variability of the Heat Content and Steric Height, *J. Clim.*, 29, 1305–1323, <https://doi.org/10.1175/JCLI-D-15-0028.1>, 2016.
 - Good, S. A., Martin, M. J., and Rayner, N. A.: EN4: Quality controlled ocean temperature and salinity profiles and monthly objective analyses with uncertainty estimates, *J. Geophys. Res. Oceans*, 118, 6704–6716, <https://doi.org/10.1002/2013JC009067>, 2013.
 - Gregory, J. M. and Lowe, J. A.: Predictions of global and regional sea-level rise using AOGCMs with and without flux adjustment, *Geophys. Res. Lett.*, 27, 3069–3072, <https://doi.org/10.1029/1999GL011228>, 2000.

- Gregory, J. M., Griffies, S. M., Hughes, C. W., Lowe, J. A., Church, J. A., Fukimori, I., Gomez, N., Kopp, R. E., Landerer, F., Cozannet, G. L., Ponte, R. M., Stammer, D., Tamisiea, M. E., and van de Wal, R. S. W.: Concepts and Terminology for Sea Level: Mean, Variability and Change, Both Local and Global, *Surv. Geophys.*, 40, 1251–1289, <https://doi.org/10.1007/s10712-019-09525-z>, 2019.
- Hamlington, B. D., Frederikse, T., Nerem, R. S., Fasullo, J. T., and Adhikari, S.: Investigating the Acceleration of Regional Sea Level Rise During the Satellite Altimeter Era, *Geophys. Res. Lett.*, 47, <https://doi.org/10.1029/2019GL086528>, 2020.
- Han, W., Stammer, D., Thompson, P., Ezer, T., Palanisamy, H., Zhang, X., Domingues, C. M., Zhang, L., and Yuan, D.: Impacts of Basin-Scale Climate Modes on Coastal Sea Level: a Review, *Surv. Geophys.*, 40, 1493–1541, <https://doi.org/10.1007/s10712-019-09562-8>, 2019.
- Hermans, T. H. J., Le Bars, D., Katsman, C. A., Camargo, C. M. L., Gerkema, T., Calafat, F. M., Tinker, J., and Slangen, A. B. A.: Drivers of Interannual Sea Level Variability on the Northwestern European Shelf, *J. Geophys. Res. Oceans*, 125, e2020JC016325, <https://doi.org/10.1029/2020JC016325>, 2020.
- Horwath, M., Gutknecht, B. D., Cazenave, A., Palanisamy, H. K., Marti, F., Marzeion, B., Paul, F., Le Bris, R., Hogg, A. E., Otosaka, I., Shepherd, A., Döll, P., Cáceres, D., Müller Schmied, H., Johannessen, J. A., Nilsen, J. E. Ø., Raj, R. P., Forsberg, R., Sandberg Sørensen, L., Barletta, V. R., Simonsen, S., Knudsen, P., Andersen, O. B., Rannald, H., Rose, S. K., Merchant, C. J., Macintosh, C. R., Von Schuckmann, K., Novotny, K., Groh, A., Restano, M., and Benveniste, J.: ESA Sea Level Budget Closure Climate Change Initiative (SLBC_cci): Time series of global mean sea level budget and ocean mass budget elements (1993-2016, at monthly resolution), version 2.2, <https://doi.org/10.5285/17C2CE31784048DE93996275EE976FFF>, 2021.
- Horwath, M., Gutknecht, B. D., Cazenave, A., Palanisamy, H. K., Marti, F., Marzeion, B., Paul, F., Bris, R. L., Hogg, A. E., Otosaka, I., Shepherd, A., Döll, P., Cáceres, D., Schmied, H. M., Johannessen, J. A., Nilsen, J. E. Ø., Raj, R. P., Forsberg, R., Sørensen, L. S., Barletta, V. R., Simonsen, S. B., Knudsen, P., Andersen, O. B., Randall, H., Rose, S. K., Merchant, C. J., Macintosh, C. R., Schuckmann, K. von, Novotny, K., Groh, A., Restano, M., and Benveniste, J.: Global sea-level budget and ocean-mass budget, with focus on advanced data products and uncertainty characterisation, *Earth Syst. Sci. Data*, 14, 411–447, <https://doi.org/10.5194/essd-14-411-2022>, 2022.
- Hosoda, S., Ohira, T., and Nakamura, T.: A monthly mean dataset of global oceanic temperature and salinity derived from Argo float observations, *JAMSTEC Rep. Res. Dev.*, 8, 47–59, <https://doi.org/10.5918/jamstecr.8.47>, 2008.
- Hugonnet, R., McNabb, R., Berthier, E., Menounos, B., Nuth, C., Girod, L., Farinotti, D., Huss, M., Dussaillant, I., Brun, F., and Kääb, A.: Accelerated global glacier mass loss in the early twenty-first century, *Nature*, 592, 726–731, <https://doi.org/10.1038/s41586-021-03436-z>, 2021.
- IPCC (2019). IPCC Special Report on the Ocean and Cryosphere in a Changing Climate, edited by Portner, H.-O., Roberts, D. C., Masson-Delmotte, V., Zhai, P., Tignor, M., Poloczanska, E., Mintenbeck, K., Alegría, A., Nicolai, M., Okem, A., Petzold, J., Rama, B., and Weyer, N. M.
- IPCC (2021), Climate Change 2021. The Physical Science Basis. Contribution of Working Group I to the Sixth Assessment Report of the Intergovernmental Panel on Climate Change [Masson-Delmotte, V., P. Zhai, A. Pirani, S.L. Connors, C. Péan, S. Berger, N. Caud, Y.

- Chen, L. Goldfarb, M.I. Gomis, M. Huang, K. Leitzell, E. Lonnoy, J.B.R. Matthews, T.K. Maycock, T. Waterfield, O. Yelekçi, R. Yu, and B. Zhou (eds.)). Cambridge University Press. In Press.
- Kemgang Ghomsi, F. E., Raj, R. P., Bonaduce, A., Halo, I., Nyberg, B., Cazenave, A., Rouault, M., and Johannessen, O. M.: Sea level variability in Gulf of Guinea from satellite altimetry, *Sci. Rep.*, 14, 4759, <https://doi.org/10.1038/s41598-024-55170-x>, 2024.
 - Kolodziejczyk, N., Prigent-Mazella, A., and Gaillard, F.: ISAS temperature, salinity, dissolved oxygen gridded fields, <https://doi.org/10.17882/52367>, 2023.
 - Leclercq, L., Cazenave, A., Leger, F., Birol, F., Nino, F., Tolu, L., and Legeais, J.-F.: Coastal sea level rise at altimetry-based virtual stations in the Gulf of Mexico, *Adv. Space Res.*, 75, 1636–1652, <https://doi.org/10.1016/j.asr.2024.11.069>, 2025.
 - L'Ecuyer, T. S., Beaudoin, H. K., Rodell, M., Olson, W., Lin, B., Kato, S., Clayson, C. A., Wood, E., Sheffield, J., Adler, R., Huffman, G., Bosilovich, M., Gu, G., Robertson, F., Houser, P. R., Chambers, D., Famiglietti, J. S., Fetzer, E., Liu, W. T., Gao, X., Schlosser, C. A., Clark, E., Lettenmaier, D. P., and Hilburn, K.: The Observed State of the Energy Budget in the Early Twenty-First Century, *J. Clim.*, 28, 8319–8346, <https://doi.org/10.1175/JCLI-D-14-00556.1>, 2015.
 - Little, C. M., Piecuch, C. G., and Ponte, R. M.: North American East Coast Sea Level Exhibits High Power and Spatiotemporal Complexity on Decadal Timescales, *Geophys. Res. Lett.*, 48, e2021GL093675, <https://doi.org/10.1029/2021GL093675>, 2021.
 - Liu, C., Liang, X., Chambers, D. P., and Ponte, R. M.: Global Patterns of Spatial and Temporal Variability in Salinity from Multiple Gridded Argo Products, <https://doi.org/10.1175/JCLI-D-20-0053.1>, 2020.
 - Llovel, W., Purkey, S., Meyssignac, B., Blazquez, A., Kolodziejczyk, N., and Bamber, J.: Global ocean freshening, ocean mass increase and global mean sea level rise over 2005–2015, *Sci. Rep.*, 9, 17717, <https://doi.org/10.1038/s41598-019-54239-2>, 2019.
 - Loomis, B. D., Luthcke, S. B., and Sabaka, T. J.: Regularization and error characterization of GRACE mascons, *J. Geod.*, 93, 1381–1398, <https://doi.org/10.1007/s00190-019-01252-y>, 2019.
 - Ludwigsen, C. B., Andersen, O. B., Marzeion, B., Malles, J.-H., Müller Schmied, H., Döll, P., Watson, C., and King, M. A.: Global and regional ocean mass budget closure since 2003, *Nat. Commun.*, 15, 1416, <https://doi.org/10.1038/s41467-024-45726-w>, 2024.
 - Martinec, Z., Klemann, V., van der Wal, W., Riva, R. E. M., Spada, G., Sun, Y., Melini, D., Kachuck, S. B., Barletta, V., Simon, K., A, G., and James, T. S.: A benchmark study of numerical implementations of the sea level equation in GIA modelling, *Geophys. J. Int.*, 215, 389–414, <https://doi.org/10.1093/gji/ggy280>, 2018.
 - Mu, Q., Müller, J., Wu, H., Knabe, A., and Zhong, M.: Satellite gradiometry based on a new generation of accelerometers and its potential contribution to Earth gravity field determination, *Adv. Space Res.*, 73, 3321–3344, <https://doi.org/10.1016/j.asr.2023.08.023>, 2024.
 - Nerem, R. S., Beckley, B. D., Fasullo, J. T., Hamlington, B. D., Masters, D., and Mitchum, G. T.: Climate-change–driven accelerated sea-level rise detected in the altimeter era, *Proc. Natl. Acad. Sci.*, 201717312, <https://doi.org/10.1073/pnas.1717312115>, 2018.
 - Otosaka, I. N., Horwath, M., Mottram, R., and Nowicki, S.: Mass Balances of the Antarctic and Greenland Ice Sheets Monitored from Space, *Surv. Geophys.*, 44, 1615–1652, <https://doi.org/10.1007/s10712-023-09795-8>, 2023.
 - Peltier, W. R., Argus, D. F., and Drummond, R.: Comment on “An Assessment of the

- ICE-6G_C (VM5a) Glacial Isostatic Adjustment Model” by Purcell et al., J. Geophys. Res. Solid Earth, 123, 2019–2028, <https://doi.org/10.1002/2016JB013844>, 2018.
- Piecuch, C. G., Bittermann, K., Kemp, A. C., Ponte, R. M., Little, C. M., Engelhart, S. E., and Lentz, S. J.: River-discharge effects on United States Atlantic and Gulf coast sea-level changes, Proc. Natl. Acad. Sci., 115, 7729–7734, <https://doi.org/10.1073/pnas.1805428115>, 2018.
 - Ponte, R. M., Sun, Q., Liu, C., and Liang, X.: How Salty Is the Global Ocean: Weighing It All or Tasting It a Sip at a Time?, Geophys. Res. Lett., 48, e2021GL092935, <https://doi.org/10.1029/2021GL092935>, 2021.
 - Rietbroek, R., Brunnabend, S.-E., Kusche, J., Schröter, J., and Dahle, C.: Revisiting the contemporary sea-level budget on global and regional scales, Proc. Natl. Acad. Sci., 113, 1504–1509, <https://doi.org/10.1073/pnas.1519132113>, 2016.
 - Rodell, M., Beaudoing, H., L’Ecuyer, T., Olson, W., Famiglietti, J., Houser, P., Adler, R., Bosilovich, M., Clayson, C., Chambers, D., Clark, E., Fetzer, E., Gu, G., Hilburn, K., Huffman, G., Lettenmaier, D., Liu, W. T. L., Robertson, F., Sheffield, J., and Gao, X.: The Observed State of the Water Cycle in the Early Twenty-First Century, 2015.
 - Roemmich, D. and Gilson, J.: The 2004–2008 mean and annual cycle of temperature, salinity, and steric height in the global ocean from the Argo Program, Prog. Oceanogr., 82, 81–100, <https://doi.org/10.1016/j.pocean.2009.03.004>, 2009.
 - Royston, S., Vishwakarma, B. D., Westaway, R., Rougier, J., Sha, Z., and Bamber, J.: Can We Resolve the Basin-Scale Sea Level Trend Budget From GRACE Ocean Mass?, J. Geophys. Res. Oceans, 125, <https://doi.org/10.1029/2019jc015535>, 2020.
 - Save, H., Bettadpur, S., and Tapley, B. D.: High-resolution CSR GRACE RL05 mascons, J. Geophys. Res. Solid Earth, 121, 7547–7569, <https://doi.org/10.1002/2016jb013007>, 2016.
 - Spada, G. and Melini, D.: SELEN⁴ (SELEN version 4.0): a Fortran program for solving the gravitationally and topographically self-consistent sea-level equation in glacial isostatic adjustment modeling, Geosci. Model Dev., 12, 5055–5075, <https://doi.org/10.5194/gmd-12-5055-2019>, 2019.
 - Spada, G., Barletta, V. R., Klemann, V., Riva, R. E. M., Martinec, Z., Gasperini, P., Lund, B., Wolf, D., Vermeersen, L. L. A., and King, M. A.: A benchmark study for glacial isostatic adjustment codes, Geophys. J. Int., 185, 106–132, <https://doi.org/10.1111/j.1365-246X.2011.04952.x>, 2011.
 - Steinberg, J. M., Piecuch, C. G., Hamlington, B. D., Thompson, P. R., and Coats, S.: Influence of Deep-Ocean Warming on Coastal Sea-Level Decadal Trends in the Gulf of Mexico, J. Geophys. Res. Oceans, 129, e2023JC019681, <https://doi.org/10.1029/2023JC019681>, 2024.
 - Storto, A. and Yang, C.: Acceleration of the ocean warming from 1961 to 2022 unveiled by large-ensemble reanalyses, Nat. Commun., 15, 545, <https://doi.org/10.1038/s41467-024-44749-7>, 2024.
 - Thompson, B., Jevrejeva, S., Zachariah, J., Faller, D. G., and Tkalic, P.: Impact of Mass Redistribution on Regional Sea Level Changes Over the South China Sea Shelves, Geophys. Res. Lett., 50, e2023GL105740, <https://doi.org/10.1029/2023GL105740>, 2023.
 - Wang, O., Lee, T., Piecuch, C. G., Fukumori, I., Fenty, I., Frederikse, T., Menemenlis, D., Ponte, R. M., and Zhang, H.: Local and Remote Forcing of Interannual Sea-Level Variability at Nantucket Island, J. Geophys. Res. Oceans, 127, e2021JC018275, <https://doi.org/10.1029/2021JC018275>, 2022.
 - WCRP Global Sea Level Budget Group: Global sea-level budget 1993–present, Earth Syst.

- Sci. Data, 10, 1551–1590, <https://doi.org/10.5194/essd-10-1551-2018>, 2018.
- Wiese, D. N., Landerer, F. W., and Watkins, M. M.: Quantifying and reducing leakage errors in the JPL RL05M GRACE mascon solution, *Water Resour. Res.*, 52, 7490–7502, <https://doi.org/10.1002/2016WR019344>, 2016.
 - Wise, A., Calafat, F. M., Hughes, C. W., Jevrejeva, S., Katsman, C. A., Oelmann, J., Piecuch, C., Polton, J., and Richter, K.: Using Shelf-Edge Transport Composition and Sensitivity Experiments to Understand Processes Driving Sea Level on the Northwest European Shelf, *J. Geophys. Res. Oceans*, 129, e2023JC020587, <https://doi.org/10.1029/2023JC020587>, 2024.
 - Wong, A. P. S., Gilson, J., and Cabanes, C.: Argo salinity: bias and uncertainty evaluation, *Earth Syst. Sci. Data*, 15, 383–393, <https://doi.org/10.5194/essd-15-383-2023>, 2023.
 - Yin, J.: Rapid Decadal Acceleration of Sea Level Rise along the U.S. East and Gulf Coasts during 2010–22 and Its Impact on Hurricane-Induced Storm Surge, <https://doi.org/10.1175/JCLI-D-22-0670.1>, 2023.
 - Zemp, M., Jakob, L., Dussaillant, I., Nussbaumer, S. U., Gourmelen, N., Dubber, S., A, G., Abdullahi, S., Andreassen, L. M., Berthier, E., Bhattacharya, A., Blazquez, A., Boehm Vock, L. F., Bolch, T., Box, J., Braun, M. H., Brun, F., Cicero, E., Colgan, W., Eckert, N., Farinotti, D., Florentine, C., Floricioiu, D., Gardner, A., Harig, C., Hassan, J., Hugonnet, R., Huss, M., Jóhannesson, T., Liang, C.-C. A., Ke, C.-Q., Khan, S. A., King, O., Kneib, M., Krieger, L., Maussion, F., Mattea, E., McNabb, R., Menounos, B., Miles, E., Moholdt, G., Nilsson, J., Pálsson, F., Pfeffer, J., Piermattei, L., Plummer, S., Richter, A., Sasgen, I., Schuster, L., Seehaus, T., Shen, X., Sommer, C., Sutterley, T., Treichler, D., Velicogna, I., Wouters, B., Zekollari, H., Zheng, W., and The GlaMBIE Team: Community estimate of global glacier mass changes from 2000 to 2023, *Nature*, 639, 382–388, <https://doi.org/10.1038/s41586-024-08545-z>, 2025.

1.4. Acronyms

Table 2 *List of abbreviations and acronyms.*

Acronyms	Description
C3S	Copernicus Climate Change Service
CCI	The ESA Climate Change Initiative
CDS	Climate Data Store
ECV	Essential Climate Variable
ERA5	ECMWF Atmospheric Reanalysis v5
ESA	European Space Agency
ECMWF	European Centre for Medium-range Weather Forecasts
GIA	Glacial Isostatic Adjustment
HOAPS	Hambourg Ocean-Atmosphere Fluxes and Parameters from Satellite

ISBA-CTRIP	Interaction Soil-Biosphere-Atmosphere, Total Runoff Integrating Pathways from the Centre National de Recherches Météorologiques
LWS	Land Water Storage
SLBC	Sea level budget closure
SLBC_cci	Sea Level Budget Closure of the ESA Climate Change Initiative (first phase)
SLBC_cci+	Sea Level Budget Closure of the ESA Climate Change Initiative (second phase, this activity)
SL_cci	The Sea Level component of the ESA Climate Change Initiative
TCWV	Total Column Water Vapour
TWS	Terrestrial Water Storage
WaterGAP	Water Global Assessment and Prognosis
WGHM	WaterGAP Hydrological Model
w.r.t	With respect to
WTC	Wet Troposphere Correction

2. Scientific Context

Assessing the sea level budget at global, regional and local scales over the altimetry era, i.e., comparing the altimetry-based sea level time series with the sum of components is of primary importance for many reasons. This allows (1) improved process understanding, (2) detection of temporal changes in one or several components, e.g., acceleration, abrupt change, with inference on sea level evolution; (3) identification and quantification of missing contributions if the budget is not closed, (4) detection of systematic instrumental bias & drifts and coverage gaps in the observing systems used to compute the components of the sea level budget, and (5) validation of models developed for sea level (e.g., reanalyses, coupled climate models) and components. At global scale, assessment of the sea level budget has been the object of numerous publications (e.g. Barnoud et al., 2021, 2023; Cazenave et al., 2018; Chen et al., 2018, 2022; Dieng et al., 2017; Horwath et al., 2021; Nerem et al., 2018; WCRP Global Sea Level Budget Group, 2018, just to quote a few recent studies). While there is general consensus on closure of the global mean sea level budget within data uncertainties until about 2016 (see above references and IPCC 2019, 2021), recent studies (e.g., Barnoud et al., 2021, 2023; Chen et al., 2022; Mu et al., 2024) have pointed out lack of closure since then, possibly a consequence of instrumental problems (e.g., radiometer drift onboard the Jason-3 altimetry mission and accelerometer breakdown on the GRACE/GRACE FO satellites). This well highlights the imperative necessity of continuously comparing the altimetry-based sea level data with the sum of contributions.

At regional scale, sea level budget studies are much less numerous. A few recent studies have assessed the closure of the sea level budget at the basin-scale, over the altimetry era (e.g., Camargo et al., 2023; Frederikse et al., 2016, 2018, 2020; Hamlington et al., 2020; Mu et al., 2024; Rietbroek et al., 2016; Royston et al., 2020). The regional ocean mass budget has also been investigated (Ludwigsen et al., 2024). Closure of the regional budget is only observed in some regions but not everywhere. For example, using altimetry, gravimetry and Argo data over 2005-2015, Royston et al. (2020) concluded that the regional budget cannot be closed in the Indian-South Pacific region. Similarly, Camargo et al. (2023) also found non-closure of the regional sea level budget in a number of oceanic areas. Using machine learning techniques, these authors were able to identify processes not well captured by the observations that are considered to assess closure of the regional sea level budget. Thus reinvestigating closure of the regional sea level budget with novel approaches is definitely an important task. This is one of the objectives of this project. This should allow deeper insight into the regions where the budget is not closed and into the suspected component (s) responsible for lack of closure. In the above quoted studies, closure of the regional budget was assessed by averaging the data either at basin-scales or sub-basin scales. Assessing the regional sea level budget without averaging the data at the basin-scale will also be a significant improvement.

Finally, no study exists on closure of the local/coastal sea level budget at a planetary scale. This is quite understandable, considering that at the coast a variety of local processes are superimposed to the global mean and regional sea level signal, causing sea level change at the coast to significantly vary from one region to another. However, a number of studies have focused on sea level changes over shelf areas in specific oceanic regions; e.g., Northeast America (Camargo et al., 2023; Dangendorf et al., 2023; Little et al., 2021; Piecuch et al., 2018), Gulf of Mexico (Leclercq

et al., 2025; Steinberg et al., 2024; Wang et al., 2022; Yin, 2023), northern Europe (Frederikse et al., 2016; Hermans et al., 2020; Wise et al., 2024), western Africa (Dieng et al., 2021; Dièye et al., 2023; Kemgang Ghomsi et al., 2024), Indian Ocean (Han et al., 2019), Southeast Asia (Thompson et al., 2023), etc. The purpose of these studies was to analyze how coastal sea level evolves from monthly to interannual time scale, identify and/or quantify the contribution of local underlying drivers (e.g., river runoff) and estimate the respective importance of ocean mass redistribution on the shelf versus remote steric effects (e.g., Dangendorf et al., 2021). Although not focusing on the local sea level budget, these studies constitute a very useful first step for further assessment of budget closure at the coast.

3. Intercomparison of each SLBC components

3.1. Altimetric component

3.1.1. Description of the product

The altimetry-based sea level component is computed using the approach described in AD3. This method relies on the C3S Level-4 sea level product, which provides gridded monthly sea level anomalies derived from multiple satellite altimeters.

To obtain the global sea level component from altimetry, we first compute the global mean sea level (GMSL) time series by averaging sea level anomalies over the ice-free ocean. This computation accounts for instrumental corrections, including orbit adjustments, wet and dry tropospheric corrections, ionospheric corrections, and dynamic atmospheric corrections.

3.1.2. Validation Strategy

To validate the altimetry-based sea level component, we performed an intercomparison with multiple reference datasets.

First, we compared our results with the time series from the first phase of the project, which also relies on the Copernicus Climate Change Service (C3S) sea level dataset. This allows us to assess the consistency of the methodology and detect potential differences introduced by updates in the C3S processing chain.

In addition, we used external altimetry-based products such as the CMEMS (Copernicus Marine Environment Monitoring Service) global sea level product provided by the U.S. NOAA Laboratory for Satellite Altimetry (Global Ocean Gridded L 4 Sea Surface Heights And Derived Variables Reprocessed 1993 Ongoing, 2025). This product, based on a multi-mission approach, offers an independent reference for assessing the stability and accuracy of our computed sea level anomalies.

Furthermore, we directly used Level-2P (L2P) altimetry products to evaluate the impact of different processing choices on the computed sea level time series. This approach has the advantage of leveraging the most recent L2P DT 2024 data, which are not yet included in the C3S Level-4 (L4)

sea level product. By comparing the L2P-derived sea level trends with those from the C3S L4 dataset, we can assess the effects of various corrections applied in the C3S processing chain.

A key aspect of our validation focuses on the impact of specific instrumental corrections, particularly:

- The TOPEX-A drift correction, which is applied to ensure the long-term stability of the sea level record.
- The Jason-3 radiometer drift correction, which can be addressed using the official Shannon Brown correction (Brown et al., 2023).
- Alternative wet tropospheric correction approaches, such as those based on climate data records (CDR), following the methodology of Barnoud et al. (2021).

These comparisons help quantify the impact of different correction strategies and ensure the robustness of the derived sea level trends.

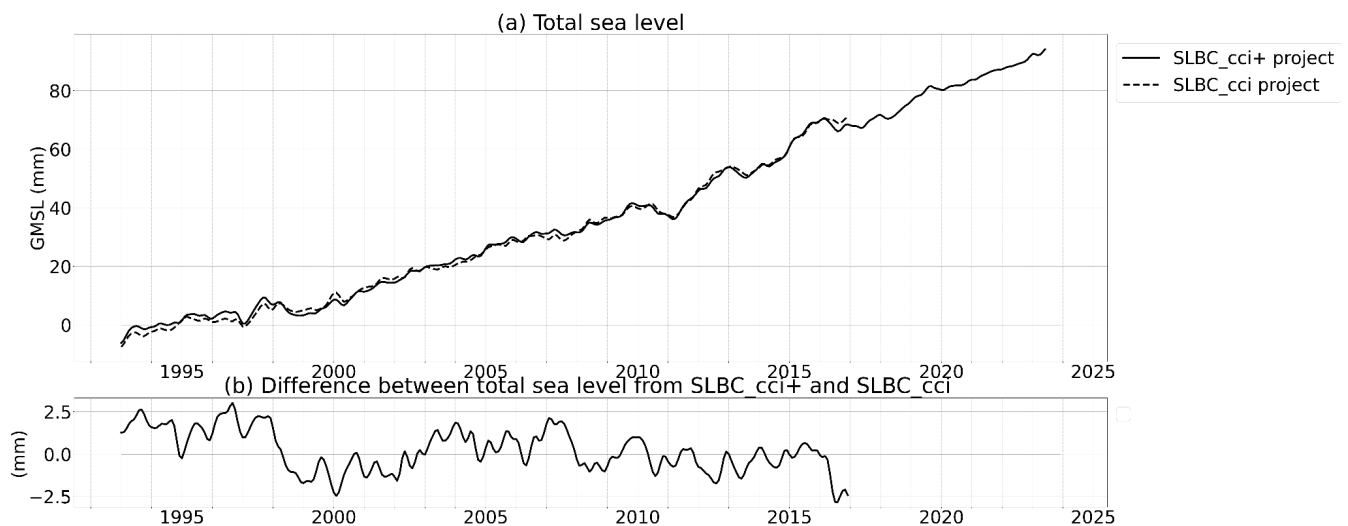


Figure 1 *Comparison between the total sea level component of the SLBC_CCI Phase I project and the total sea level component of the SLBC_CCI+ Phase II project. Panel (a) presents the GMSL time series, and Panel (b) shows the difference between the time series.*

Figure 1 shows a comparison between the total sea level component proposed in the second phase of the SLBC CCI project and that from phase I. It can be observed that there is very little difference between the two GMSL time series. The time series of the differences reveals a trend of approximately 0.15 mm/yr over 23 years, which is not significant compared to the uncertainties associated with the GMSL trend. The highest uncertainties are observed at the beginning of the time series, during the TOPEX/Poseidon period, when it was shown that the TOPEX A altimeter had a drift. A correction must therefore be applied to these data. The observed differences are likely related to variations in the correction of this drift between phases I and II.

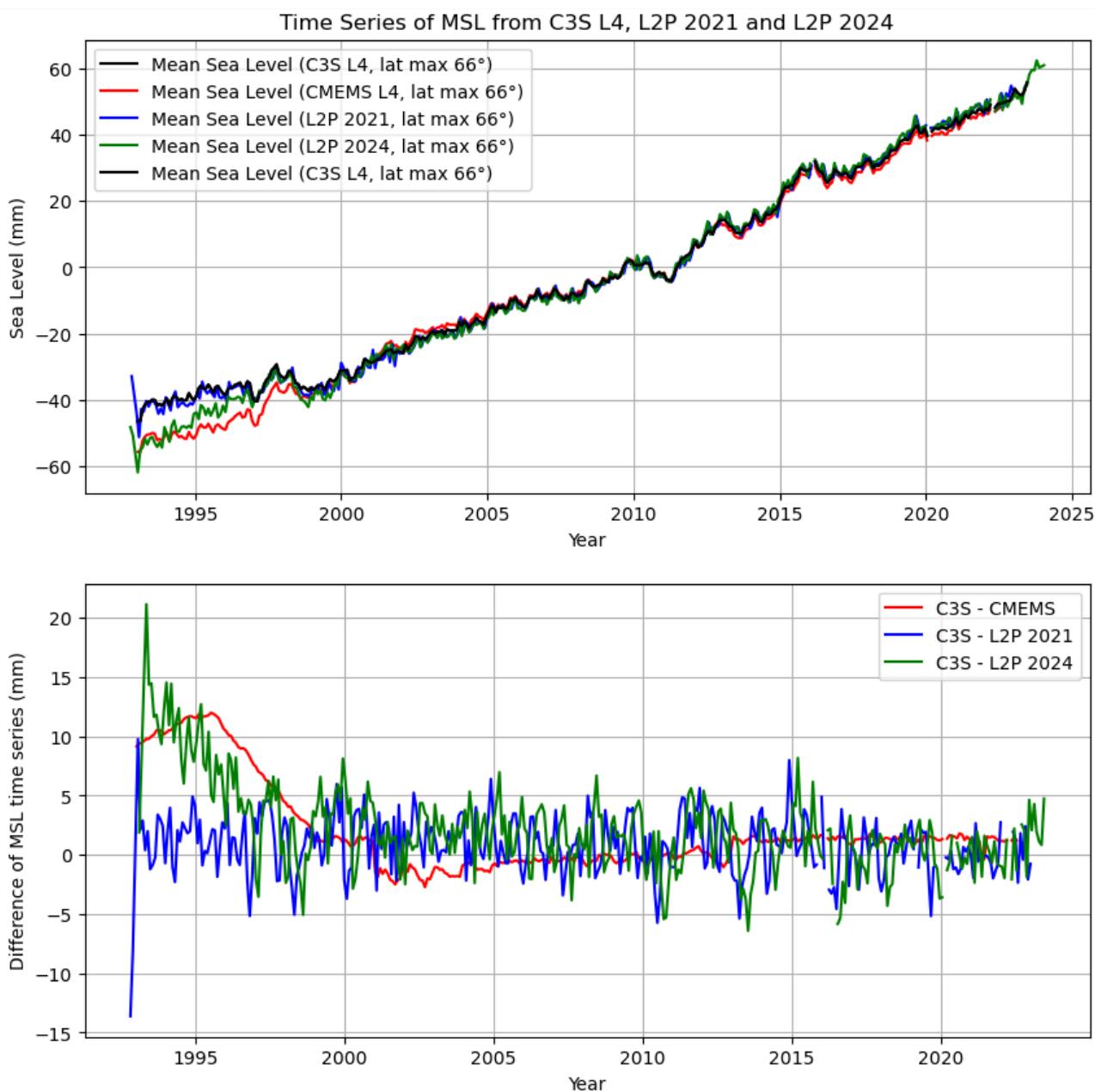


Figure 2 *Comparison between the total sea level component of the SLBC_CCI+ project (C3S) and alternative data such as GMSL from L4 CMEMS, from L2P DT 2021 and L2P DT 2024. Panel (a) presents the GMSL time series, and Panel (b) shows the difference between the time series.*

Figure 2 presents a comparison between the global mean sea level (GMSL) time series derived from the SLBC_CCI+ altimetry component (based on the C3S Level-4 product) and several alternative datasets: the CMEMS global L4 product, and GMSL derived directly from Level-2P altimetry data using both DT 2021 and DT 2024 reprocessing versions. Panel (a) displays the GMSL time series, while panel (b) shows the differences between each alternative product and the C3S-derived time series.

The overall agreement across the different datasets is good at long time scale, with only minor short time scale discrepancies observed. Most of the divergence is concentrated during the early part of the record, particularly in the TOPEX/Poseidon era. During this period, two distinct approaches can be identified: on one side, C3S and the L2P DT 2021 datasets recommend applying a correction for the TOPEX-A instrumental drift; on the other side, CMEMS and the L2P DT 2024 dataset currently do not recommend applying a TOPEX-A correction, although discussions are still ongoing regarding this point for L2P 2024.

At present, we observe that applying the TOPEX-A drift correction to the C3S data results in GMSL time series more closely aligned with what was provided during the first phase of the project for the altimetry component. Beyond this period, the variations between the datasets are negligible, indicating a high degree of consistency in recent years across the different processing approaches.

This comparison reinforces the robustness of the C3S Level-4 altimetry product used in the SLBC_CCI+ project. Despite differences in processing methodologies and applied corrections, the resulting GMSL time series remain very consistent, especially over the past two decades. The main differences stem from known uncertainties in the early altimetry era, which are well-documented and actively corrected in the latest reprocessing efforts.

In conclusion, the validation against multiple independent altimetry datasets confirms the reliability and stability of the SLBC_CCI+ altimetric component. While some sensitivity to processing choices exists during the TOPEX/Poseidon period, particularly regarding the treatment of TOPEX-A drift in the latest Level-2P DT 2024 dataset, the long-term GMSL trend remains robust across all datasets.

3.2. Steric component

The steric sea level change was calculated for several products: MOAA GPV ((Hosoda et al., 2008), hereafter JAMSTEC), EN4.2.2.109. (hereafter EN4,(Good et al., 2013)), SCRIPPS (Roemmich and Gilson, 2009) and ISAS20 (Gaillard et al., 2016; Kolodziejczyk et al., 2023). The four products are analyses based on an optimal interpolation of Argo data. The steric component is calculated for all of them and compared between 2005 and 2020 (the common period). As these products have different continental masks, interpolation must be done for some computation. When calculating direct differences: Product - ISAS20, ISAS20 is interpolated onto the grid of Product. When calculating the inter-product spread, the four analyses are compared and are all interpolated onto JAMSTEC's grid, which is the most confined.

Seasonal variability:

The monthly mean climatology is calculated for JAMSTEC, EN4, SCRIPPS and ISAS between 2005 and 2020. The temporal standard deviations of each climatology are displayed in Figure 3. The differences between ISAS's monthly standard deviation and that of the other products is shown in Figure 4, along with the ensemble spread of the four standard deviations.

ISAS seasonal variability is comparable with the other products, except in the Southern Ocean where strong differences are found with JAMSTEC (Figure 3 a-d, Figure 4 a-c). Regions of disagreement between all the products are located in the Southern Ocean, and in the Kuroshio, and Gulf Stream regions (Figure 4 d).

Seasonal STD (mm)

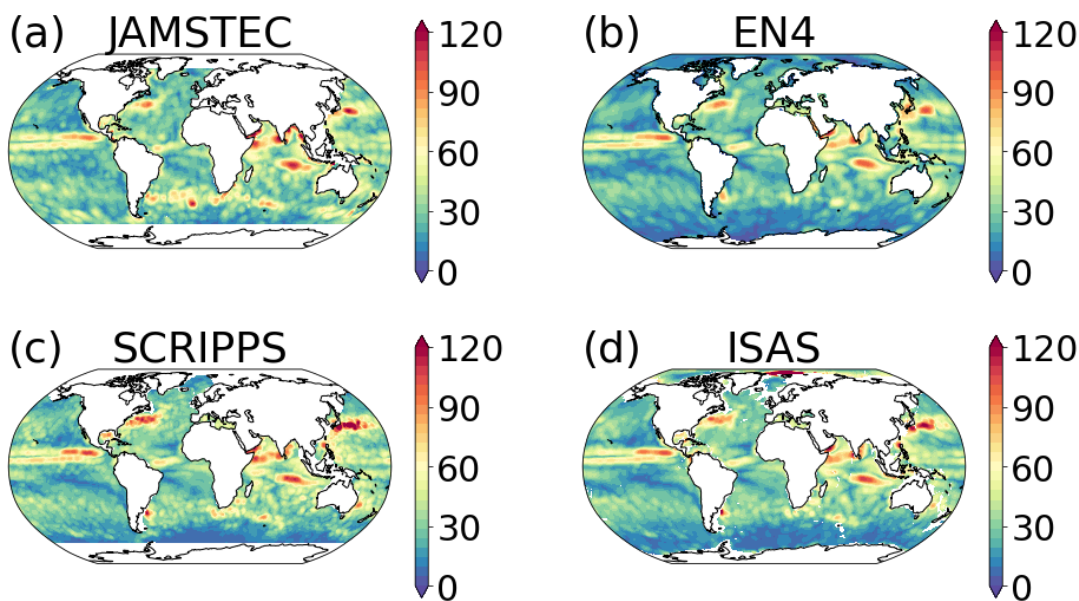


Figure 3 *Standard deviation of the monthly climatology estimated from JAMSTEC (a), EN4 (b), SCRIPPS (c) and ISAS (d).*

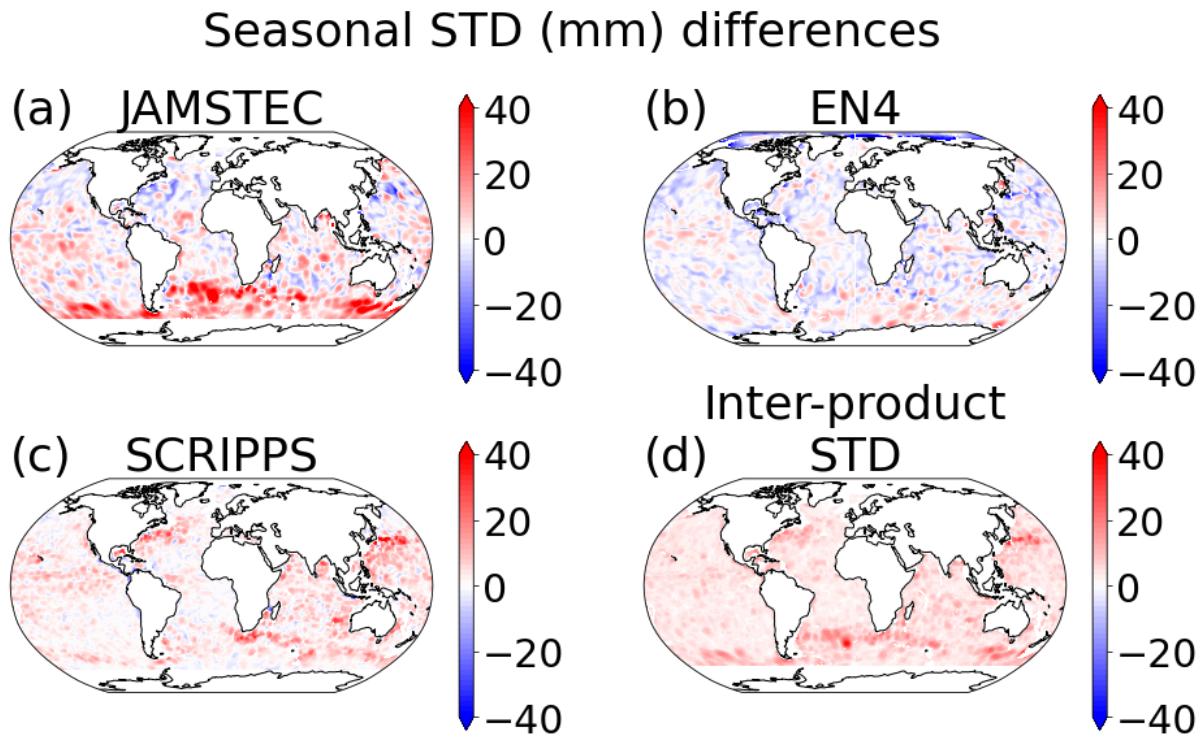


Figure 4 *Differences between the climatology standard deviations of JAMSTEC (a), EN4 (b) and SCRIPPS (c) with this of ISAS). (d) Interproduct standard deviation of the climatology standard deviations*

Global evaluation:

With the removal of the monthly climatology, we can focus on the anomalies of the four products.

The global average of these anomalies (between 60°S and 70°N, for common latitudes) is shown in Figure 5a. The difference of these averages with ISAS solution is shown in Figure 5b. A significant long-term change is observed, consistent between all the products (Figure 5a). The linear trend is about 1 mm per year for ISAS, 1.13 for JAMSTEC, 0.73 for EN4 and 1.27 for SCRIPPS. ISAS evolves close to JAMSTEC, and exhibits larger inter-product differences before 2008 and after 2018, at the edges of the time period (Figure 5 a and b). Part of the differences are associated with the reconstruction of interannual variability (Figure 5 b).

With removal of long-term trend from the global averages, we can better assess the differences of reconstruction of interannual variability among the products (Figure 6 a and b). Variations at interannual scale are of the order of 2mm and can reach 5mm (Figure 6 a).

Interannual anomalies of ISAS are similar to those of the JAMSTEC product (Figure 6 b). Higher differences are among ISAS and EN4. Again, most important differences between the products are found at the edges of the time period.

The uncertainty associated with ISAS (dark gray shades, 95% C.I.) captures the other product signals within its interval, prior to 2009, and between 2014 and 2018 (Figure 5a and Figure 6a). Before 2008, there is to be an overestimation of the error of analysis (due to an insufficient amount of Argo observations) while it is more accurately estimated between 2014 and 2018. The error may be underestimated between 2009 and 2014, and after 2018.

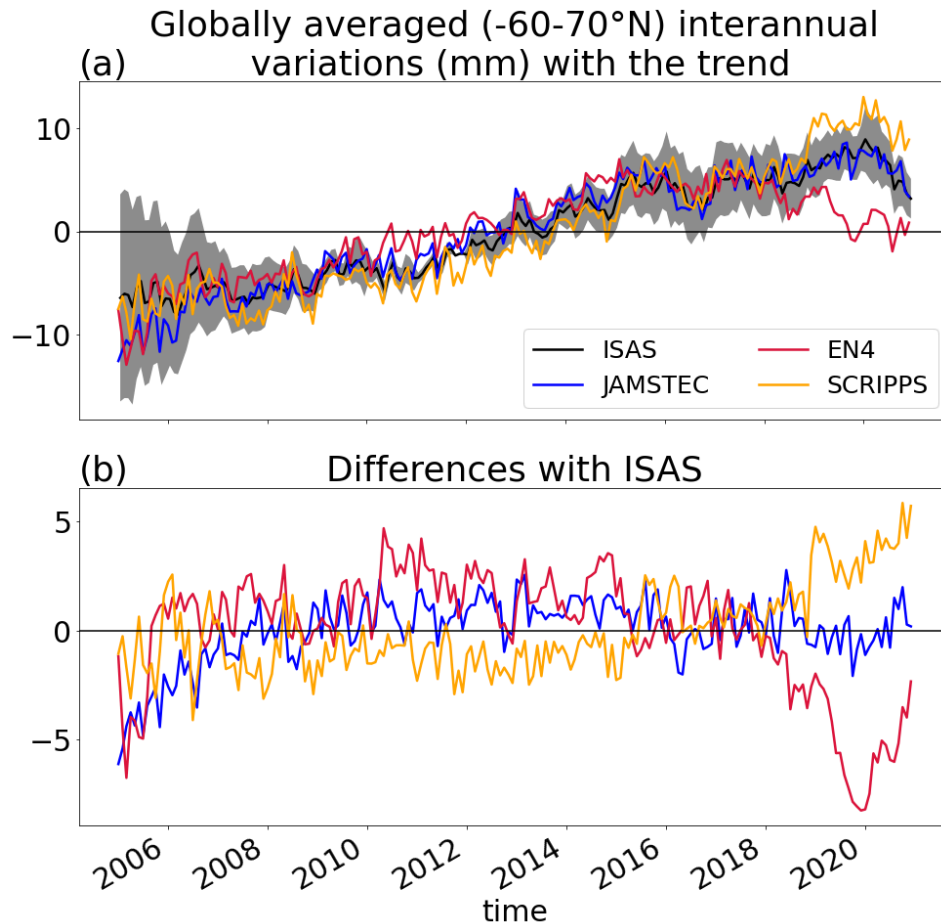


Figure 5 (a) Globally average of anomalies of JAMSTEC, EN4, SCRIPPS and ISAS, following the removal of the monthly climatology, but with the linear trend still present. (b) Differences of the global averages of JAMSTEC, EN4 and SCRIPPS with ISAS'.

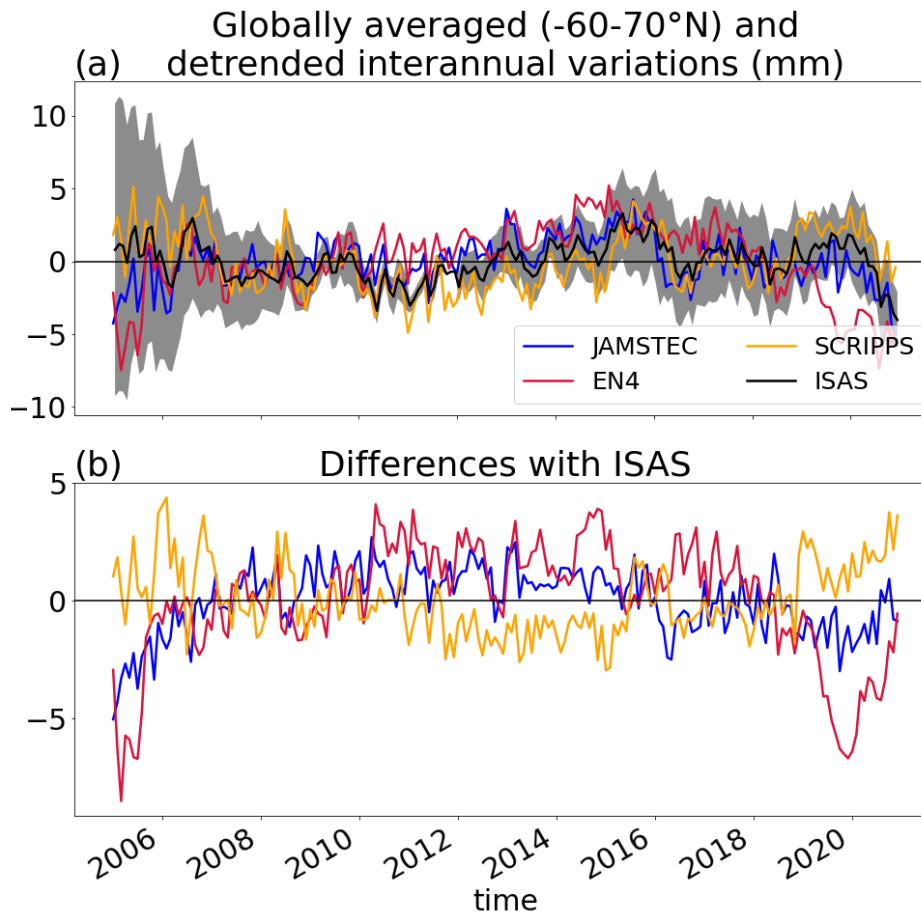


Figure 6 (a) Globally average of interannual anomalies of JAMSTEC, EN4, SCRIPPS and ISAS, following the removal of the monthly climatology and the linear trend. (b) Differences of the global averages of JAMSTEC, EN4 and SCRIPPS with ISAS'.

Regional long-term change:

The long-term steric sea level changes at the regional scale are shown in Figure 7, with linear trends as represented by the different products. The differences between these trends are represented in Figure 8.

Sea level changes due to steric effects are positive in most of the oceans, with most important rise in the vicinity of strong oceanic currents (Gulf Stream, Kuroshio, Antarctic Circumpolar Current) and notably in the eastern tropical Pacific. Regions where the sea level decreases due to steric effects (with agreement among the four products) are in the western Tropical Pacific, the Tropical Atlantic, the Labrador Sea, and the Ross Sea (Figure 7 a-d).

The disagreements between ISAS and the other products do not indicate a notable bias in ISAS (Figure 8 a-c). There are significant discrepancies among all the products, as revealed by their mutual standard deviation (Figure 8 d). However, ISAS may be underestimating the trends in the Southern Ocean and the Southern Atlantic Ocean, relative to the other products (Figure 8 a-c).

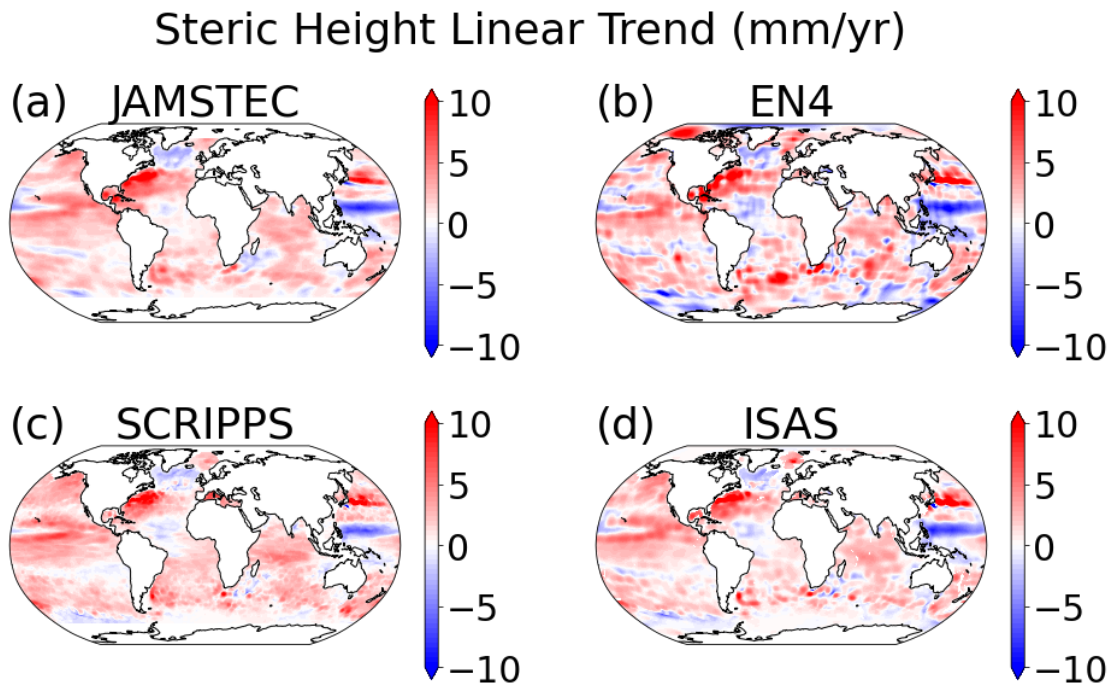


Figure 7 *SSL linear trends for JAMSTEC (a), EN4 (b) SCRIPPS (c) and ISAS (d).*

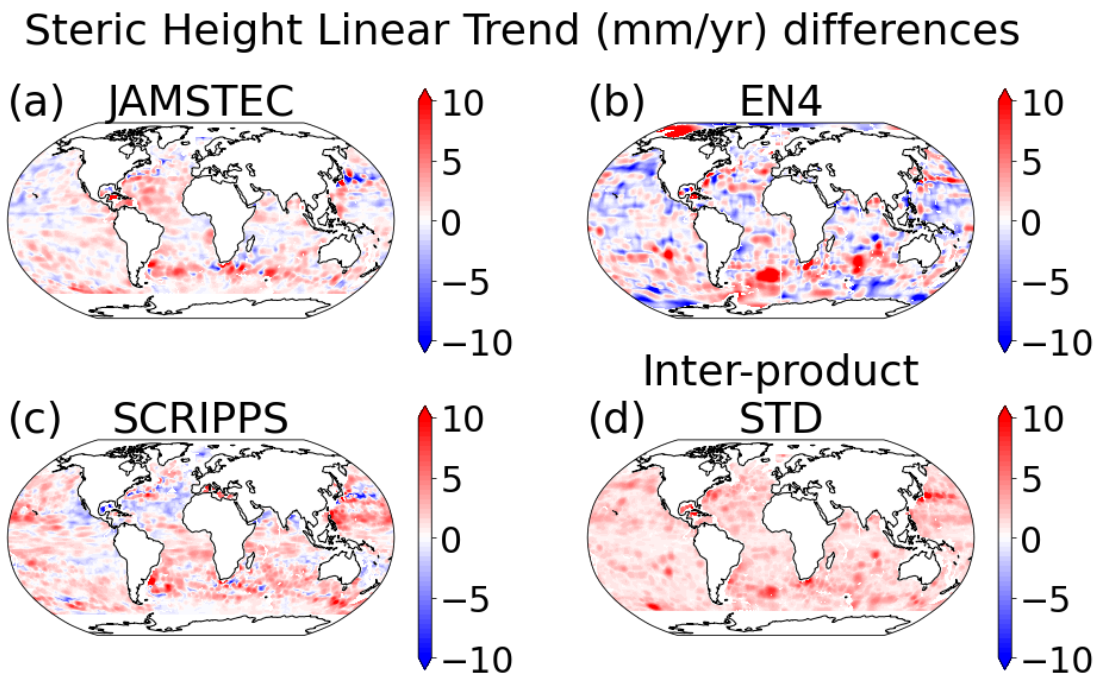


Figure 8 *Differences of the linear trends of JAMSTEC (a), EN4 (b) SCRIPPS, SCRIPPS (c) with ISAS. (d) Inter-product standard deviations of the trends.*

The distribution of the linear long-term changes along the latitudes is represented in Figure 9. It shows a sea level rise due to steric effects (up to 5 mm/year, at 35°N) at most latitudes and a

decrease around 15°N (around -2 mm/year), around 60°N and in the south of 55°S (Figure 9 a). The meridional limitation of JAMSTEC and SCRIPPS prevent a more robust estimation of the changes north of 70°N and south of 55°S, especially as ISAS and EN4 have significantly different results (Figure 9 a and b). South of 50°N, ISAS linear trends are found among the spread of the other products, but its uncertainty appears underestimated (Figure 9 a). Concerning the differences between ISAS trends and the others, they range between -1 – 1 mm/year, apart from the higher latitudes. ISAS trends are strong relative to other products at 60°N, and 70°N.

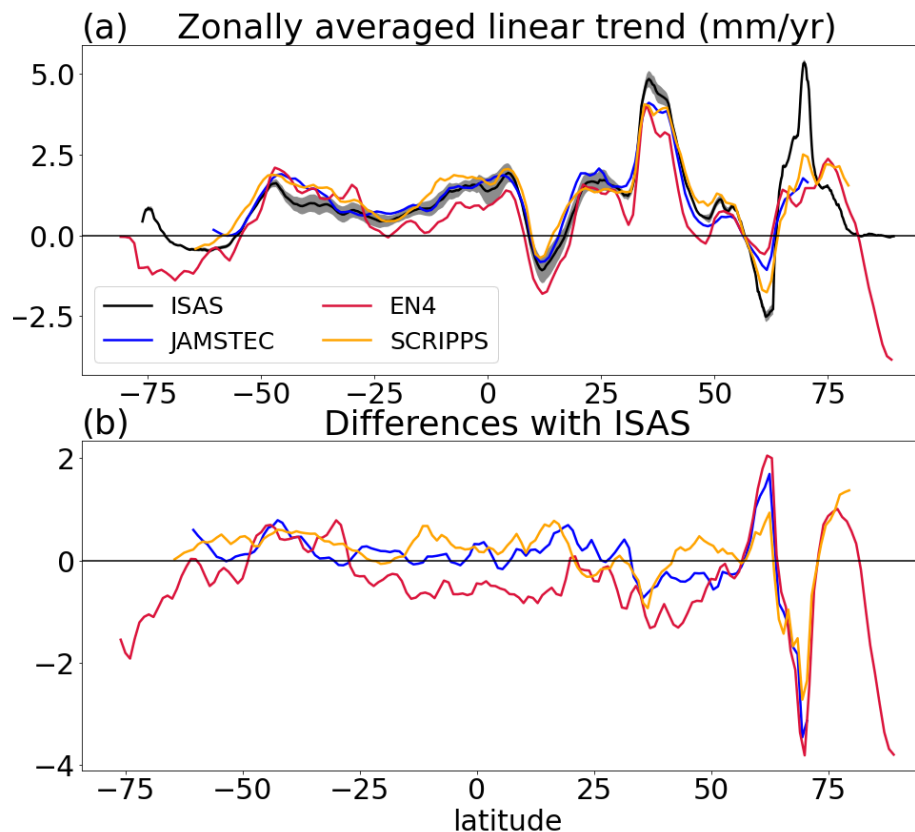


Figure 9 (a) Zonally averaged SSL linear trends for JAMSTEC, EN4, SCRIPPS and ISAS. (b) Differences of the zonally averages SSL linear trends of JAMSTEC, EN4 and SCRIPPS with ISAS'.

Regional interannual variability:

With removal of the climatology and the linear trend, we can analyse the interannual variability in the steric component of sea level changes (Figure 10) and how ISAS differs from other products (Figure 11). Regions where the associated fluctuations are important are consistently identified by the four products. They are the Gulf Stream, the Tropical Pacific basin, the Kuroshio, the Central Indian Ocean, the Malvinas Current, and the Agulhas Current. These regions are roughly the same as previously identified for the climatology, although with more intense variations (Figure 3 and Figure 10).

The intensity of the interannual variability differs from one product to another (Figure 10 a-d and Figure 11 d). Differences between ISAS and other products suggest ISAS may underestimate the interannual variability in the Southern Ocean and the Northern Atlantic Ocean. Differences with EN4 are significant, with EN4 representing stronger variability than ISAS, excepted in the region of the Kuroshio Current.

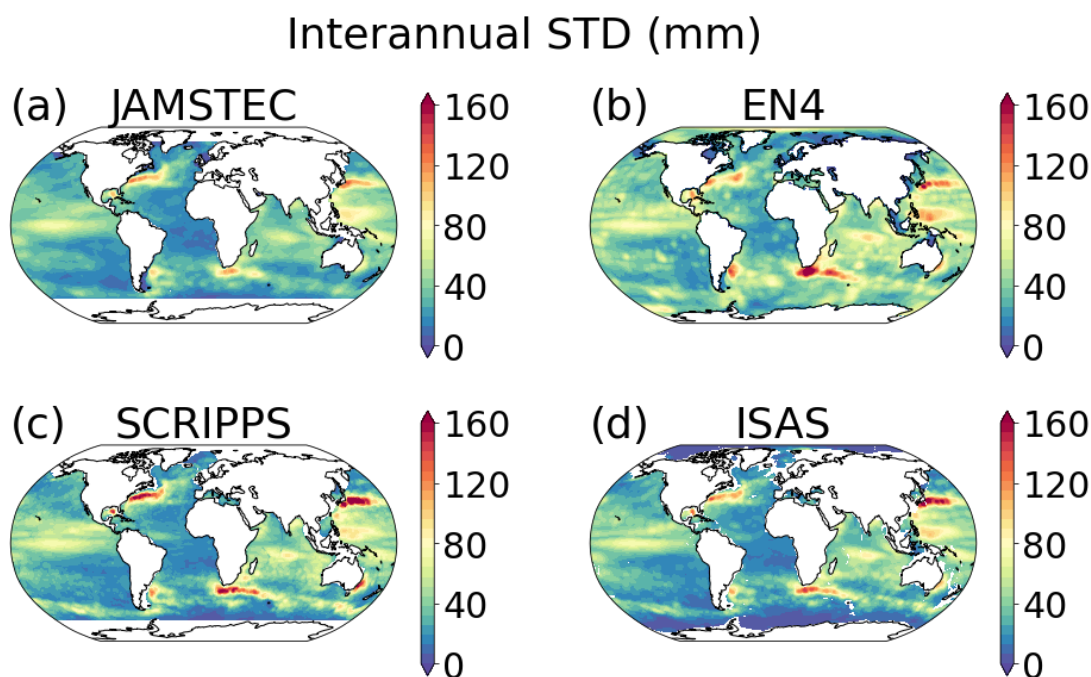


Figure 10 *Standard deviations associated with SSL anomalies, following the removal of the monthly climatology and linear trend, for JAMSTEC (a), EN4 (b) SCRIPPS (c) and ISAS (d).*

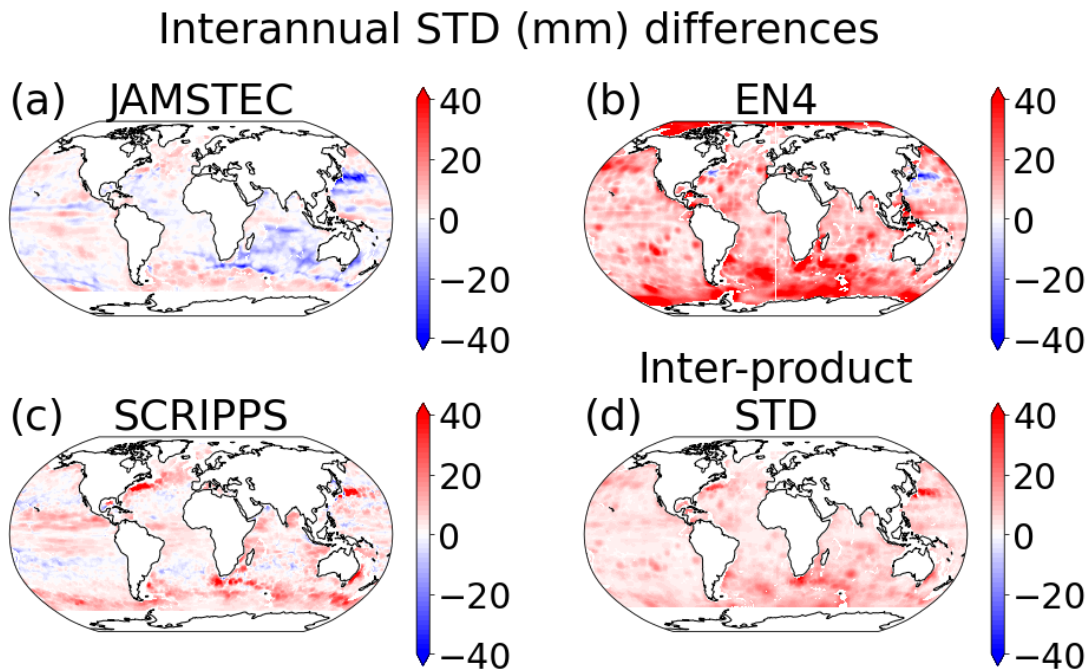


Figure 11 *Differences of the interannual standard deviations of JAMSTEC (a), EN4 (b) SCRIPPS, SCRIPPS (c) with ISAS. (d) Inter-product standard deviations of the interannual standard deviations.*

3.3. Manometric and Barystatic component from GRACE

For validation of the GRACE-derived mass changes we performed an intercomparison with different alternative GRACE-based data sets.

The first comparison is performed with the time series of the ocean-mass component of the global ocean from the first SLBC_cci project (SLBC-1) (Figure 12). This comparison is intended to validate the methodological changes made in the current phase of the project.

To further validate the TU Dresden mass change product we compare the time series of the ocean-mass component of the global ocean with time series derived from three alternative mascon products (Loomis et al., 2019; Save et al., 2016; Wiese et al., 2016), (Figure 13, Table 3).

We further use these three mascon products to validate spatially resolved trends of mass changes over the global ocean in our third comparison (Figure 14).

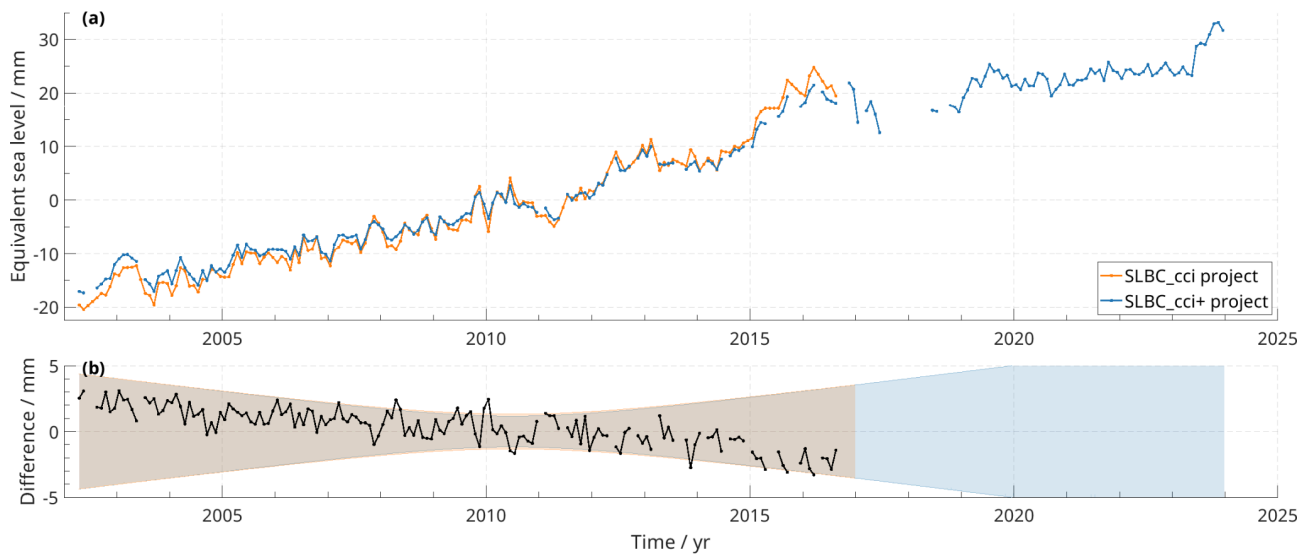


Figure 12 *Comparison between (a) mass-change time series for the global ocean from the SLBC-1 ocean-mass change solutions (orange) and the current ocean-mass change solution (blue). For the current solution, different from its standard run, the GIA model by Caron et al. (2018) was applied for GIA correction, to be consistent with SLBC-1. Seasonal components are removed. (b) Difference between the two time series and the associated uncertainties assessed in SLBC-1 (light orange) and in the current project (light blue). (Note that the uncertainties for the current phase are clipped following 2020).*

Figure 12 shows the comparison between global ocean mass time series of SLBC-1 and the current phase of the project. A seasonal component is removed from both time series. Furthermore, for the specific comparison in Figure 12, the same GIA correction as in SLBC-1 was used (Caron et al., 2018) in order to focus this comparison on other methodological differences. The difference time series does not only show a noise component but also a systematic trend. However, the differences stay well within the assessed 1- σ uncertainties of both time series. This is to be expected as these uncertainties also include error components (e.g., errors introduced by the GIA correction) that are not visible here due to the same treatment in both time series.

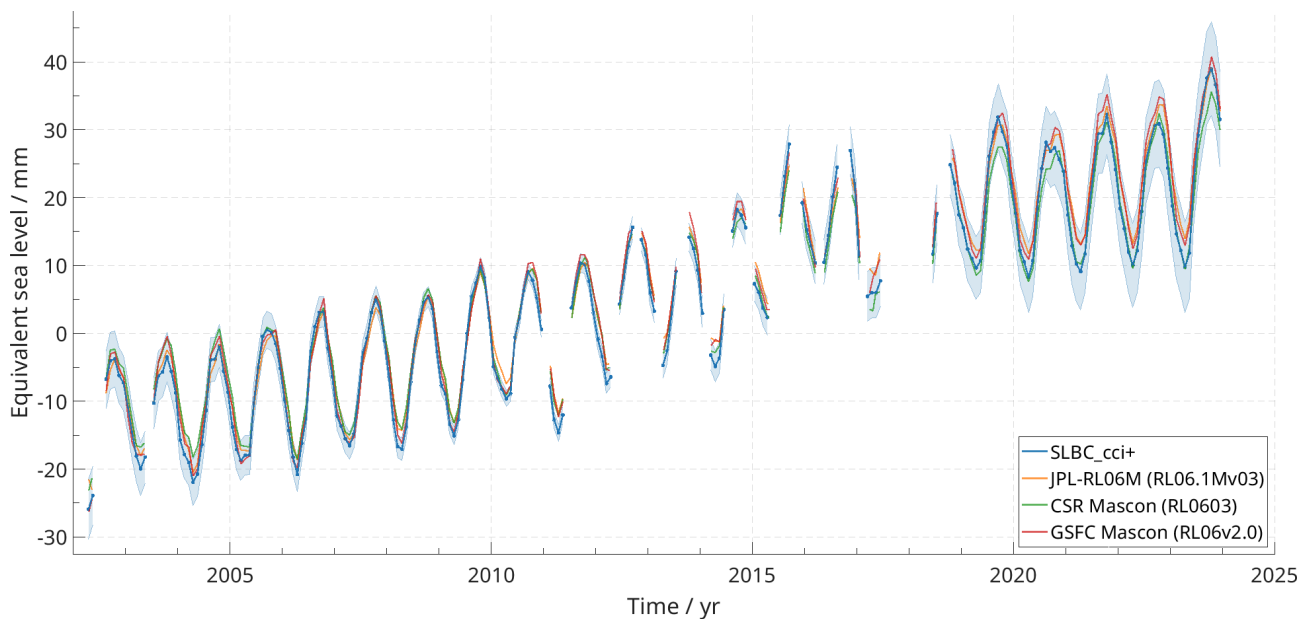


Figure 13 *Comparison between time series of global ocean mass change from this project (blue) and derived from alternative mascon solutions.*

Figure 13 shows the comparison between the global ocean mass time series of this project and time series derived from alternative Mascon products. As all three mascon solutions use the ICE-6G_D GIA model (Peltier et al., 2018) correction, the same GIA correction was applied to the time series of this project. The time series derived in this project does not exceed the differences between the three time series of the alternative mascon products. All time series fit well within the assessed uncertainties of the time series of this project, too, and the trends also agree within the assessed uncertainties (Table 3).

Table 3 *Trends of global ocean mass change*

Mascon product:	SLBC_cci+	JPL-RL06M	CSR-Mascon	GSFC-Mascon
Trend (2002–2024):	1.96 mm yr ⁻¹	2.01 mm yr ⁻¹	1.74 mm yr ⁻¹	2.03 mm yr ⁻¹

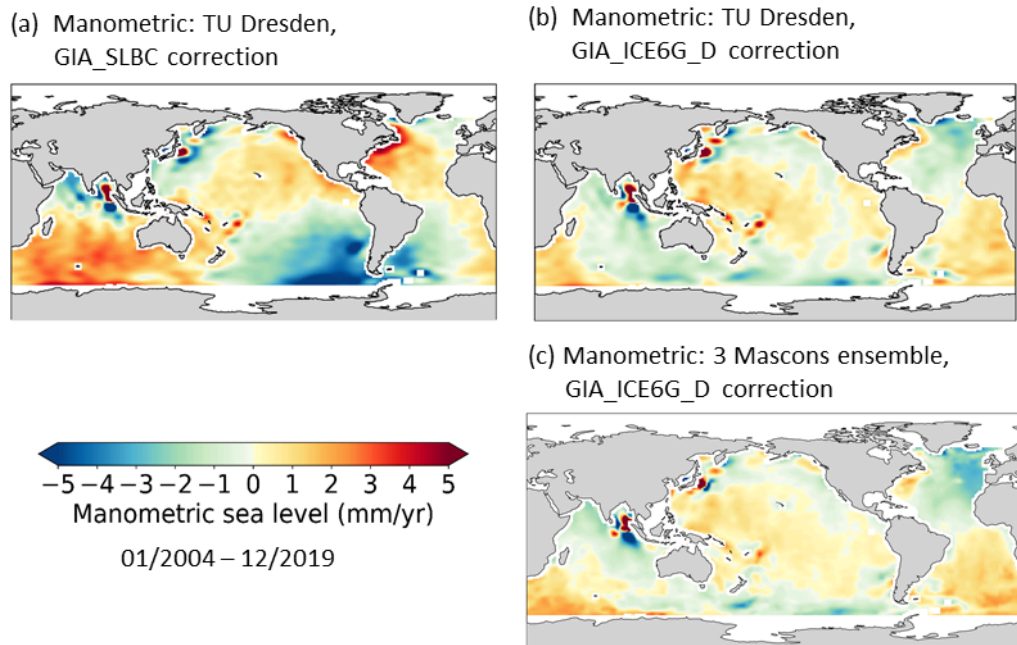


Figure 14 *Comparison between manometric sea level trends. (a): Trends derived in this project using the UNIBO SLBC_cci+ GIA correction. (b): Trends derived in this project using the ICE-6G_D GIA correction. (c): Trend from an ensemble of three alternative mascon solutions using the ICE-6G_D GIA model.*

Figure 14 shows three maps of manometric sea level trends. The trends estimated in this study (Figure 14b) and estimated from an ensemble of the three alternative mascon products (Figure 14c) are both derived using the ICE-6G_D GIA model (Peltier et al., 2018) correction. Spatial patterns in both maps agree well for different oceans with minor differences in amplitude. This comparison validates the manometric estimates derived with the method used in this project. However, a comparison with trends derived using the UNIBO GIA correction of this project (Figure 14a) highlights the impact of the GIA correction: the derived trends are dominated by a visible $C_{2,1}/S_{2,1}$ pattern compared to Figure 14b.

3.4. Individual mass contributions

3.4.1. Land Water Storage component

The Land Water Storage component has been estimated using GRACE-REC, ISBACTRIP and WGHM hydrological models (Figure 15). The GRACE-REC model is an estimate of the climate-driven Total Water Storage based on precipitation and calibrated against GRACE data (Humphrey and Gudmundsson, 2019) using three climate forcing models (ERA5, GSWP3 and MSWEP) and two GRACE datasets (from GSFC and JPL) until the end of 2014 when using GSWP3, until the end of 2016 when using MSWEP and until the end of 2019 when using ERA5.

These estimates based on precipitations include the contribution of land ice. The ISBA-CTRIP (Interaction Soil-Biosphere-Atmosphere, Total Runoff Integrating Pathways from the Centre National de Recherches Météorologiques) hydrological model provides estimates of climate-driven LWS until the end of 2018 (Decharme et al., 2019). The Water Global Assessment and Prognosis (WaterGAP) Hydrological Model (WGHM) version 22e (Müller Schmied et al., 2023) provides estimates of LWS using the fifth generation of the European Centre for Medium-range Weather Forecasts (ECMWF) atmospheric reanalysis (ERA5) and W5E5 datasets for the climate-forcing, with and without the anthropogenic contribution. The W5E5-based data are provided until the end of 2019 while the ERA5-based data are provided until the end of 2022.

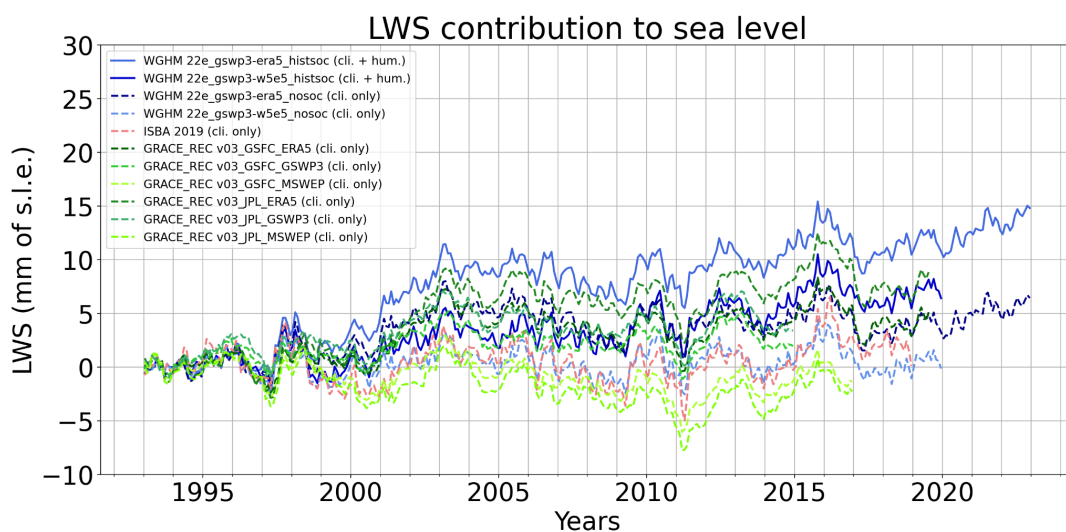


Figure 15 *Comparison of the estimate of land water storage variation contribution to sea level change from various hydrological models: four estimates of the WaterGAP Hydrological Model (WGHM) version 22e, the ISBA-CTRIP hydrological model and six estimates of the GRACE_REC model. Plain lines indicate estimates including the human-induced contribution (“hum.”) while dotted lines indicate estimates taking into consideration only the climate-driven contribution (“cli.”). Only the GRACE-REC estimates include the land ice contribution.*

From gridded LWS data, we compute the global mean LWS variations over land areas excluding Greenland, Antarctica and glacier areas. The global mean LWS variation over land is then converted to contribution to sea level change using the total surface of oceans.

The time series of the WGHM 22e model with ERA5 and W5e5 climate forcing, which includes anthropogenic contributions, remained similar from 1993 to 1998 before diverging by up to 5 mm (Figure 16). We use the LWS time series obtained by averaging these WGHM 22e times series. Besides, this estimate does not include the contribution of land ice which is taken into account by the glacier component (see section 3.4.4).

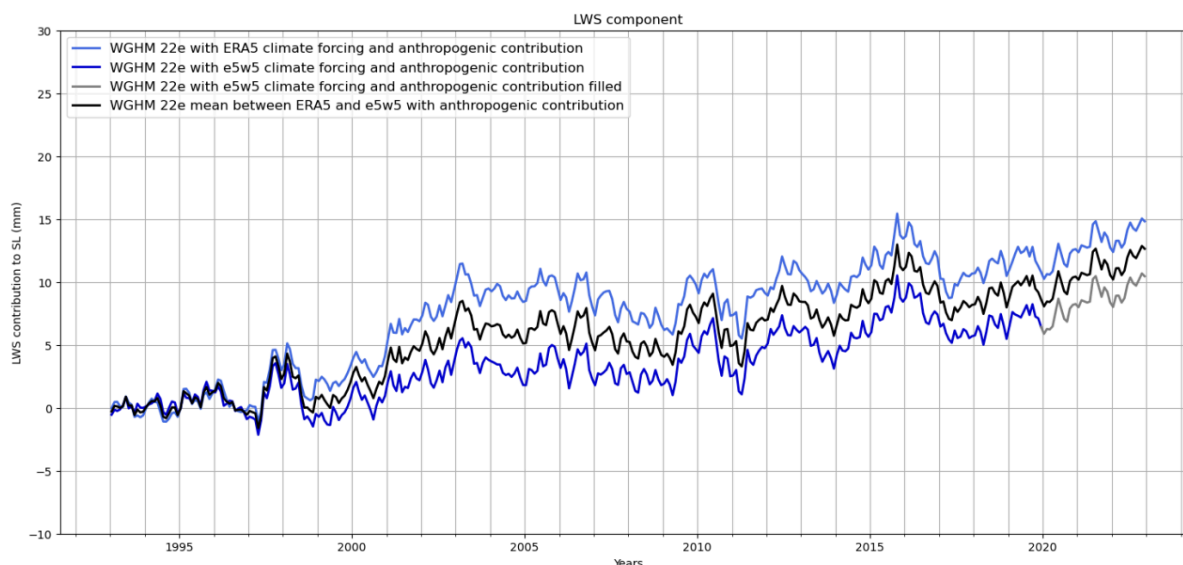


Figure 16 *Land water storage variations contribution to global mean sea level change, from the WaterGap Hydrological Model (WGHM) version 22e with ERA5 (light blue) and W5e5 (blue) climate forcing and including the anthropogenic contribution. The LWS time series obtained by averaging the WGHM 22e times series is in black. The LWS time series estimated with W5e5 climate forcing was completed by overlapping WGHM with ERA5 forcing data.*

Figure 17 shows the LWS time series used as a component for the sea level budget with its standard uncertainty. The uncertainty budget of the land water storage component includes the combination of the two trend uncertainties (Cáceres et al. (2020)) and of the white noise results in a full covariance matrix of the LWS component, following the same methodology as for altimetry (Ablain et al., 2019; Guérou et al., 2023). The uncertainty estimation approach of the LWS time series is detailed in section 2.4.1 of the D3-5.

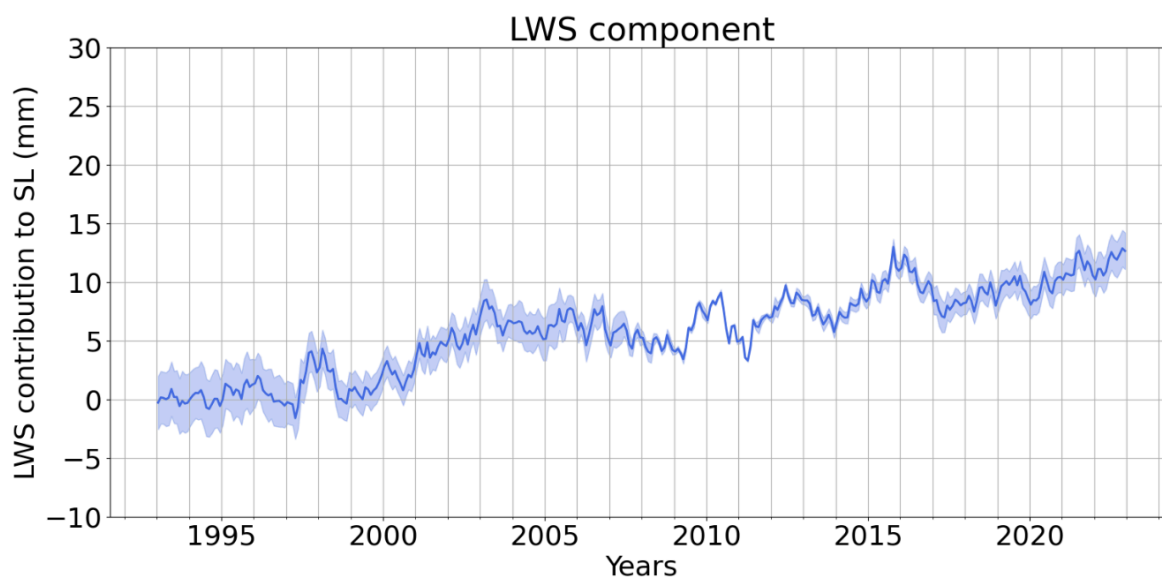


Figure 17 *Land water storage variations contribution to global mean sea level change obtained by averaging the WGHM 22e with ERA5 and W5e5 climate forcing and including the anthropogenic contribution with its standard uncertainty.*

3.4.2. Atmosphere water vapour component

The Atmosphere water vapour component has been estimated with the water vapour content from ERA5 dataset which are summed over the whole globe and converted to sea level change using the total surface of the oceans. There are other datasets that provide this water vapour content such as the ESA CCI over land and from the Hambourg Ocean-Atmosphere Fluxes and Parameters from Satellite (HOAPS) data or the GRACE Atmosphere and Ocean De-aliasing dataset (called AOD1B). More details about the processing of the data is provided in the ATBD ([AD3]).

However, the ERA5 dataset provides a full period coverage of the altimetry era (1993-present) with a high spatial and temporal resolution (monthly, $1/4^\circ \times 1/4^\circ$). The other estimates (HOAPS, AOD1B) have limited spatial and temporal resolutions but provide very accurate datasets for comparison activities.

When comparing the datasets over their respective periods (Figure 18), we can observe a good agreement between the different estimates over the period 2005-2016 but with more important discrepancies after 2016 especially between ERA5 and AOD1B. We can also observe that there is no particular trend observed over the period 2005-2015 with an increase of the Global Mean atmosphere mass change after 2015.

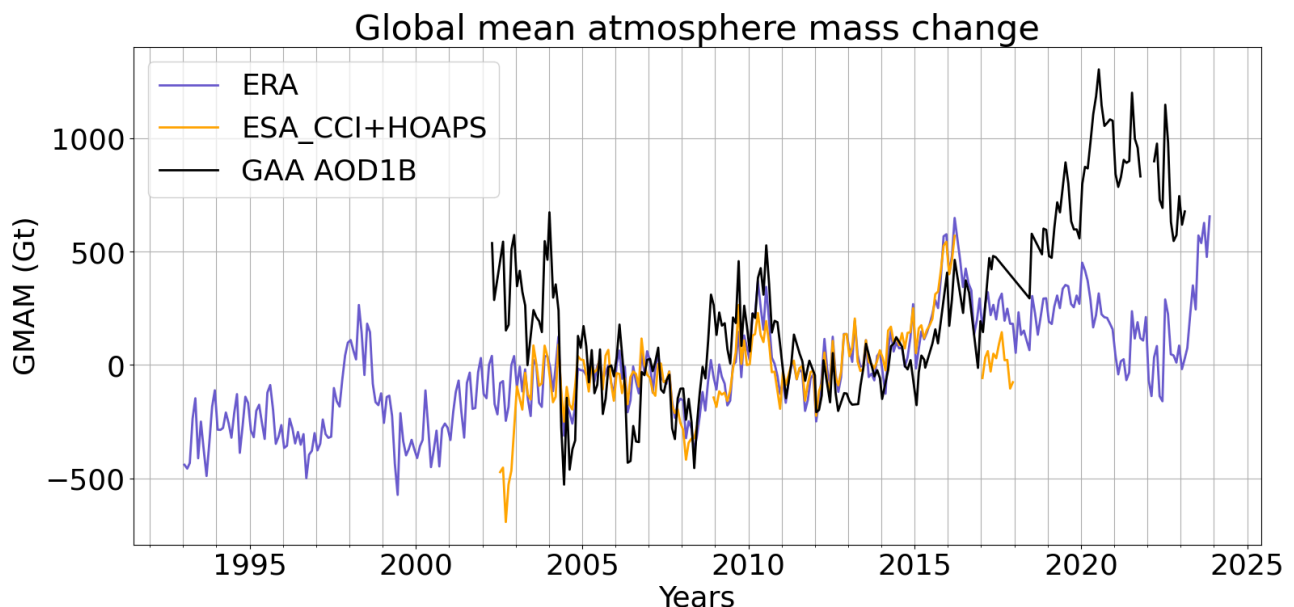


Figure 18 *Comparison of the global mean atmosphere mass change estimated from ERA5 (blue line), HOAPS (orange line) and AOD1B (black line) over the period 1993-2024*

Comparisons have also been made over the common period of 2005-2016 in terms of inter-annual variations (Figure 19). We can observe a very good agreement between the different datasets over this period with a variation around 2010 (likely due to an important El-niño event).

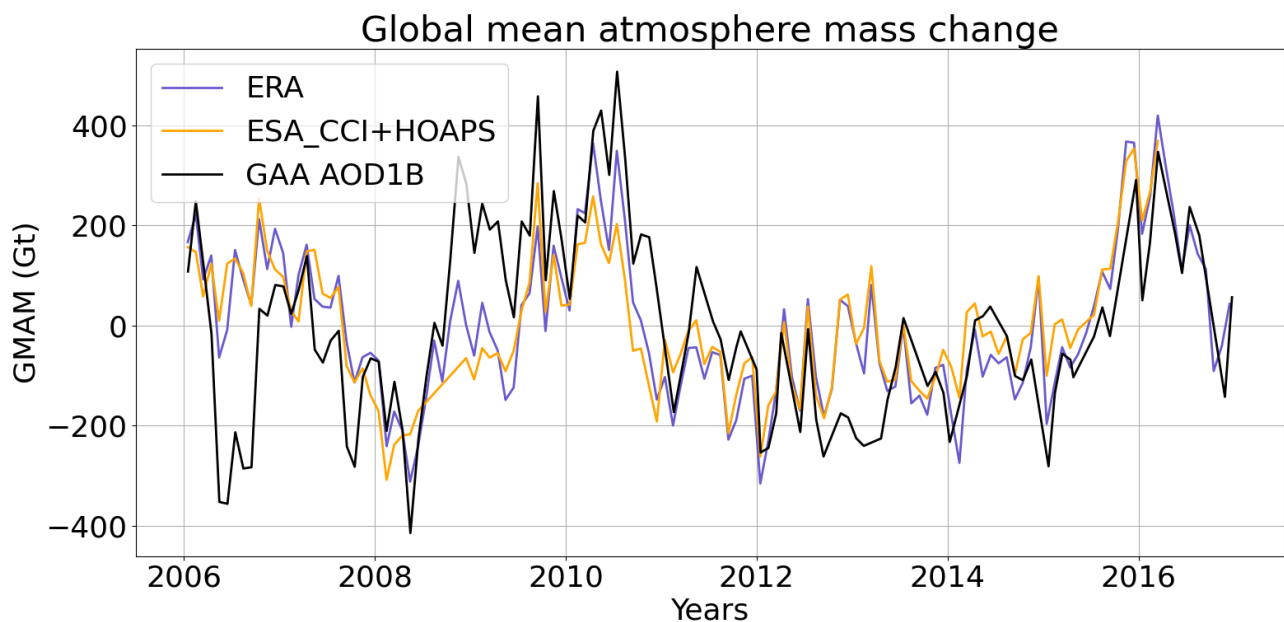


Figure 19 *Comparison of the global mean atmosphere mass change estimated from ERA5 (blue line), HOAPS (orange line) and AOD1B (black line) over the period 2005-2016, trend has been removed from each dataset*

3.4.3. Ice Sheets component

The SLBC_cci+ project relies on established datasets for ice sheet mass balance (cf. ATBD), Namely, the IMBIE_R2 aggregated assessments and the CCI GMB products. State-of-the art estimates of ice sheet mass balance have been compared regularly, e.g. within IMBIE (Otosaka et al, 2023). These comparisons have revealed good agreement between the different estimates for the GIS and somewhat larger differences for the AIS. The most recent IMBIE assessment (Otosaka et al., 2023) particularly revealed discrepancies between results of the input output method (contributed from a single group) and the gravimetric method and altimetric method for the EAIS, where the latter two methods are in a better agreement.

Here we compare the IMBIE aggregated assessment and the CCI GMB assessments with each other. In addition, we compare these two assessments with the ice sheet mass balance assessments used by the first SLBC_cci project (SLBC-1) (Horwath et al., 2021). SLBC-1 used two alternative ice sheet assessments: one from gravimetry and one from altimetry. For Greenland,

SLBC-1 added an assessment for the peripheral glaciers according to a global glacier model. This peripheral glacier assessment is not included in the present comparison.

For the **Greenland Ice Sheet**, Figure 20 compares the four assessments on a time series level. All time series show a very similar long-term behaviour, e.g. with an acceleration of mass loss between 1995 and 2012 and some deceleration around 2012. Differences occur w.r.t. the short-term signals. The pronounced seasonal signal is only visible in the CCI GMB time series. This is because seasonal signals were removed from the SLBC-1 GRACE-based time series and are not present in the IMBIE and SLBC-1 altimetry-based time series. The latter two, by their generation, have an effective temporal resolution of 3 years and 3 to 5 years, respectively. This difference in temporal resolution also explains the smoother appearance of the IMBIE and altimetry-based time series. The comparison of the uncertainty bounds (shaded areas) illustrates the role of the reference time to which mass anomalies refer. This reference time is 1992.0 for IMBIE, hence the error bars increase from the starting point of the time series. For the other three time series, the reference state is the mean over a ten-year interval centered in 2011.0. Hence, uncertainty 'wedges' converge to values close to zero at this central time.

Linear trends over the common period of the four time series (from 2003-01 to 2016-08) are given in Table 5. They are calculated as the rate of a linear function fitted together with an annual sinusoid. The trends range from -253 Gt/yr to -282 Gt/a. The spread is slightly larger than the uncertainty quoted for the individual assessments. Part of the differences likely arises from the different degrees of inclusion of peripheral glaciers. Their contribution is partly included in the GRACE-based assessment (due to the low spatial resolution of satellite gravimetry), while it is not included in the altimetry-based assessments used here. Hugonnet et al., 2021 estimate the peripheral glacier mass change between 2000 and 2019 on the order of -35 Gt/yr, which could explain the larger mass losses indicated by GRACE-only assessments.

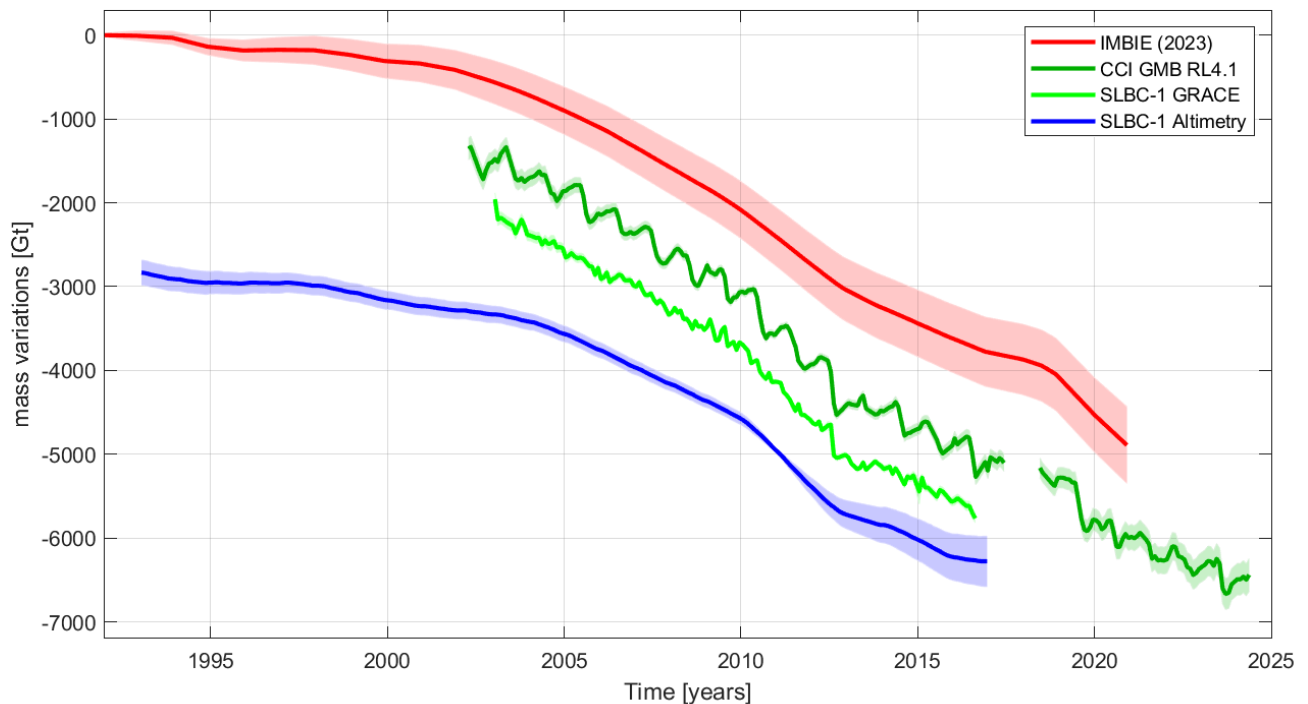


Figure 20 *Mass changes of the Greenland Ice Sheet according to the latest IMBIE assessment (red), the GIS_cci+ Gravimetric Mass Balance (GMB) RL4.1 assessment (dark green), the GRACE-based assessment used by the first SLBC_cci project (light green) and the altimetry-based assessment used by the first SLBC_cci project (blue). The curves are offset along the y-axis for better legibility. Error bars provided with the assessments refer to mass anomalies w.r.t. 1992 for the case of IMBIE and w.r.t. 2011.0 for the case of the other three assessments.*

For the **Antarctic Ice Sheet**, Figure 21 compares the four assessments on time series level. The observations of different short term content in the time series and their explanation is analogous to what was stated for the GIS time series. The GRACE time series for the AIS exhibits a notable month-to-month noise component, partly related to the uncertainties of low-degree spherical harmonic components of the underlying gravity field solutions. The altimetry-based SLBC-1 time series is a monthly interpolation of an originally 140-day resolution.

Mean linear trends for the common period from 2003-01 to 2016-08 (Table 4) are between -98 Gt/a and -135 Gt/yr. This range reflects the well-known spread among results from different techniques (and even from different realisations of the same techniques). Uncertainties quoted for the gravimetric results are in line with this spread, while uncertainties quoted for IMBIE and SLBC-1 altimetry are smaller. A possible underestimation of the IMBIE uncertainties might arise from their methodology of uncertainty aggregation, which relies on the uncertainties per epoch stated by the individual contributors and has limited account for temporal error correlations.

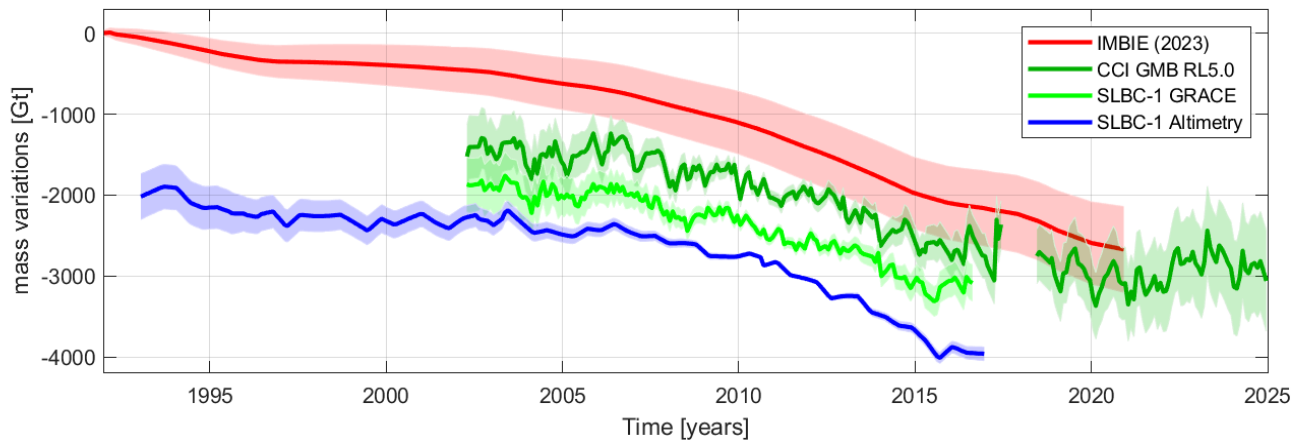


Figure 21 *Mass changes of the Antarctic Ice Sheet according to the latest IMBIE assessment (red), the AIS_cci+ Gravimetric Mass Balance (GMB) RL5.0 assessment (dark green), the GRACE-based assessment used by the first SLBC_cci project (light green) and the altimetry-based assessment used by the first SLBC_cci project (blue). The curves are offset along the y-axis for better legibility. Error bars provided with the assessments refer to mass anomalies w.r.t. 1992 for the case of IMBIE and w.r.t. 2011.0 for the case of the other three assessments.*

Table 5 *Mean linear trends of ice sheet mass over the period 2003-01 – 2016-08 for the Greenland Ice Sheet (GIS) and the Antarctic Ice Sheet (AIS) from the four assessments considered here. Uncertainties are quoted from the data sources. They exceed the formal uncertainties that would just result from the linear regression. In the case of the IMBIE assessment, uncertainties are calculated from the uncertainties quoted by Otosaka et al. (2023) for three consecutive 5-year intervals under the assumption of uncorrelated errors, in line with the uncertainty aggregation approach of IMBIE.*

	GIS [Gt/a] 2003-01 – 2016-08	AIS [Gt/a] 2003-01 – 2016-08
IMBIE	-253 ± 23	-135 ± 25
CCI GMB	-282 ± 14	-98 ± 44
SLBC-1 GRACE	-281 ± 8	102 ± 40
SLBC-1 Altimetry	-246 ± 22	-125 ± 14

3.4.4. Glaciers component

The GIC data provided here were compared to a community-based intercomparison exercise involving 233 estimates of regional mass balance change using all available methods (Zemp et al, 2025). The data set used here compares well with the GLAMBIE ensemble estimate when

averaged over all regions (Figure 22) but there are some differences locally that are difficult to constrain in terms of cause.

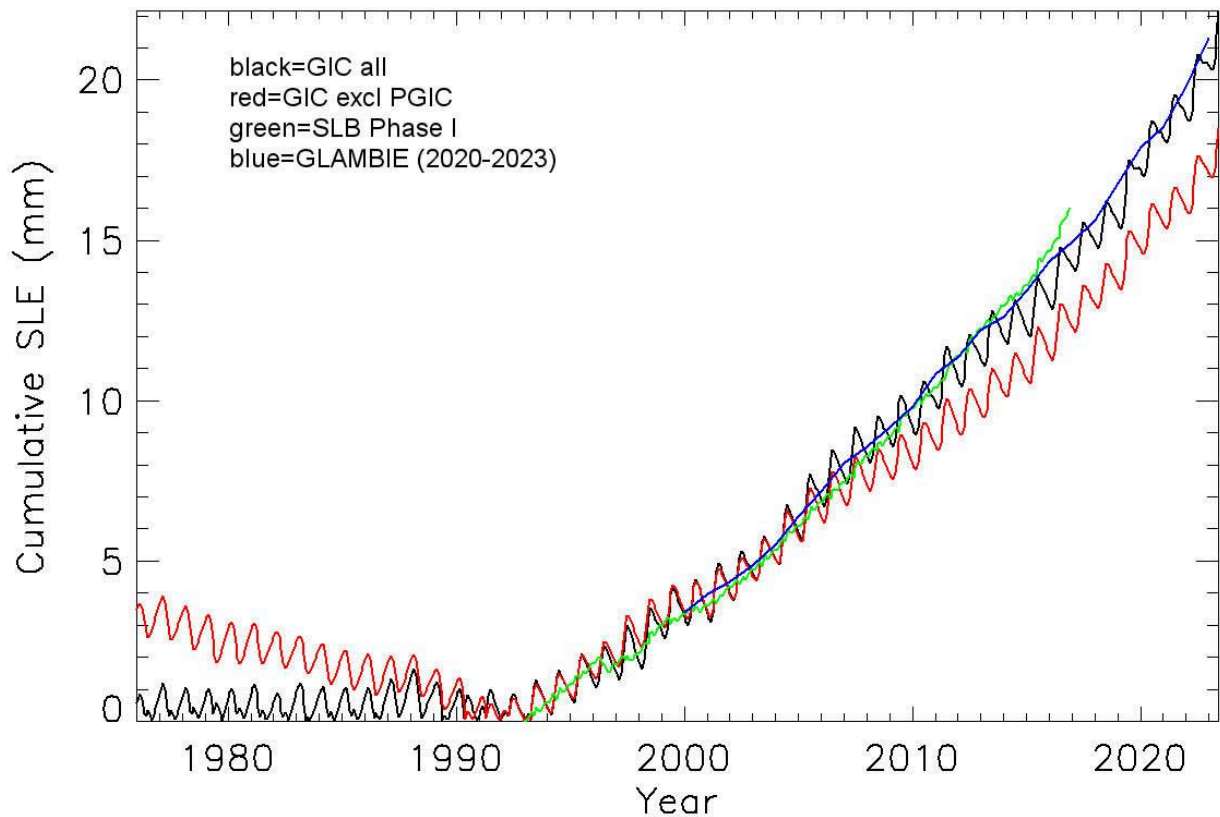


Figure 22 *Comparison of spatially integrated GIC mass balance for the data set used here (black), the SLB P1 product and the community intercomparison ensemble for 2000-2023 (blue).*

Figure 22 compares our data at global scale with the SLB P1 and the Glacier Mass Balance Intercomparison Exercise (GLAMBIE). The P1 estimates for 2010-17 were slightly more positive (~ 1 mm SLE cumulative) compared to the P2 product but the latter was derived in an entirely different way, contains new and comprehensive mass balance data that was not available previously and compares favourably and within errors to the ensemble mean from GLAMBIE. Note, however, that the seasonal cycle is idealised and cannot easily be compared to other products. In addition, the GLAMBIE project (funded by ESA) undertook an extensive comparison with the P2 and all other available data sets (Zemp et al., 2025). Figure 23 illustrates the comparison undertaken in the GLAMBIE project for a region that is challenging for many EO methods but which has relatively large signal.

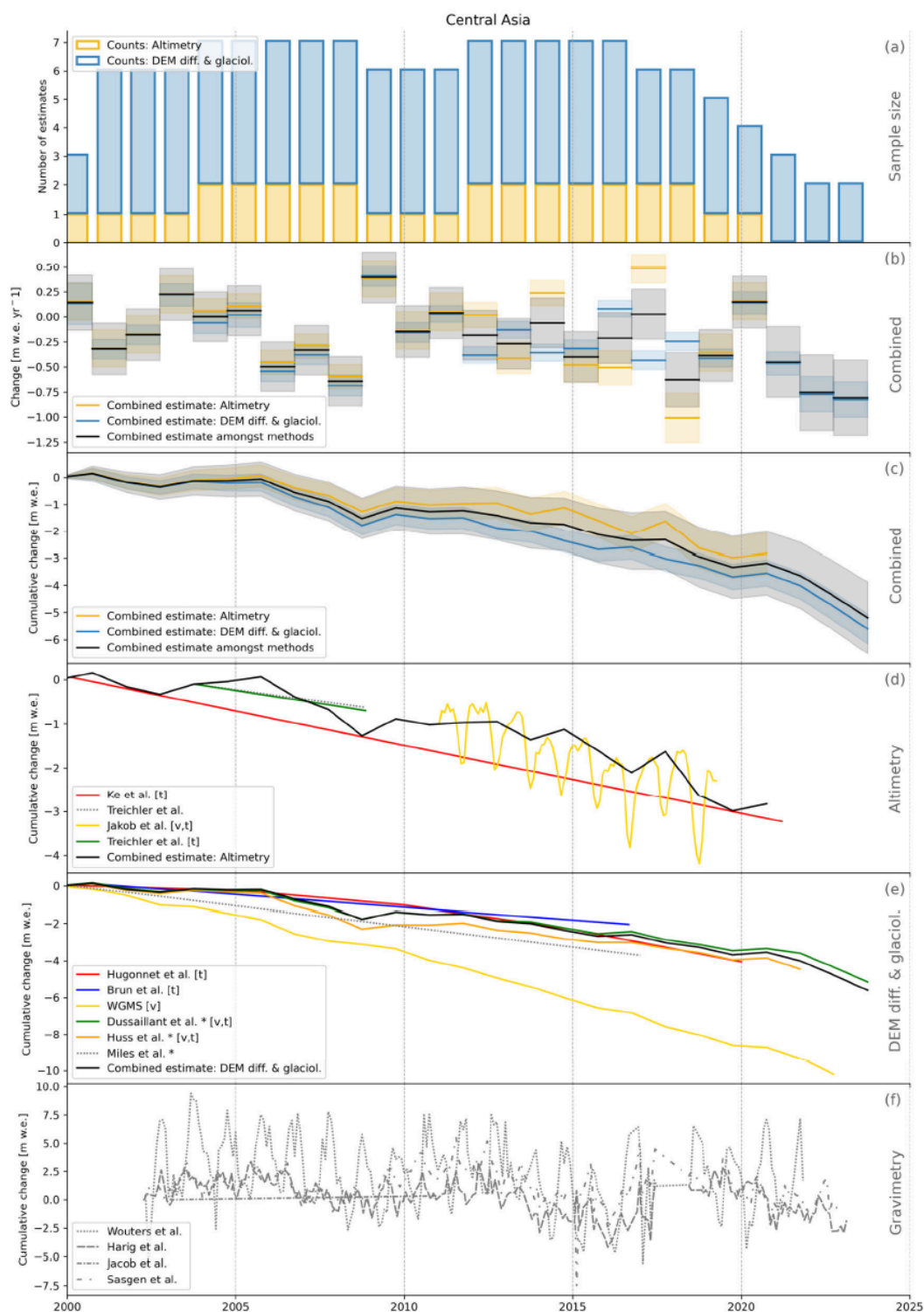


Figure 23 *Comparison of different data sets undertaken in Zemp et al, 2025 for RGI region Central Asia. The GLAMBIE ensemble estimate is in black and the P2 product used here in green. Similar figures are provided for all 19 RGI regions and in all cases the P2 product is in close agreement with the GLAMBIE ensemble which currently must be considered as the benchmark data set for the post 2000 period. It does not, however, include a seasonal component and does not extend back before 2000.*

3.5. Glacial Isostatic Adjustment and Present Days Ice Melting component

The GIA and PDIM components of sea level provided by UNIBO have been evaluated using the open source program SELEN⁴ (Spada and Melini, 2019). The GIA and the elastic fingerprint data produced so far in the framework of this collaboration are made available from the site <https://doi.org/10.5281/zenodo.12755218>

The evaluation of the GIA and of the elastic fingerprints data have required fundamentally two steps. Step i) consists in the computation, for a given spherically symmetric Earth model, of the loading love number for an elastic rheology (fingerprints) and for a Maxwell viscoelastic rheology (GIA) whereas Step ii) consists in the solution of the Sea Level Equation in order to retrieve the patterns of spatial variability of the geophysical quantities (absolute and relative sea level variations, vertical displacements of the solid Earth, and geoid height changes).

For step i), comparison with other, independently obtained data have been performed on the load-deformation coefficients using standard results from the validation and intercomparison work of Spada et al. (2011). Tidal Love numbers have been validated as well, since these are necessary for the evaluation of the rotational feedback on sea-level change.

For step ii), we have taken advantage of the results of the Sea Level Equation benchmark of Martinec et al. (2018), validating the most critical parts of the sea level equation solvers employed within the framework of this collaboration, including the modelization of the migration of the shorelines in response to GIA.

Figure 24 shows the nominal solution for the GIA model ICE-6G_C, obtained using the Sea Level Equation solver SELEN⁴. To allow a comparison with another GIA data set, in Figure 25 we have considered the GIA absolute sea level change according to the models progressively developed at the Australian National University (ANU) by Kurt Lambeck and collaborators. The global and regional differences in the two fingerprints reflect different assumptions regarding i) the distribution of the ice at the Last Glacial Maximum ii) the rheological profile of the mantle and of the lithosphere and iii) different constraining datasets. Results in Figure 24 and Figure 25 have been obtained using the same Sea Level Equation solver (SELEN⁴).

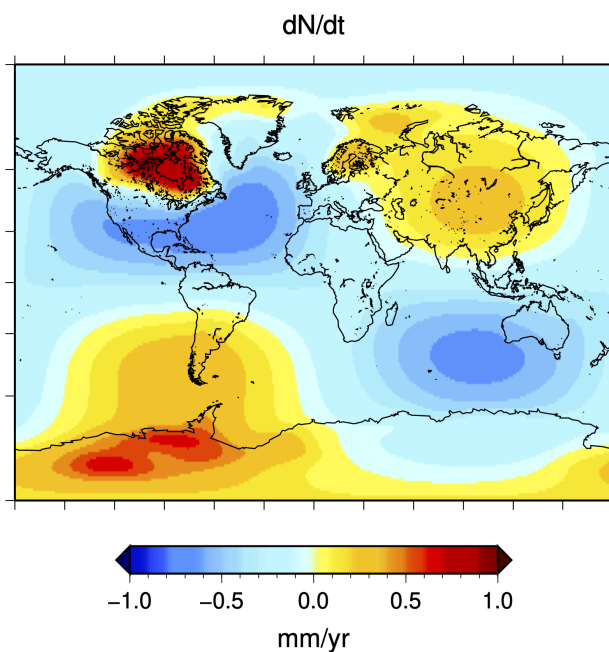


Figure 24 *GIA rate of present day absolute sea level change (mm/yr), according to the implementation of the nominal ICE-6G_C mode of [Argus et al. \(2014\)](#) and [Peltier et al. \(2015\)](#), obtained using SELEN⁴ of [Spada and Melini \(2019\)](#).*

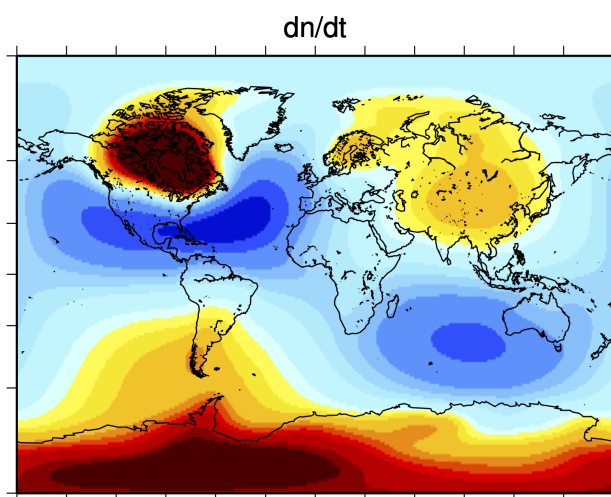


Figure 25 *GIA rate of present-day absolute sea level change (mm/yr) according to the ANU model. Same color table as in Figure 24.*

4. Analysis of the unconstrained SLBC: Historical Approach

4.1. Overview

This section presents the main outcomes of the classical approach to Sea Level Budget Closure (SLBC), as initially developed during Phase 1 of the SLBC_cci project (Horwath et al., 2022). The analysis involves computing the sea level budget and its residuals from the sum of individual components, using the input datasets described in [AD4] and [AD5]. This allows us to assess how well the budget closes and to investigate potential sources of discrepancy between data sources and methods.

The global analysis includes two key aspects. First, the mass budget, which compares the barystatic sea level derived from satellite gravimetry (GRACE) to the sum of individual mass components (ice sheets, glaciers, and land water storage). Second, the sea level budget, which compares the sum of individual contributions (thermsteric and barystatic) to the observed global mean sea level from satellite altimetry, with particular attention paid to trend variations. Together, these elements provide insight into the global SLB closure and highlight the agreements or mismatches between different observation systems and methods.

The regional analysis extends this comparison to spatially resolved patterns of sea level change. The analysis is focused on regions and periods for which observations are available.

Section 4.2 presents the global SLBC analysis using the SLBC_cci+ project datasets. The analysis focuses on the closure of the mass and total sea level budgets at global scale, assessing the consistency between different components (barystatic, thermsteric, and observed sea level from altimetry) and evaluating the performance of the project's data in reproducing observed trends and variability.

Section 4.3 extends this analysis to the regional scale. It investigates spatially resolved patterns of sea level change and budget closure over selected regions, still using the SLBC_cci+ datasets. This regional perspective helps highlight possible local discrepancies and better understand spatial variability in the SLBC.

In both sections, we then summarize the main results of Bouih et al. (2025), which has recently been accepted for publication. These results were obtained using external datasets, independent of those produced within the current project. They represent a preliminary version of the SLB analysis, based on readily available and well-documented ancillary datasets. This preliminary choice was made to ensure timely progress in the project.

In Section 4.4, we build upon these results to introduce the first elements of a more advanced analysis. The outcomes of the classical SLBC approach—both global and regional—will serve as a

benchmark for validating the new methodologies developed within the project. Moreover, several open issues identified in the classical analysis are discussed.

4.2. At global mean

4.2.1. Validation of the SLB product

This section aims to evaluate the consistency of the global mean sea level budget by comparing the different components contributing to sea level change. Using both satellite gravimetry (GRACE/GRACE-FO) and the sum of individual mass contributions, we assess the closure of the budget through three complementary formulations.

4.2.1.1. Input data

We use the following notations for input components see ATBD ([\[AD3\]](#)) for detailed descriptions:

Table 6 *Table describing the input data used in the sea level and ocean mass budget equations*

Notation	Name of the variable
ΔSL_{abs}	Absolute sea level changes
ΔSL_{rel}	Relative sea level changes
ΔVLM	Vertical land motions contribution to sea level including GIA and current days ice melting
ΔSL_{thermo}	Thermosteric sea level
ΔSL_{halo}	Halosteric sea level
$\Delta SL_{steric} = \Delta SL_{thermo} + \Delta SL_{halo}$	Steric sea level
ΔSL_{manGIA}	Manometric sea level change from gravimetric data excluding the effect of GIA
$\Delta GM SL_{abs}$	Global mean absolute sea level
$\Delta GM SL_{rel}$	Global mean relative sea level
$\Delta GM SL_{thermo}$	Global mean thermosteric sea level

$(\Delta GMSL_{bary})_{sat}$	Barystatic sea level
$\Delta GMVLM = GMN_{GIA} + \Delta GMVLM_{current}$	Global mean vertical land motions
$(\Delta GMSL_{bary})_{GIS}$	Greenland ice-sheet contribution to sea level
$(\Delta GMSL_{bary})_{GIS}$	Antarctica ice-sheet contribution to sea level
$(\Delta GMSL_{bary})_{GIC}$	Land glaciers and ice-cap contribution to sea level
$(\Delta GMSL_{bary})_{LWS}$	Land water storage contribution to sea level
$(\Delta GMSL_{bary})_{WV}$	Atmosphere water vapour contribution to sea level

4.2.1.2. Ocean mass budget and sea level budget

The global mean sea level budget residuals R are computed from the global mean components as follows:

$$R = (\Delta GMSL_{rel})_{alti} - (\Delta GMSL_{bary})_{gravi} - (\Delta GMSL_{thermo})_{in situ}. \quad \text{Equation 1}$$

In global mean, the halosteric sea level is negligible (Gregory and Lowe, 2000; Llovel et al., 2019). Considering only the thermosteric component avoids including halosteric data with spurious drifts (Barnoud et al., 2021). The global mean ocean mass budget residuals S are computed from the barystatic component from GRACE and the individual mass contributions to sea level change as:

$$S = (\Delta GMSL_{bary})_{gravi} - (\Delta GMSL_{bary})_{GIS} - (\Delta GMSL_{bary})_{AIS} \\ - (\Delta GMSL_{bary})_{GIC} - (\Delta GMSL_{bary})_{LWS} - (\Delta GMSL_{bary})_{WV} \quad \text{Equation 2}$$

The global mean sea level budget residuals T can also be computed by replacing the GRACE estimate of the barystatic component by the sum of the individual contributions to ocean mass change as follows:

$$T = \Delta GMSL_{rel} - \Delta GMSL_{thermo} - (\Delta GMSL_{bary})_{GIS} - (\Delta GMSL_{bary})_{AIS} - (\Delta GMSL_{bary})_{GIC} - (\Delta GMSL_{bary})_{LWS} - (\Delta GMSL_{bary})_{WV} \quad \text{Equation 3}$$

Note that these three budget equations (Equation 1, Equation 2 and Equation 3) are not independent as any of these equations is the sum or the difference of the other two equations. Only two of these equations are sufficient to fully describe the sea level and ocean mass budgets.

This section presents the results of the barystatic sea level estimated using the two different methods described above. We compare the time series derived from the sum of individual mass components with those derived from GRACE/GRACE-FO data, and also examine how both compare to the results obtained during Phase 1 of the SLBC_cci project.

In all figures, the mean value over the period 2005–2015 is subtracted to align the different time series for comparison. Additionally, constant offsets are applied for visualization purposes, allowing the various components to be more clearly distinguished within the plots.

Figure 26 shows the global mean barystatic sea level time series derived from the SLBC CCI+ project datasets. Two estimates are compared: the barystatic component computed as the sum of individual mass contributions (shown as a blue dashed line), and the barystatic component directly estimated from GRACE/GRACE-FO satellite gravimetry (solid blue line).

A good agreement is observed between the two estimates over most of their common period, particularly between 2004 and 2015. However, the difference between the two time series (Figure 26b) reveals a noticeable trend from 2016 to 2024. This divergence coincides with a period where the sea level budget does not fully close, suggesting potential inconsistencies in the mass components or gravimetric measurements during this time.

The following Figure 27 presents the global mean sea level budget components using the ISAS20 thermosteric datasets. This analysis covers the satellite altimetry period starting in 2002, during which ISAS20 data are available. The comparison of observed sea level with the sum of individual components allows us to assess the consistency of the sea level budget closure based on project datasets.

Over the 2002–2020 period, the budget residuals (Figure 27b) exhibit a clear trend, both when using the barystatic component derived from GRACE/GRACE-FO and when using the barystatic component obtained from the sum of individual mass contributions. However, the trend in the residuals estimated with GRACE/GRACE-FO is slightly smaller, suggesting that the sea level budget closes better when the GRACE-based barystatic component is used.

The analysis shows a generally good agreement between the GRACE-based barystatic estimates and the sum of individual mass contributions, especially over the 2004–2015 period. However, the budget residuals consistently exhibit low-frequency variations, which remain an open question. These trends may reflect inconsistencies or errors in one or more of the input components, but

alternative explanations are also possible. Ongoing research within this project explores these signals further, including through the application of an innovative sea level budget closure approach developed as part of the SLBC_cci+ effort. This method may offer new insights into the origin of these residual trends and improve the robustness of future sea level budget assessments.

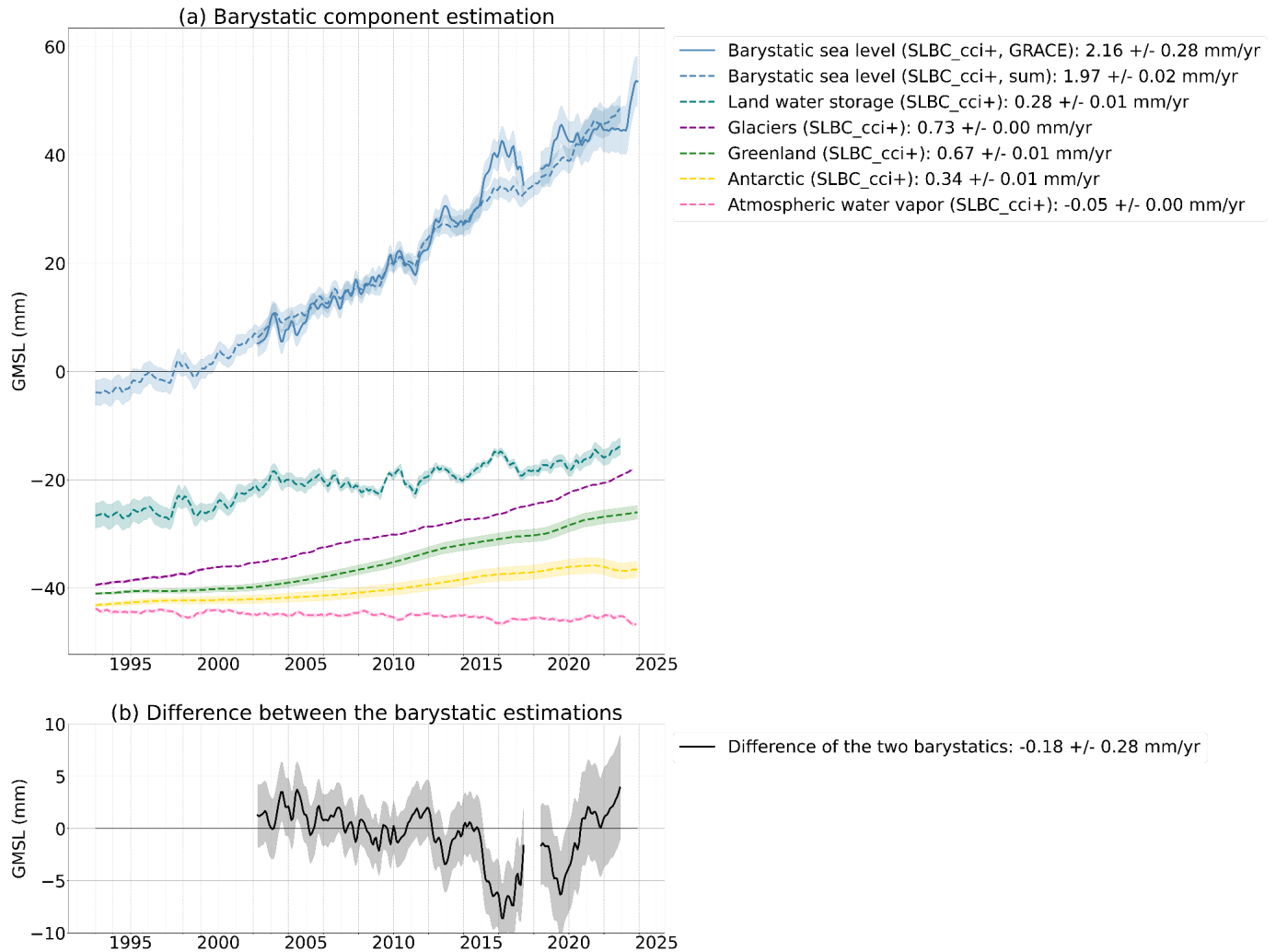


Figure 26 (a) Global mean barystatic sea level time series for SLBC CCI+. Blue lines show the total barystatic component: solid for barystatic from GRACE/GRACE-FO data, and dashed for barystatic from the sum of individual mass components. Teal lines show land water storage, purple lines show glacier melt, green lines Greenland Ice Sheet mass loss, and yellow lines Antarctic Ice Sheet mass loss. (b) Difference between barystatic sea level estimates from GRACE/GRACE-FO and sum of individual mass components. Trends estimated over the period 06/2002 - 12/2022.

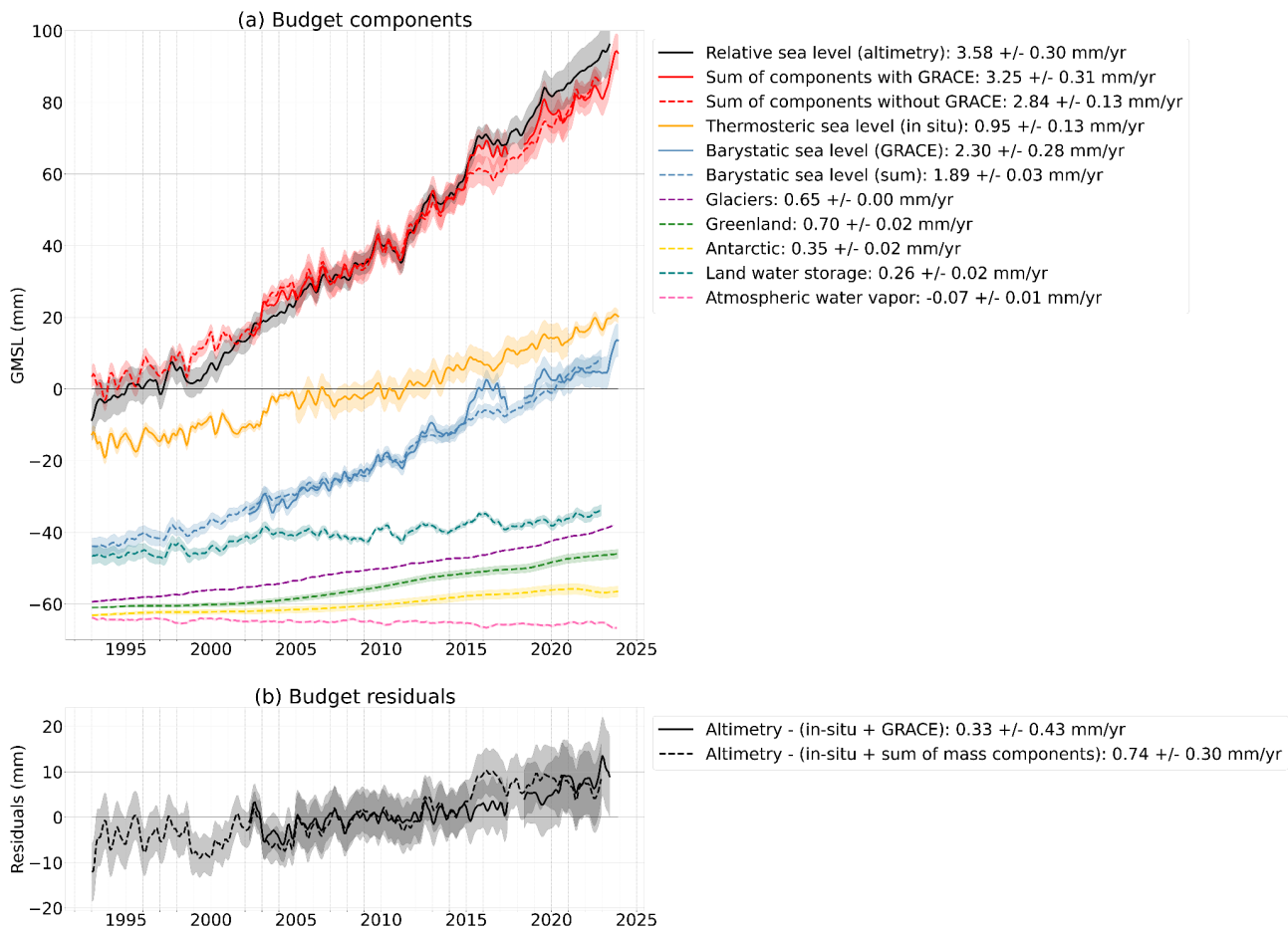


Figure 27 *Sea level budget comparison using two different barystatic components. (a) Global mean sea level budget components using SLBC CCI+ data. The black curves represent altimetry-based sea level; the blue curves show the manometric (barystatic) component from GRACE; the orange curve shows the thermosteric contribution, respectively; and the red curves show the sum of all components. Solid lines indicate values based on GRACE-derived barystatic sea level; dashed lines indicate values based on the sum of individual mass contributions. (b) Residuals of the sea level budget, computed as the difference between the observed sea level (altimetry) and the sum of all components. Trends estimated over the period 06/2002 - 06/2016.*

4.2.2. Comparison with other datasets

4.2.2.1. Comparison with Phase 1 SLBC CCI products

This section provides a comparison between the Phase 1 (SLBC_cci) and Phase 2 (SLBC_cci+) products of the SLBC project. Both GRACE-based and non-GRACE-based estimates are analyzed to understand the sources of discrepancies and their impact on budget closure.

Figure 28 presents a comparison between the barystatic sea level derived from the sum of individual mass components used in Phase 1 of the project (referred to as SLBC_cci, shown with dashed lines) and those from the current Phase 2 (referred to as SLBC_cci+, shown with solid

lines). We observe notable differences between the two barystatic time series, particularly prior to 2005, a period during which GRACE/GRACE-FO data are not available.

From 1992 to 2008, the difference between the two barystatic time series (Figure 28b) exhibits a trend of approximately 0.5 mm/yr. This difference increases to around 0.7 mm/yr over the 2008–2017 period, indicating a persistent mismatch between the two estimates throughout the record.

When examining the individual mass components contributing to the barystatic signal (solid lines for SLBC_cci+, dashed lines for SLBC_cci), significant discrepancies are also evident. In particular, large differences are observed between the SLBC_cci and SLBC_cci+ estimates of the land water storage (LWS) component before the GRACE era. This discrepancy was discussed previously in Section 3.4.1.

Notable differences also appear in the glacier (ice cap) and Greenland ice sheet (GIS) components. However, the largest divergence is observed in the LWS contribution. Given that the largest differences between the LWS components occur prior to the GRACE era, it is particularly challenging to determine which LWS time series is more reliable. In the absence of independent observations for this period, such as satellite gravimetry, we lack a direct reference to validate either of the two datasets.

During the 2008–2017 interval, the most pronounced difference appears to stem from the GIS component. The SLBC_cci estimate for GIS shows a steeper trend over this period compared to the SLBC_cci+ estimate.

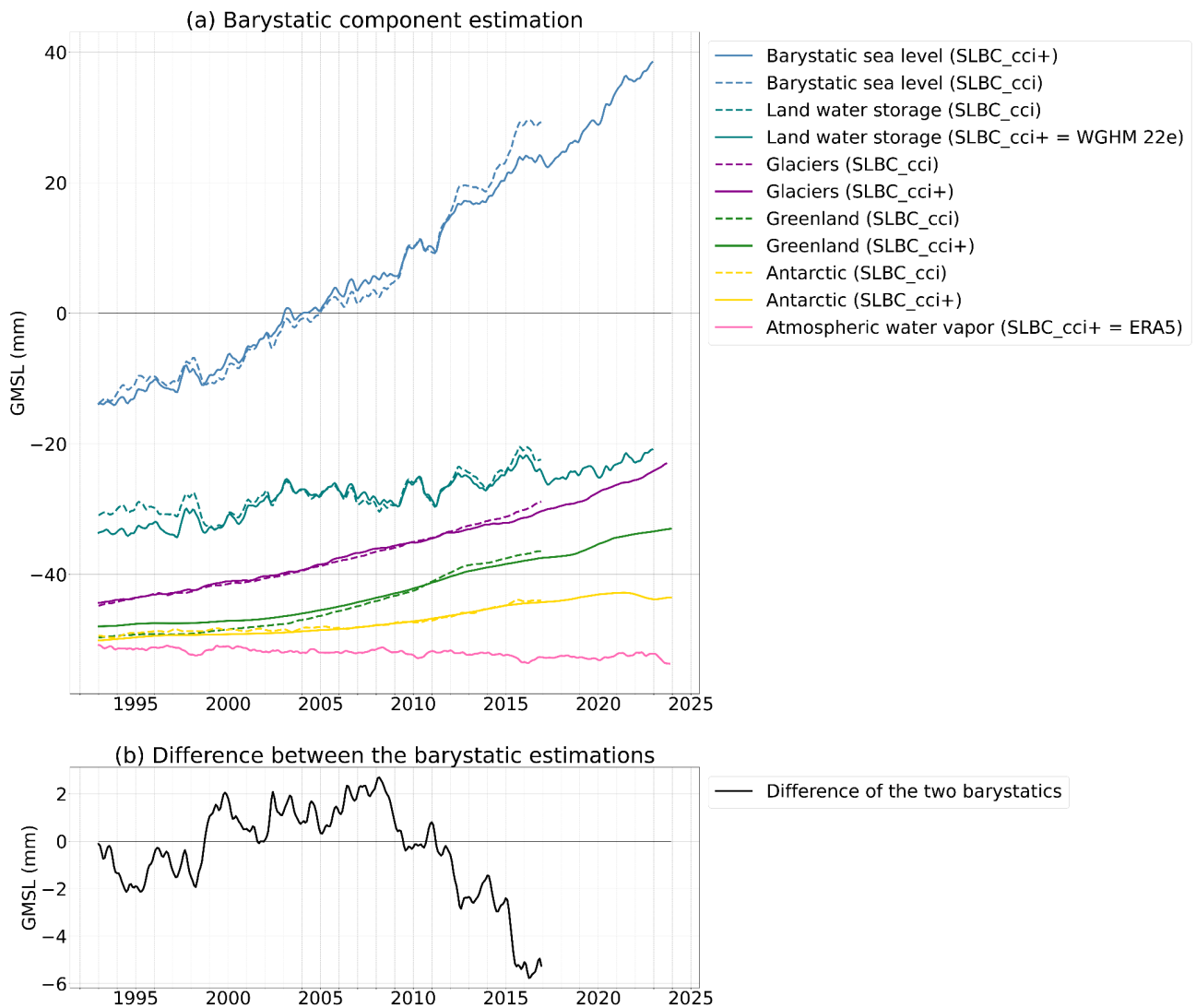


Figure 28 (a) *Global mean barystatic sea level time series. Blue lines show the total barystatic component: solid for SLBC CCI+, and dashed for SLBC CCI Phase 1. Teal lines show land water storage, purple lines show glacier melt, green lines Greenland Ice Sheet mass loss, and yellow lines Antarctic Ice Sheet mass loss — with solid lines for SLBC CCI+ and dashed lines for SLBC CCI Phase 1. (b) Difference between barystatic sea level estimates from SLBC CCI+ and SLBC CCI Phase 1.*

Figure 29 presents a comparison of the global mean sea level budget components and residuals between the two phases of the SLBC project: SLBC CCI (Phase 1, dashed lines) and SLBC CCI+ (Phase 2, solid lines). All components are computed using the barystatic contribution derived from the sum of individual mass components, excluding GRACE-based estimates. This allows us to assess the consistency of the sea level budget closure between both phases over their common period, and to identify differences in the individual components or residuals.

The altimetry-based sea level curves from both phases are consistent over the overlapping period, with small differences explained by improved corrections applied in Phase 2 (e.g., GIA and PDIM corrections described earlier). Differences between the barystatic estimates (obtained from the sum of individual mass components) of Phase 1 and Phase 2 impact the total sum of components (red curves), and the updated thermosteric contribution in Phase 2 adds to this discrepancy.

A better agreement is observed between the sea level and the sum of components in Phase 1 (dashed black and red curves), compared to Phase 2 (solid black and red curves), which is also reflected in the residual time series (Figure 29b). In particular, during the 2002–2010 period, the residuals from SLBC CCI+ (Phase 2) exhibit a trend of nearly 1 mm/yr, whereas the residuals from Phase 1 do not show significant low-frequency variations over the same period.

Over that interval, the barystatic components from both phases agree reasonably well, suggesting that the discrepancy between the altimetry-based sea level and the sum of components in Phase 2 likely originates from the thermosteric contribution. These results are still under investigation and may be better understood through more detailed analyses of the individual components and through the innovative budget closure methodology developed as part of this project.

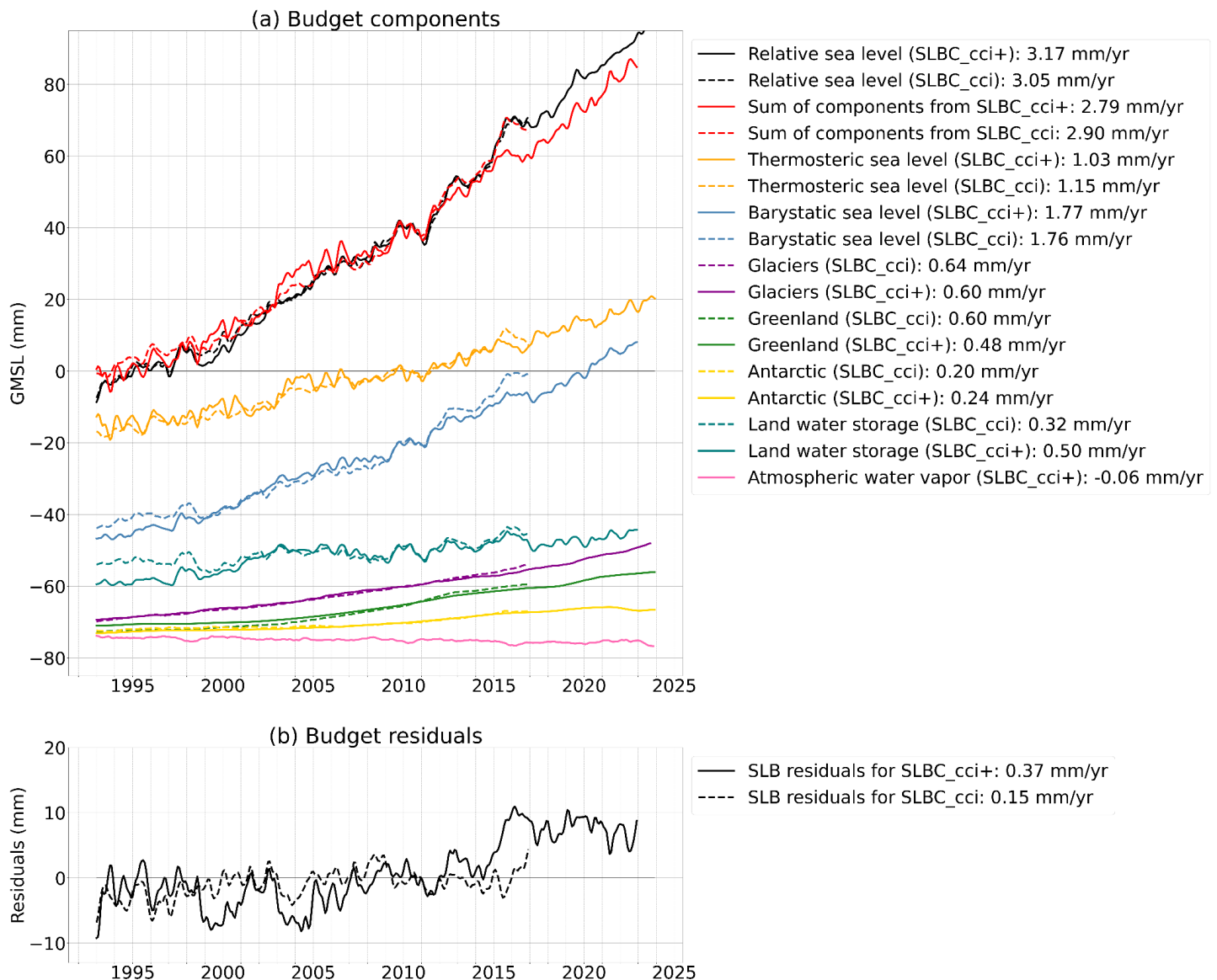


Figure 29 *Sea level budget comparison (SLBC CCI vs. SLBC CCI+).* (a) *Global mean sea level budget components estimated using the sum of individual mass contributions. Black curves show the observed sea level from altimetry; orange curves represent the thermosteric component; blue curves show the barystatic component (from the sum of mass contributions); and red curves indicate the total sea level from the sum of all components. Solid lines correspond to SLBC CCI+ (Phase 2), while dashed lines represent SLBC CCI (Phase 1).* (b) *Residuals of the sea level budget, computed as the difference between the observed sea level (altimetry) and the sum of all components, for both SLBC CCI+ (solid line) and SLBC CCI Phase 1 (dashed line). Trends estimated over the period 01/1993 - 12/2016.*

Using the GRACE-based barystatic components from SLBC_cci and SLBC_cci+, we observe a clear trend in the budget residuals shown in Figure 30b. In Phase 1, the residuals exhibit a negative trend, whereas in Phase 2, the trend is positive.

Looking at the individual budget components in Figure 30a, we see a generally good agreement between the altimetry-based sea level and GRACE-derived barystatic time series across both project phases. A slight trend difference between the two GRACE-based barystatic estimates is visible, consistent with what was previously discussed.

The most notable differences, however, arise in the thermosteric component. The thermosteric time series from Phase 2 (based on ISAS20) exhibits a slightly lower trend compared to that from Phase 1 over their common period. This discrepancy affects the total sum of components (red curve), which shows a weaker trend than the altimetry-based sea level estimate in Phase 2, thereby contributing to the larger residual trend.

Overall, the intercomparison between SLBC_cci (Phase 1) and SLBC_cci+ (Phase 2) highlights meaningful differences in both barystatic and thermosteric components, which translate into distinct behaviors in sea level budget residuals. While the barystatic estimates from both phases show reasonable agreement during the GRACE era, the thermosteric component remains a key driver of the observed discrepancies—particularly in Phase 2, where a weaker thermosteric trend results in a larger positive residual trend. Further investigation, including the application of innovative sea level budget closure method developed in this project, may help to better constrain these residual trends and improve our understanding of the underlying causes.

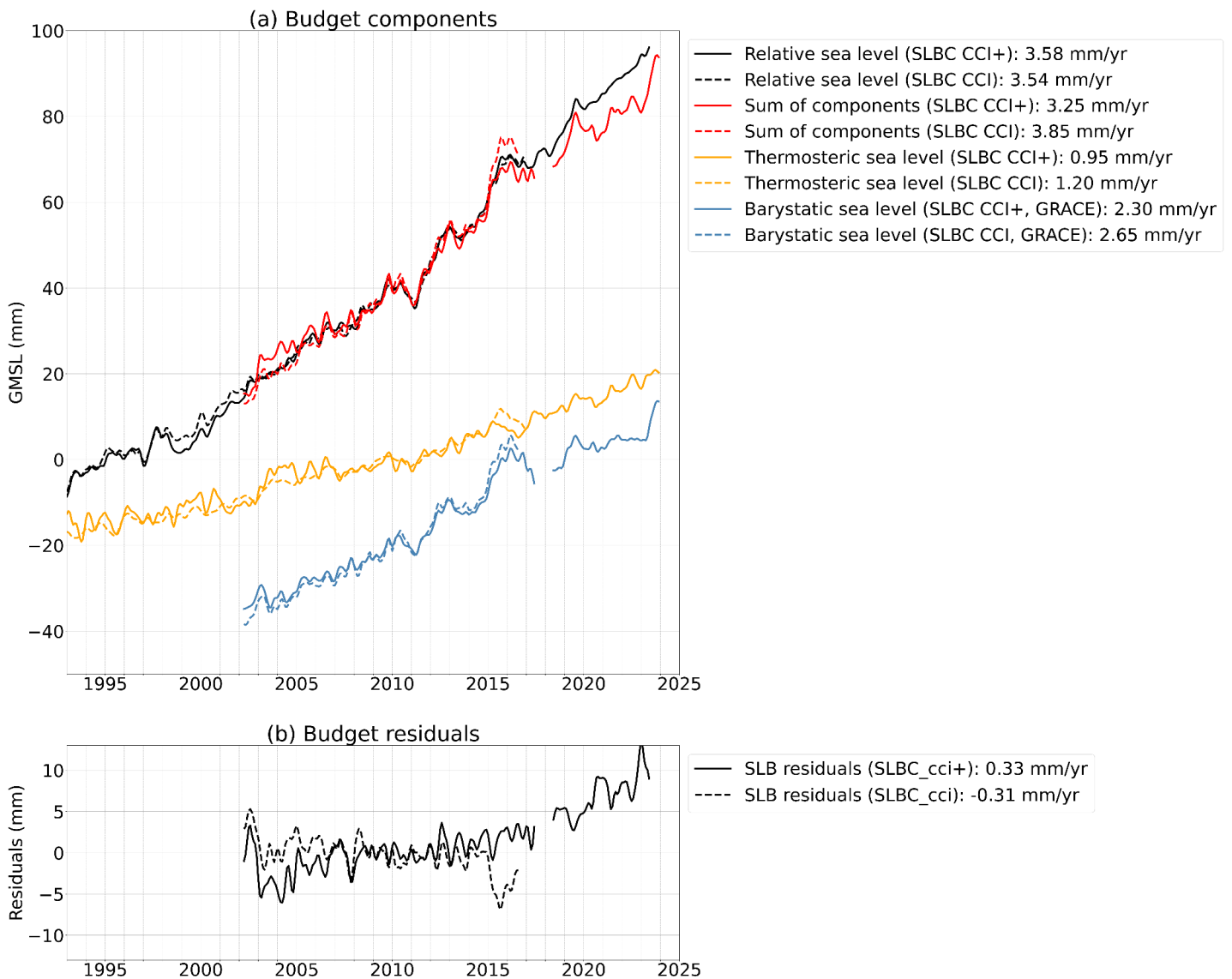


Figure 30 (a) Global mean sea level budget components using the GRACE-derived barystatic estimate, for SLBC CCI (Phase 1, dashed lines) and SLBC CCI+ (Phase 2, solid lines). The black curves represent altimetry-based sea level; the blue curves show the barystatic component from GRACE; the orange curves show the thermosteric contribution; and the red curves show the sum of all components. (b) Residuals of the sea level budget, computed as the difference between the observed sea level (altimetry) and the sum of thermosteric and GRACE-based barystatic components. Trends are estimated over 06/2002-06/2016 period.

4.2.2.2. Complementary work using other datasets

The task concerning the global mean sea level (GMSL) budget in this project is an extension of earlier work performed in the ESA CCI Sea Level Budget Closure (SLBC) over the 1993-2016 time

span (Horwath et al., 2021). In the ESA CCI SLBC project, datasets used for the components were those estimated within the ESA CCI. The conclusion was that over that 1993-2016, the sea level budget was considered as closed within error bars.

Here, the objective is to extend in time (beyond 2016) the GMSL budget closure assessment using the conventional method (called here 'historical' method), i.e., comparing the altimetry-based GMSL with the sum of components. The work done so far focuses on the ARGO & GRACE time span and concerns the time span 2005-present. It is found that beyond 2016 the budget is no more closed (Barnoud et al., 2021; Chen et al., 2020). In that study, it is shown that errors in Argo salinity measurements are responsible for about 40% of the budget error while the altimetry data cannot explain the remaining error. The remaining budget non closure is attributed partly for the radiometer drift onboard the Jason-3 mission and partly for instrumental errors (failure of one onboard accelerometer) that have affected the GRACE mission at the end of its lifetime and the GRACE-Follow On mission. The figure below shows the GMSL budget over 2005-2022 accounting for the halosteric component (right panel) and deleting the halosteric component (to avoid the salinity measurements errors that have affected some Argo floats in the recent years and considering that at a global scale the halosteric component is negligible) (right panel) (Barnoud et al., 2023).

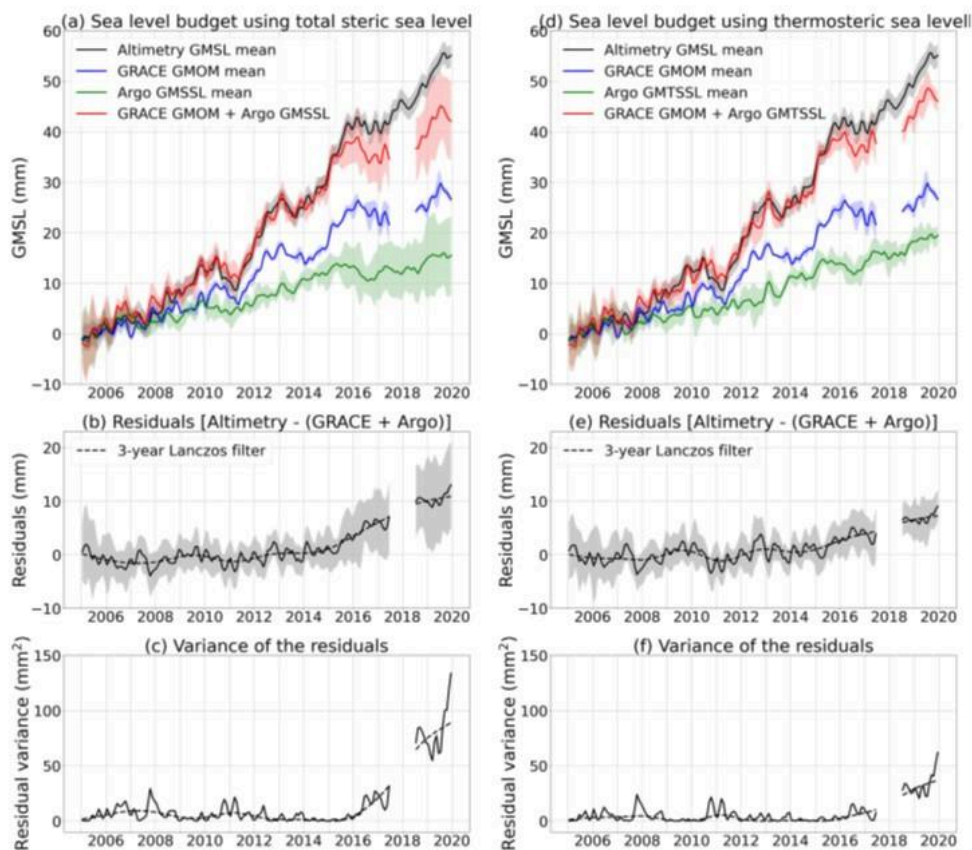


Figure 31 *Sea level budget over the January 2005–December 2019 period. The shaded areas correspond to the estimated 1-sigma uncertainties. (a) Budget with altimetry, Gravity Recovery and Climate Experiment and steric Argo contributions. (b) Residuals of the budget. (c) Variance of the residuals. The right three panels (d, e and f) are similar to the left, but with only Argo thermosteric effect considered. From Barnoud et al., 2021.*

In a second step, the GMSL budget has been reassessed without the halosteric component but accounting for the Jason-3 radiometer drift; This is shown below. The residuals between the altimetry-based GMSL and sum of components has been reduced when accounting for the Jason-3 radiometer drift, but non closure beyond 2016 is still observed. We cannot exclude that there is a remaining error contribution from GRACE data.

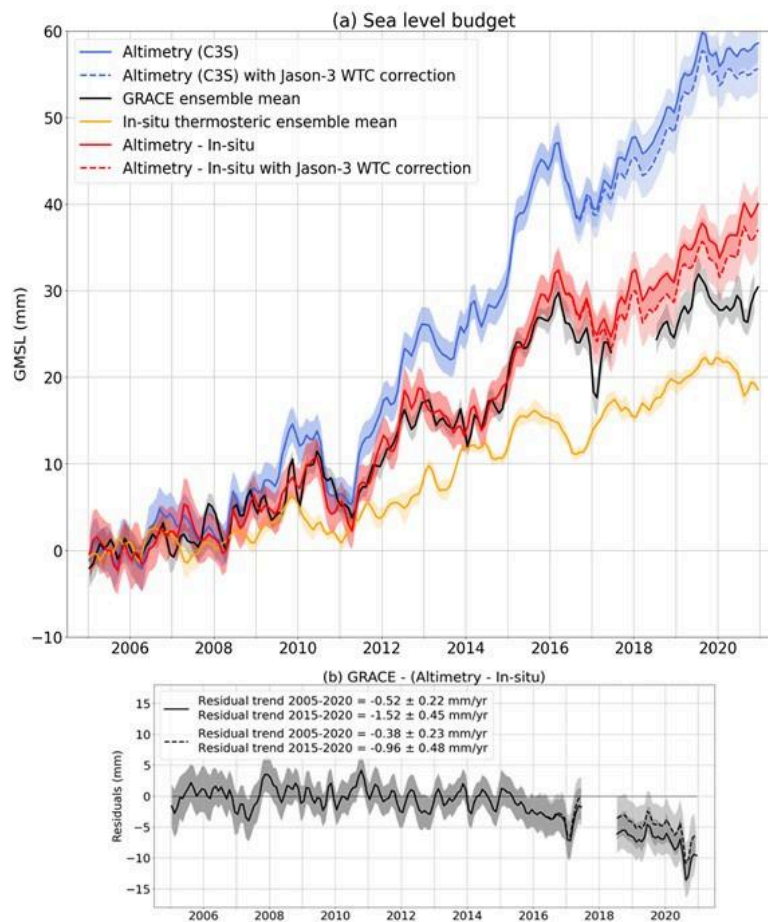


Figure 32 *Upper panel: Altimetry-based GMSL with and without the Jason-3 radiometer correction (dashed and solid blue curves); Altimetry-based base GMSL minus steric component with and without the Jason-3 radiometer drift (dashed and solid red curves). Lower panel; residuals. From Barnoud et al., 2023.*

Improvements & planned work

From the work already performed, two significant improvements have been brought to the GMSL budget assessment that have led to the reduction of the GMSL budget non closure:

- Identification of errors from salinity data
- Account of the Jason-3 radiometer drift

However, beyond 2016, the GMSL budget is still not closed. To go further with the 'historical' approach of the GMSL budget closure, three lines of improvements are proposed:

- (1) Use of the newly reprocessed altimetry-based GMSL (GDRF L2P-DT2024 data). Investigation shows that significant differences exist at interannual time scale between the current C3S and the new reprocessed data (Cazenave & Leclercq, unpublished).
- (2) Investigate further the mass budget closure comparing GRACE/GRACE FO ocean mass (manometric component) with updated mass contributions (newly published global glacier dataset by Dusaillant et al., ESSD, 2025; updated estimates of ice sheet mass loss from the literature; updated estimates of the land water storage contribution -e.g., updated WGHM model) to validate the GRACE/GRACE FO data beyond 2016
- (3) Use of reanalyses data (i.e., the steric sea level corrected for steric effects) as an alternative for the GRACE-based manometric component (see section 4.2 for details)
- (4) Investigate the use of satellite laser ranging data (SLR) to replace GRACE/GRACE FO data for the manometric component, as recently proposed by Chen et al. (in review).

4.3. At regional scale

4.3.1. Validation of the SLB product

This section presents the regional budget derived from the components of the SLBC CCI+ project. It includes the altimetry-based sea level described in Section 3.1, corrected for GIA and PDIM using the models outlined in Section 3.5; the manometric component described in Section 3.3, also corrected for GIA as detailed in Section 3.5; and the thermosteric and halosteric components described in Section 3.2.

Only the GRACE-based manometric component is presented here, as it is the only mass-related component available at the regional scale. The barystatic component, derived from the sum of individual mass contributions, is only estimated at the global scale, and is therefore not included in the regional analysis.

Here, we present trend maps for each of these components as well as the residuals of the budget, covering the common period between all data sets, from April 2002 to December 2019. In the next version of this document, the budget will be updated to cover the 2003–2023 period, once all components are available for that full timeframe.

The accompanying figures show both trend maps and trend anomaly maps (i.e., trend maps from which the mean value has been subtracted to highlight spatial patterns of trend variability).

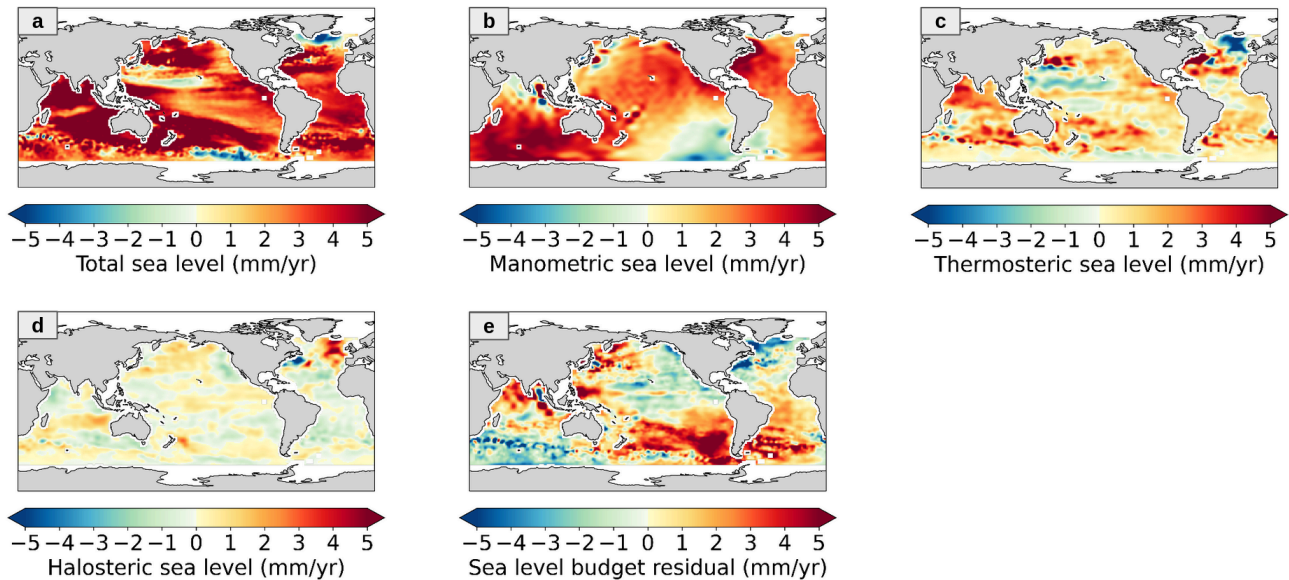


Figure 33 *Sea level trends over April 2002 to December 2019 in observed altimetry-based sea level (a), components (b, c, d: GRACE-based manometric, Argo-based thermosteric and Argo-based halosteric sea level) and budget residual trends (observed sea level minus sum of components) (e).*

Figure 33 shows the regional trends of individual sea level budget components as well as the residual trends, computed as the difference between the observed sea level and the sum of the individual components.

Figure 34 displays the corresponding trend anomalies, obtained by subtracting the global mean from each trend map. This approach highlights the finer spatial structures and regional patterns of variability that may be obscured by dominant global trends.

The trend maps in Figure 33 reveal that, globally, the manometric component exhibits the largest amplitude of sea level trend variations among all components. This is followed by the thermosteric component, while the halosteric component displays the weakest signal. The map of budget residual trends (panel e) shows local amplitudes that are comparable in magnitude to those of the individual components.

A particularly striking feature is the strong spatial similarity between the manometric component (panel b) and the budget residuals (panel e). In many regions, these two appear to be negatively correlated. For instance, the positive residual trend observed off the eastern coast of South America corresponds to a negative trend in the manometric component in the same region, suggesting a compensatory relationship.

To better understand these relationships, Figure 34 presents trend anomalies, allowing for the examination of spatial patterns independent of the global mean trend. Comparing panels b and e, a

broad-scale anticorrelation between the manometric component and the residuals becomes evident across multiple ocean basins, including the Indian, Pacific, and Atlantic Oceans. This pattern supports the idea that the manometric signal strongly influences the residual structure.

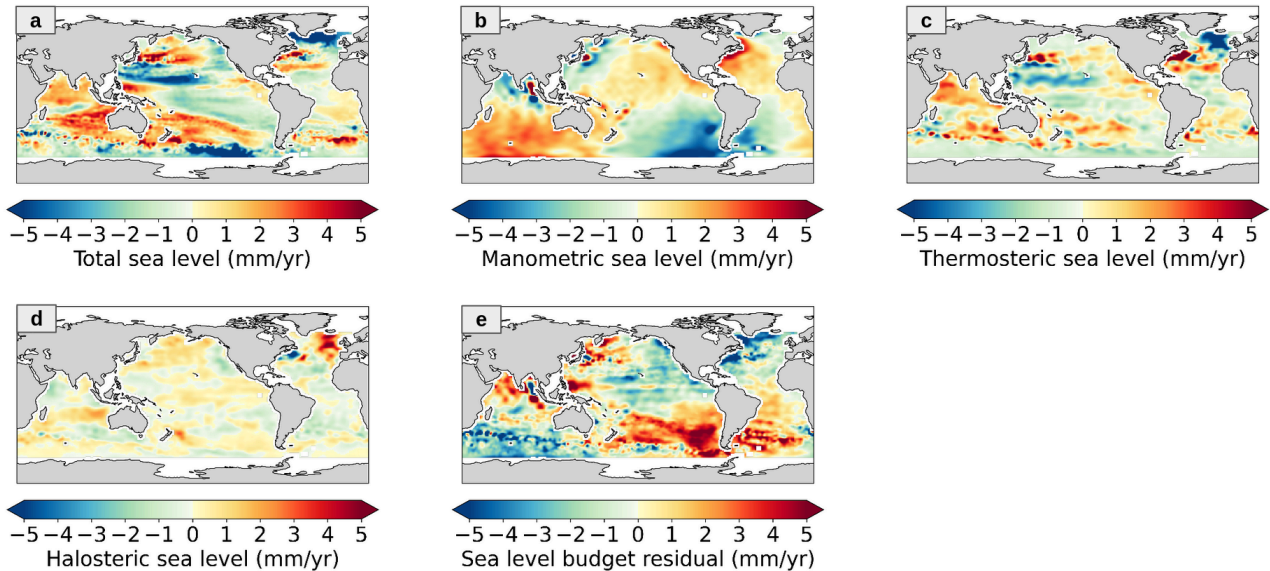


Figure 34 *Sea level trends anomalies over April 2002 to December 2019 in observed altimetry-based sea level (a), components (b, c, d: GRACE-based manometric, Argo-based thermosteric and Argo-based halosteric sea level) and budget residual trends (observed sea level minus sum of components) (e).*

Moreover, a clear positive correlation is observed between the thermosteric component (panel c) and the observed sea level trends (panel a), indicating that temperature-driven expansion plays a major role in shaping regional sea level changes. Conversely, the thermosteric and halosteric components appear to be negatively correlated, reflecting opposing effects of temperature and salinity on ocean density.

Overall, the manometric component shows the strongest spatial coherence with the residual trends, suggesting it may be the primary driver of the unexplained signals in the regional sea level budget. Notably, the anticorrelation between the residuals and the manometric component occurs over very large spatial scales, spanning entire ocean basins. This spatial coherence at basin-wide scales underscores the significance of mass redistribution processes in shaping the residual budget.

These large-scale patterns and their implications will be further explored in the following sections.

Sensitivity to GIA and PDIM Corrections

As a complementary remark, we highlight the sensitivity of the regional budget to the choice of GIA and PDIM corrections. In particular, the previous analysis relied on the GIA correction from Spada et Melini that we have chosen in the scope of the SLBC CCI+, while Figures 37 and 38 present the

same budget components and residuals, but using the ICE-5G GIA model (Peltier, 2004) and PDIM correction from Frederikse et al., 2017.

This modification significantly alters the spatial patterns of the trends and residuals, underlining the critical role of the correction models applied. It is worth noting that the study by Bouih et al. (2025) used the ICE-5G model, making this comparison directly relevant for understanding differences in residual structure and interpretation.

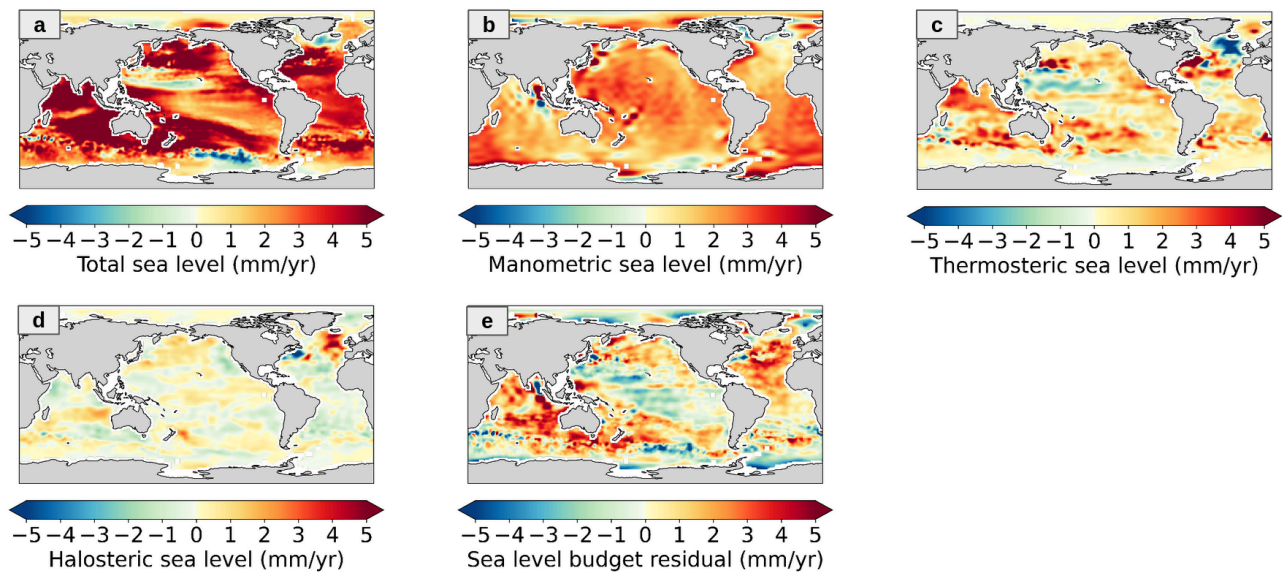


Figure 35 *Sea level trends over April 2002 to December 2019 in observed altimetry-based sea level corrected using ICE-5 GIA model (Peltier, 2004) and PDIM correction from Frederikse et al., 2017 (a), components (b, c, d: GRACE-based manometric corrected using ICE-6 GIA model (Peltier et al., 2015), Argo-based thermosteric and Argo-based halosteric sea level) and budget residual trends (observed sea level minus sum of components) (e).*

Figure 35 shows the sea level trends over the April 2002 to December 2019 period, with the ICE-5G and alternative PDIM corrections applied to the altimetry-based sea level (panel a) and the manometric component (panel b). Panels c and d represent the thermosteric and halosteric components, and panel e shows the resulting budget residuals.

Figure 36 displays the corresponding trend anomalies, highlighting the spatial differences induced by the alternative correction scheme.

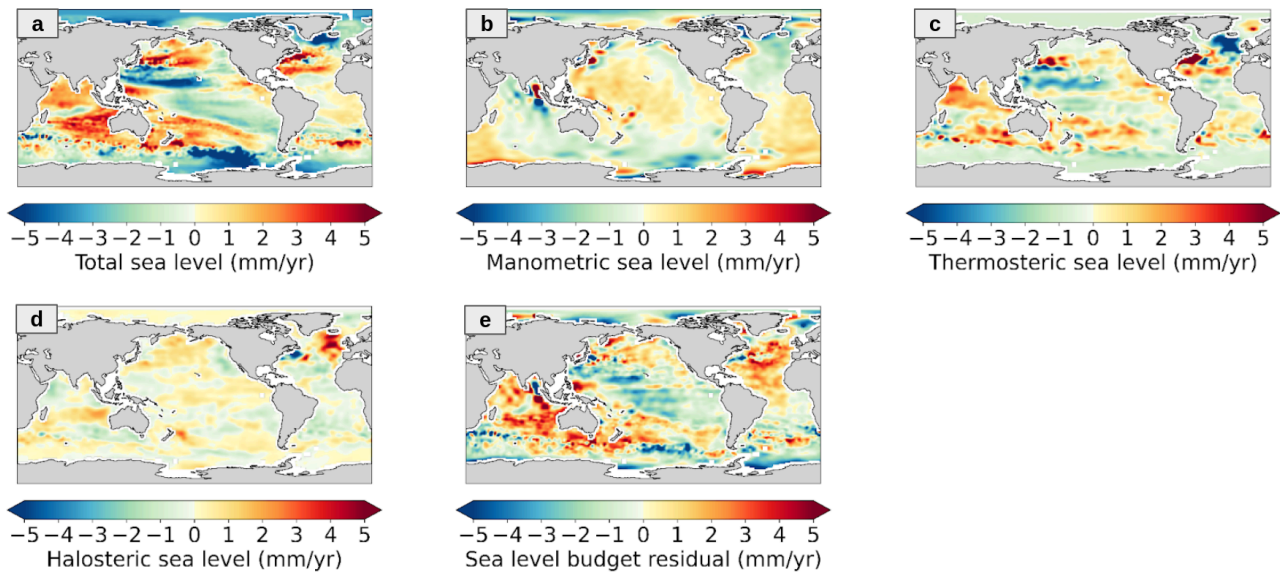


Figure 36 *Sea level trends anomalies over April 2002 to December 2019 in observed altimetry-based sea level corrected using ICE-5 GIA model (Peltier, 2004) and PDIM correction from Frederikse et al., 2017 (a), components (b, c, d: GRACE-based manometric corrected using ICE-6 GIA model (Peltier et al., 2015), Argo-based thermosteric and Argo-based halosteric sea level) and budget residual trends (observed sea level minus sum of components) (e).*

A comparison between the anomaly maps in Figure 34 and Figure 36, particularly panels b (manometric component), reveals markedly different large-scale spatial patterns depending on the GIA and PDIM corrections applied. While both exhibit large-scale structures, the patterns show opposite signs in several regions, most notably in the Indian Ocean and the North Atlantic. These differences have been previously discussed in Section 3.3, where the sensitivity of the GRACE-based manometric component to the choice of GIA correction model was analyzed in detail.

Regarding the altimetry-based sea level component (panels a), the differences between the two correction approaches are generally more moderate. However, one significant change can be observed in the North Atlantic, where the use of the ICE-5G and Frederikse et al. (2017) corrections leads to a more pronounced positive trend compared to the results obtained with the SLBC CCI+ GIA correction.

These changes also propagate into the residual trends (panels e), where we observe substantially different spatial patterns between Figure 34 and Figure 36. This further emphasizes the importance of correction models in shaping not only individual component trends, but also the structure and interpretation of the budget residuals.

4.3.2. Comparison with other datasets

While the novel approach proposed in this project based on the innovative approach (section 5) should be a breakthrough in sea level budget studies, it is also important to develop in parallel regional sea level budget assessment using conventional methods (called here the ‘historical’

approach). As shown below, the historical approach is still able to bring novel information. It will also represent a basis of comparison for the innovative approach.

Work has been done in this direction with contributions from several partners of the project (Magellium, LEGOS, CNR, IFREMER). It is summarized below.

Using gridded satellite altimetry data for the observed sea level changes, Argo data to estimate the thermosteric and halosteric sea level changes, and space gravimetry data from the GRACE and GRACE FO missions for the manometric component, the regional sea level budget has been assessed over the period from January 2004 to December 2022.

For sea level, gridded data from the Copernicus Climate Change Service have been considered. For the steric component, only data from SCRIPPS Institution of Oceanography have been used. The choice for this product is motivated by the fact that its post-processing corrects for the salinity drift reported in Argo floats since 2015, which misleads to a spurious increase reported in the global mean salinity (Liu et al., 2020; Ponte et al., 2021; Wong et al., 2023). For the mass component the ensemble mean of three mascon solutions (from JPL, CSR and GFZ) has been used. For the GIA and GRD fingerprints (regional sea level change due to ongoing land ice melt), models have been used (two GIA models and an update of Adhikari morel for the GRDs).

Comparing observed (altimetry-based sea level) with the sum of components lead to strong residuals in the north Atlantic region (Figure 37). A number of tests have been performed by changing the GRACE data (use of the ensemble mean -spherical harmonics- solution from Blazquez et al.) use of different geocenter models and GIA corrections applied to GRACE data, etc. led to similar results.

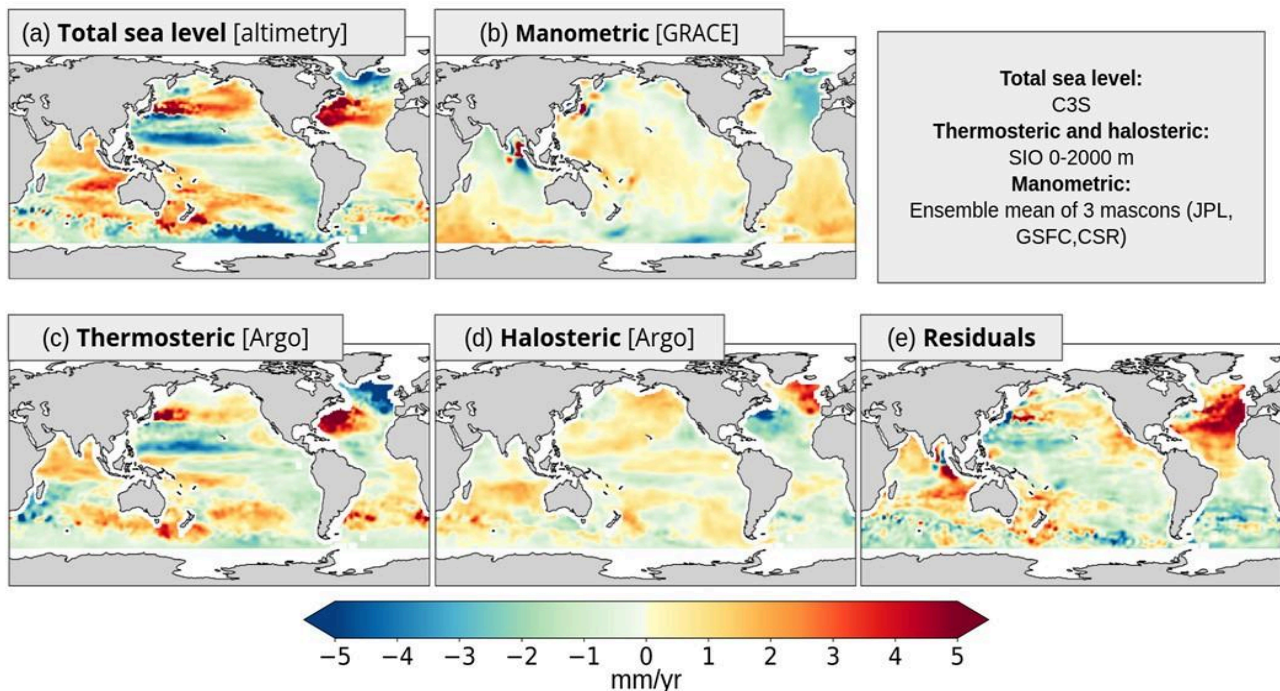


Figure 37 *Sea level trends anomalies over January 2004 to December 2022 in observed altimetry-based sea level (a), components (b, c, d: GRACE-based manometric, Argo-based thermosteric and Argo-based halosteric sea level) and budget residual trends (observed sea level minus sum of components) (e). From Bouih et al., 2025.*

An alternative approach has been developed for comparison (validation). It has consisted in using ocean reanalyses to estimate the ocean mass component (the so called manometric component). In effect, ocean models provide the stericodynamic sea level change, i.e., the sea level change due to changes in ocean density and circulation, with the inverse barometer correction applied (Camargo et al., 2023; Gregory et al., 2019; Storto and Yang, 2024). The corresponding manometric component is derived by correcting the reanalysis-based stericodynamic sea level by the local steric effect and adding the contemporary GRD fingerprints. Six different ocean reanalyses have been considered GLORYS, C-GLORS, ORAS5, FOAM, SODA and CIGAR. This variety of reanalyses offers the opportunity to evaluate the degree of consistency of the manometric signal from reanalysis-based products. The regional residuals of the budget are shown in Figure 38 for each of the six reanalyses and their mean. For comparisons the residuals with the two GRACE products are also shown.

This comparison indicates that using totally different approaches for the manometric component (GRACE versus ocean reanalyses) leads to qualitatively similar results, i.e., non closure of the regional sea level budget in the north Atlantic. However, the residuals have smaller amplitude in the case of the reanalyses. Both approaches point to a problem with the steric data used in the budget analysis, in particular with the halosteric component.

An article has been submitted to Ocean Sciences in December 2024 (Bouih et al., 2025).

A number of lessons can be learned from this 'historical' approach. In particular:

- (1) Assessment of the sea level budget at regional scale is more demanding and more informative than at global scale
- (2) It avoids compensation of spurious positive/negative sub-basin anomalies
- (3) Regional budget closure assessment allows identifying regions where the budget is not closed, offering leads for identifying the suspects (e.g., here -possibly- salinity data)

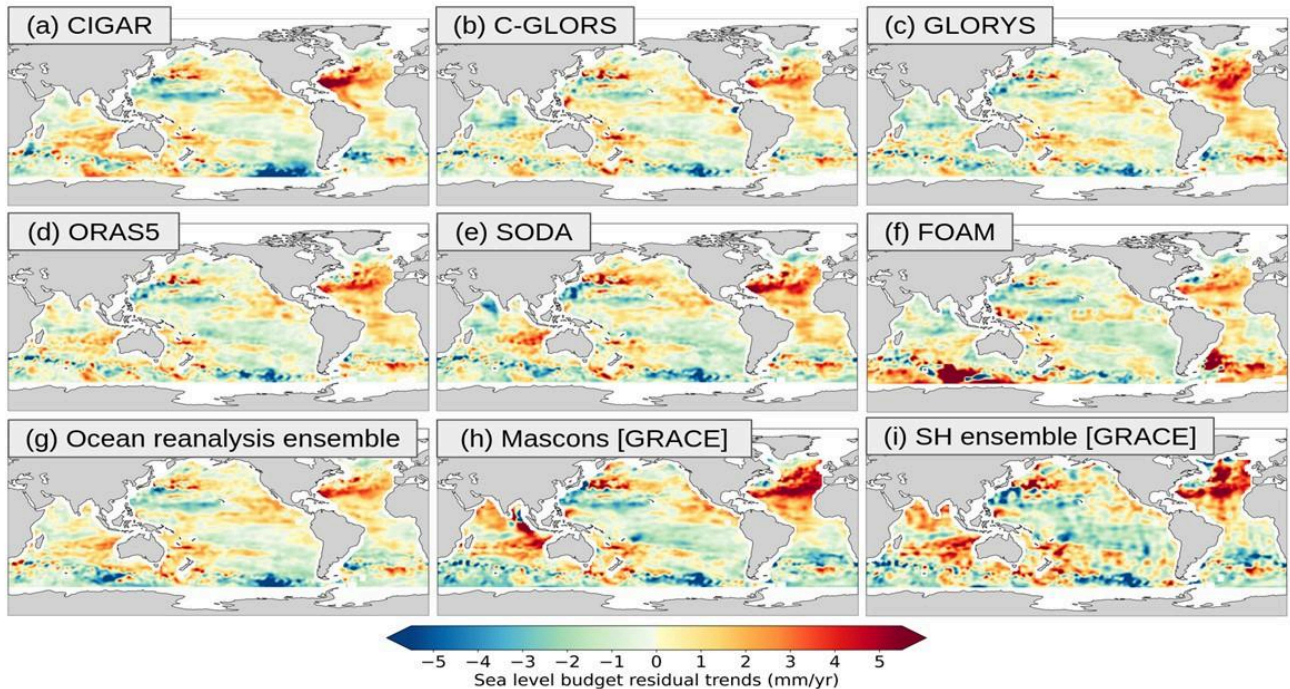


Figure 38 *Residual trends anomalies of the regional sea level budget computed with each of the six reanalyses-based manometric data sets, as well as with their mean (panels a to g) (with altimetry-based and steric components unchanged). GRACE-based residual trends for both mascons and spherical harmonic solutions are also shown (panels h and i). The period of analysis here is from January 2004 to December 2019. From Bouih et al., 2025.*

4.4. Improvements

The results summarized above with the ‘historical’ method will serve as a basis for the validation of the innovative approach proposed in this project.

Besides, these results call for further studies to understand the origin of north Atlantic budget non closure. Discussions with groups involved in processing of the Argo-based salinity data (IFREMER, SCRIPPS & others) may help clarify the question. When improved salinity data will be available, an assessment update should be performed.

The ‘historical’ approach has also revealed a number of still non-understood questions, such as ‘what is the best geocenter correction to be applied to GRACE data?’, ‘Are altimetry and GRACE data expressed in the same terrestrial reference frame?’ If time and budget permit, such questions are important issues to look at.

5. Analysis of the objectively constrained SLBC: Innovative Approach

As detailed in the project proposal ([\[AD6\]](#)), the objective of this approach aims to deliver an objective solution to the Sea Level Budget (SLB) by optimally combining sea level components in a way that minimizes the budget residuals within the uncertainty bounds of each component. This objective method will enable us to pinpoint dates and places where the SLB does not close within uncertainties along with the contribution that is most probably responsible for the misclosure.

The inverse method that is applied to the SLB is derived from approaches made in the literature (e.g., L'Ecuyer et al., 2015; Rodell et al., 2015) that were performed to close respectively the energy and the water cycle. The mathematical statement that has been used to this approach is given in section 3.4.2 of the ATBD ([\[AD3\]](#)). Thanks to this formalism, it is therefore possible to generate the optimal solution, providing both the estimated values and their associated objective uncertainties.

The uncertainties used for this approach have been estimated for each sea level component (absolute sea level, manometric sea level and steric sea level). In addition to the error variance-covariance matrix that accounts for measurement uncertainties, another source of uncertainties that describes the observability uncertainties of each observing system (i.e. altimetry, gravimetry, in-situ Argo profiles) have been estimated.

The approach is therefore applied at global mean (section 5.1) and at regional scale (section 5.2) by using the same formalism.

5.1. At global mean

Given the mathematical formalism described in the ATBD (eq. 16 and 17), the estimated values and their associated objective uncertainties that result the objective approach are the following:

$$\mathbf{m}_{\text{est}} = \mathbf{m}_{\text{obs}} - (\mathbf{K}^T \mathbf{K} + \mathbf{C}_{\text{obs}}^{-1})^{-1} \mathbf{K}^T \mathbf{K} \mathbf{m}_{\text{obs}}. \quad \text{Equation 4}$$

$$\mathbf{C}_{\text{est}} = (\mathbf{K}^T \mathbf{K} + \mathbf{C}_{\text{obs}}^{-1})^{-1}. \quad \text{Equation 5}$$

At global mean, the SLB can be performed in 2 different ways by using the barystatic sea level measured with gravimetry missions or using the sum of the individual contributions to ocean mass

change (respectively called sea level budget and ocean mass budget, cf equations 6 and 8 of the ATBD). It is therefore possible to apply the objective approach to these 2 closing methods.

5.1.1. Sea level budget

The sea level budget using barystatic measured from gravimetry is expressed as follows:

$$R = \Delta GMSL_{abs} - \Delta GMSL_{bary} - GMSL_{thermo}, \quad \text{Equation 6}$$

In order to perform the inverse method, we use the components provided within the project as well as their uncertainties and fully described in the ATBD. For each component, there are 2 sources of uncertainties that are estimated:

- 1) the measurement uncertainties of the component associated with the instrumental error and the algorithmic approximations (detailed in section 3 of the UCR, [AD1](#))
- 2) the observability uncertainty of the component associated to its effective resolution estimated from synthetic data of the OCCIPUT ocean model (detailed in section 5 of the UCR, [AD1](#))

The inversion is computed over the period 2005-2019, Figure 39 shows the sea level budget over this period and its residuals (R) without any inversion applied (i.e. the unconstrained approach). We can observe that over this period the trend residuals is about 0.58 mm/yr with an important increase after 2012.

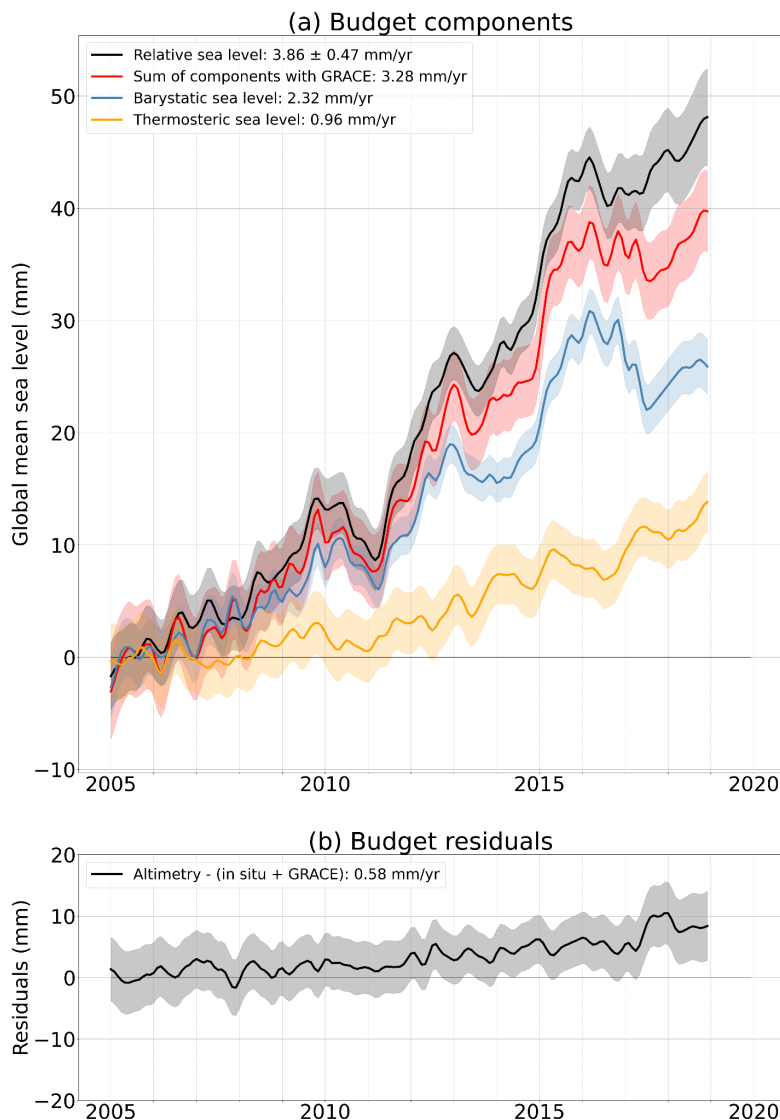


Figure 39 *Sea level budget over the period 2005-2019 (panel a) and the budget residual (panel b). The shaded areas correspond to the estimated 1-sigma uncertainties.*

After realising the inversion, the component estimated as well as their respective uncertainties are shown in Figure 40. We can observe that the budget is perfectly close over the period within their respective uncertainties. The new trend estimates of each component are slightly different from the original ones and summarised in Table 7 as well as new estimates of their respective trend uncertainties. The absolute sea level and barystatic sea level have been adjusted (respectively from 3.86 to 3.60 mm/yr and 2.32 to 2.62 mm/yr) while the thermosteric sea level trend remains unchanged.

This result indicates the existence of a solution, consistent with the estimated uncertainties of each contributing factor, that achieves a perfect closure of the sea level budget. This optimal solution was derived through a system that iteratively refined the individual components of the budget, taking into account their associated uncertainties. Notably, this optimization process has not only

identified a budget closure but has also resulted in a substantial reduction in the uncertainties associated with each component within this optimal solution. For instance, the uncertainty in the relative sea level rate has decreased from 0.47 mm/yr to 0.18 mm/yr at a 1-sigma confidence level. This significant reduction in uncertainty across the board increases the confidence in the accuracy and robustness of the identified optimal solution and provides a more precise understanding of the individual contributions to the overall sea level budget.

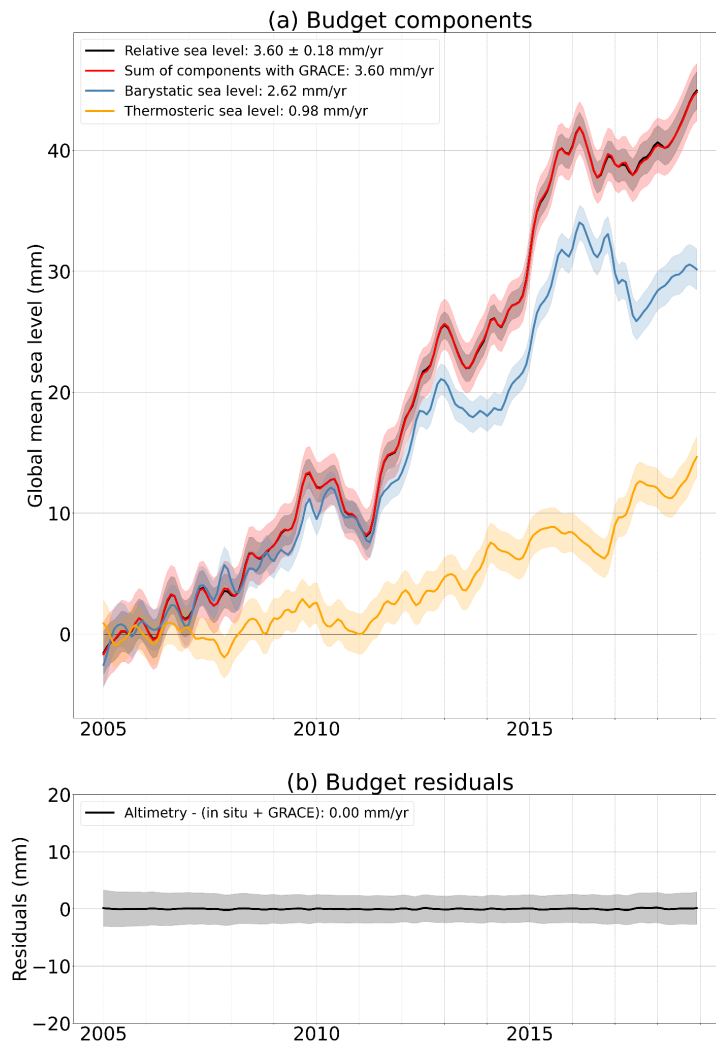


Figure 40 *Sea level budget with objectively constrained components obtained by inversion over the period 2005-2019 (panel a) and the budget residual (panel b). The shaded areas correspond to the estimated 1-sigma uncertainties.*

Table 7 *Sea level budget component trend (mm/yr) before and after inversion over the period 2005-2019*

Component	Trend (mm/yr) before inversion	Trend (mm/yr) after inversion
Relative sea level	3.86	3.60
Barystatic sea level	2.32	2.62
Thermosteric sea level	0.96	0.98

Figure 41 shows each component as well as the residuals before and after the inversion. As described above, we can observe an important trend modification on the relative sea level from altimetry while the thermosteric changes are made at short time scales (below 6 months). This result comes from the uncertainties described from each component where a linear time correlated effects have been modelised from altimetry and gravimetry which is not the case for the in-situ. This underlines the importance of how the uncertainties are described for the components, in particular the description of correlated errors that may impact a component. To date, with the prescriptions made for each component (detailed in the UCR) we can only conclude that the inversion tends to indicate an excessive trend on the altimetry that should be corrected to close the budget. However, this is a result that should not be over-interpreted because of the uncertainties modelled to date.

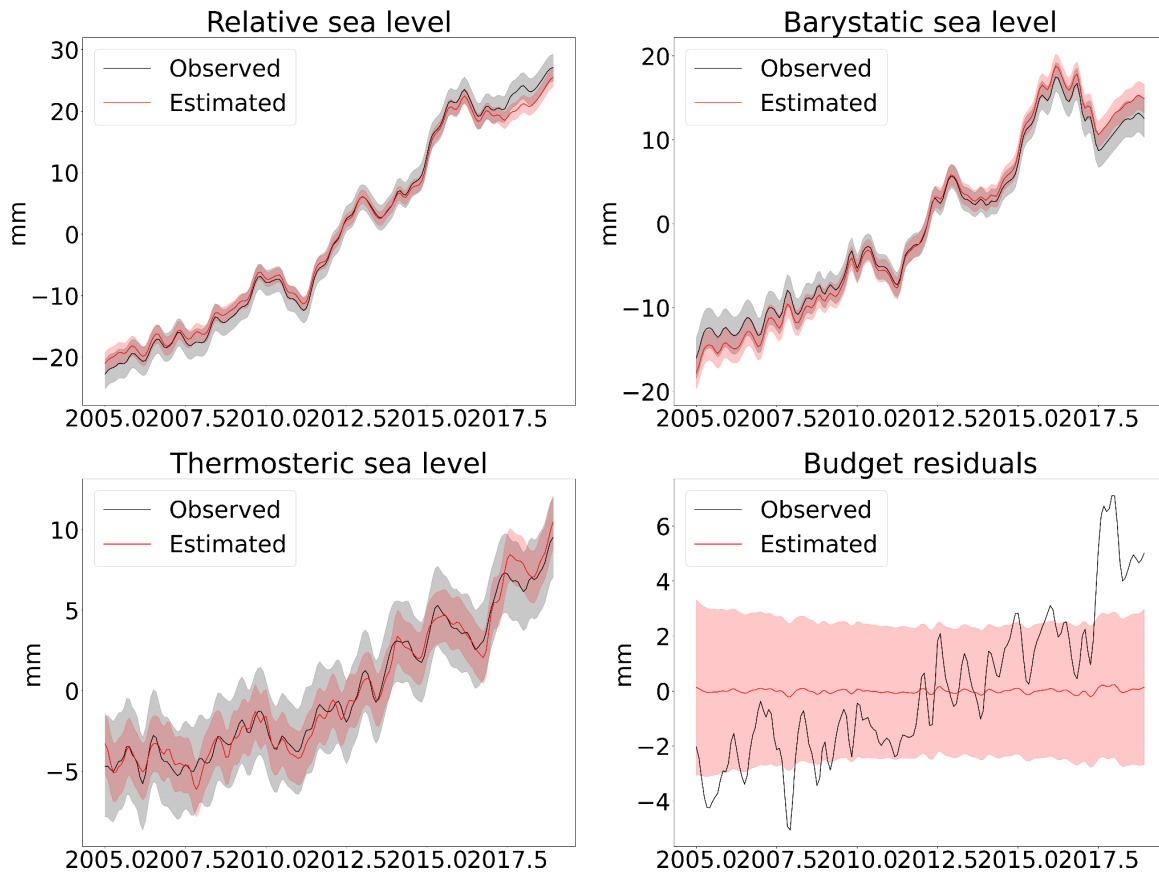


Figure 41 *Sea level budget components before inversion (black curves) and after inversion (red curves) for relative sea level by altimetry (left top), barystatic sea level by gravimetry (right top), thermosteric sea level by in-situ profiles (lower left) and budget residuals (lower right). The shaded areas correspond to the estimated 1-sigma uncertainties.*

5.1.2. Ocean mass budget

The sea level budget at global mean can also be expressed by using an ocean mass budget to estimate the barystatic sea level. Indeed, individual components of the ocean mass are measured by different systems and provide independent estimates that can be compared to satellite gravimetry measurements. It is then possible to explain the 2 budgets and inverse both simultaneously, the equations and the formula of the inversion are given in section 3.4.2.2 of the ATBD ([IAD3](#)).

$$R = \Delta GMSL_{rel} - \Delta GMSL_{bary} - \Delta GMSL_{thermo}.$$

Equation 7

$$S = (\Delta GMSL_{bary})_{sat} - (\Delta GMSL_{bary})_{GIS} - (\Delta GMSL_{bary})_{AIS} - (\Delta GMSL_{bary})_{GIC} - (\Delta GMSL_{bary})_{LWS} - (\Delta GMSL_{bary})_{WV} \quad \text{Equation 8}$$

The different components of the Equation 7 are the same as the ones used for the inversion of the sea level budget, the components of the Equation 8 (ocean mass budget) are the one provided within the project and are fully described in the ATBD.

It is important to note that for the ocean mass budget components (Greenland Ice Sheet, Antarctica, Glaciers, etc...), the uncertainties provided and described in the ATBD only describe the measurement uncertainties. The observability uncertainties for these components have not been estimated for now.

The inversion is computed over the period 2005-2019, Figure 42 shows the ocean mass budget over this period and its residuals without any inversion applied (i.e. the unconstrained approach). As for the sea level budget, we can observe that over this period the trend residuals between the barystatic estimated with gravimetry and the one observed with the mass components (S) is about 0.54 mm/yr. Before 2015, the ocean mass budget was barely closed within the uncertainties but with an important difference that appears after this date. It is important to note that there is no data in the gravimetry record between 2017 and 2018 which corresponds to the gap between GRACE and GRACE-Follow On missions.

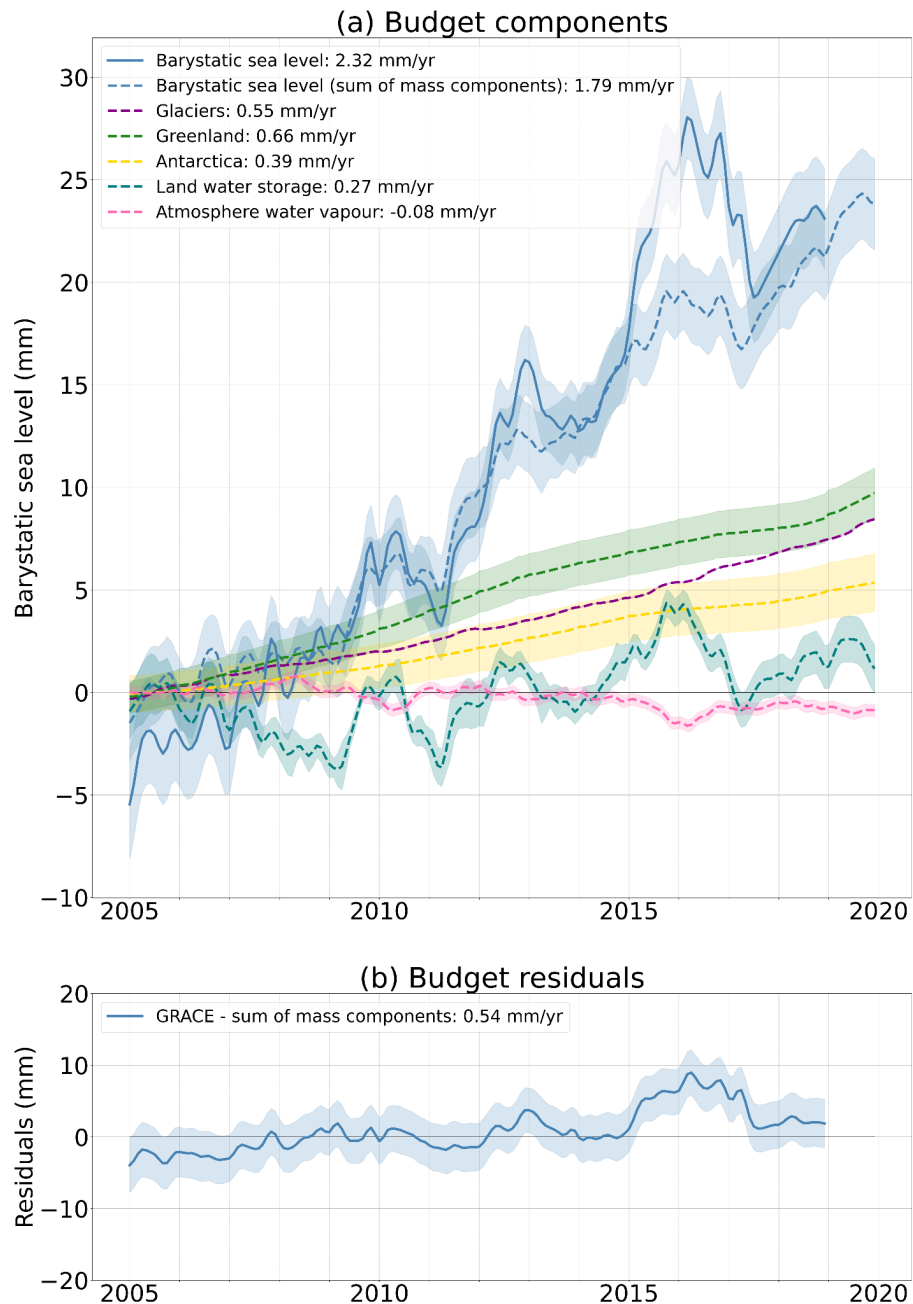


Figure 42 *Ocean mass budget over the period 2005-2019 (panel a) and the budget residual (panel b). The shaded areas correspond to the estimated 1-sigma uncertainties.*

After realising the inversion, we can observe on Figure 43 a perfect closure of the ocean mass budget over the whole period. The adjustments made by the inversion to close the budget have been performed mostly on the 2 ice sheet components (Antarctica and Greenland) because their respective uncertainties were an order of magnitude higher than others. Table 8 shows the trends of each component of the ocean mass budget before and after the inversion. The barystatic

estimated with gravimetry measurements have significantly reduced its trends from 2.32 to 1.83, this result is due to the uncertainty prescriptions of the gravimetry compared to the other datasets prescriptions which does not take into account time correlated effect.

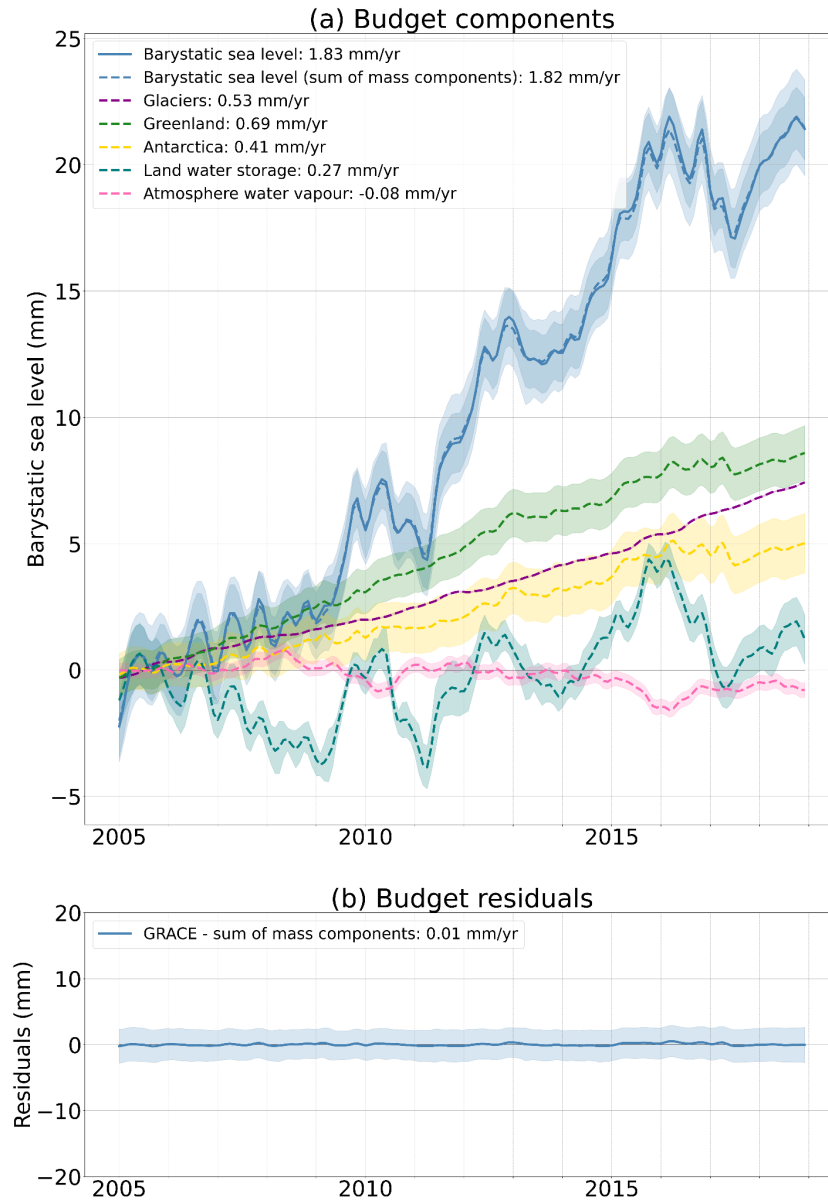


Figure 43 *Ocean mass budget with objectively constrained components obtained by inversion over the period 2005-2019 (panel a) and the budget residual (panel b). The shaded areas correspond to the estimated 1-sigma uncertainties.*

Table 8 *Ocean mass budget component trend (mm/yr) before and after inversion over the period 2005-2019*

Component	Trend (mm/yr) before inversion	Trend (mm/yr) after inversion
Barystatic sea level	2.32	1.83
Glaciers	0.55	0.53
Greenland	0.66	0.69
Antarctica	0.39	0.41
Land Water Storage	0.27	0.27
Atmosphere Water Storage	-0.08	-0.08
Sum of mass components	1.79	1.82

This result shows the current limitation of the approach regarding the budget uncertainties described to each component since it is likely probable that relative sea level could have such a low tendency over this period. The provided analysis focuses on the inversion of ocean mass and sea level budgets, examining how combining these inversions affects the estimated trends of their individual components. The core principle behind this simultaneous inversion is to optimize all contributing factors within the system, ensuring closure of the budgets while considering the inherent uncertainties associated with each component. Figure 44 visually represents the outcomes of this combined inversion.

A key observation from the ocean mass budget inversion alone indicated a barystatic sea level trend of approximately 1.83 mm/yr. Upon integrating this information into the simultaneous inversion of both budgets, a notable adjustment occurred in the relative sea level trend. Specifically, the relative sea level trend, which was initially estimated at 3.44 mm/yr based solely on the sea level budget inversion, was constrained to a lower value of 2.89 mm/yr.

This adjustment highlights a crucial aspect of the current methodology: its sensitivity to the uncertainties assigned to each component within the budgets. The significant shift in the relative sea level trend suggests that the system prioritized closing the combined budget, potentially driven by the uncertainties associated with the ocean mass budget and its influence on the overall balance.

The reduction of the relative sea level trend to 2.89 mm/yr raises questions about the plausibility of such a low tendency over the considered period. It is acknowledged that while the mathematical inversion leads to this result based on the provided data and uncertainties, there is a possibility that the actual relative sea level trend during this time frame was higher. This discrepancy underscores the importance of accurately quantifying the uncertainties associated with each component of the sea level and ocean mass budgets. Improved uncertainty estimates could lead to more robust and realistic results from the simultaneous inversion process. Further investigation and validation with independent datasets or alternative methodologies would be beneficial to

ascertain the reliability of the adjusted SLB and to refine the understanding of the budget uncertainties.

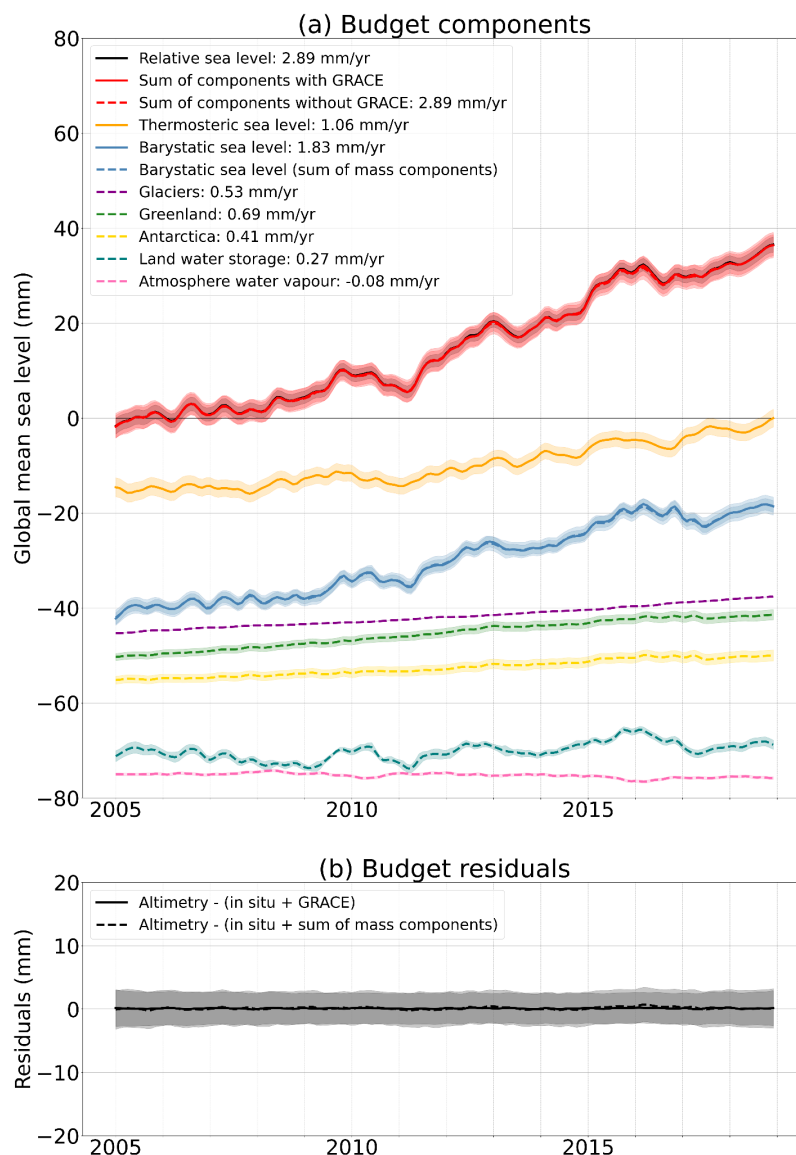


Figure 44 *Simultaneous inversion of the sea level and ocean mass budget over the period 2005-2019 (panel a) and the budgets residuals (panel b). The shaded areas correspond to the estimated 1-sigma uncertainties.*

5.2. At regional scale

The results at global mean provide valuable information about the behavior of each component, however validations activities and intercomparisons have also been performed in the frame of the project at regional scale. It would also be interesting to perform the same analysis of the objectively constrained SLB at this scale to provide feedback for each component. As at regional scale the spatial correlations of each component have not been estimated for now, we can perform an inversion at each cell independently from the one on the side. These results would be analyzed with caution since the spatial correlation would have an important impact on the inversion results.

As described in the UCR, the regional uncertainties for each component (absolute, barystatic, steric) have been provided at 1 degree resolution and at yearly timescale. Also, only the sea level budget inversion can be performed since there are no regional estimates of the ocean mass budget. Furthermore, the observability uncertainties obtained from the synthetic data of the OCCIPUT model have been estimated and can be taken into account for each component (cf section 5.2 of the UCR).

The mathematical statements regarding the inversion (cost function, model designed to minimise the cost function, etc.) are equivalent to those at global mean, and can be calculated in the same manner.

To date, the set up of the inversion at regional scale has not been carried out.

6. Conclusions and Recommendations

This intercomparison exercise offers an updated and integrated assessment of all components of the sea level budget, reflecting recent advances in data processing and methodological harmonization.

Altimetry products show a good consistency across the whole altimetric area, with the notable exception of the TOPEX period, where discrepancies between processing persist. The steric component, represented here by the ISAS20 product, aligns well with other datasets (JAMSTEC, EN4, SCRIPPS), especially in terms of long-term trends and interannual variability. However, significant differences remain in dynamically active regions, particularly major ocean currents and the Southern Ocean, where ISAS-20 tends to underestimate variability, highlighting the sensitivity to mapping and interpolation techniques.

The barystatic component, derived from GRACE and compared with various mascon-based solutions, exhibits strong agreement in global trends over 2002–2024. Differences remain within expected uncertainties, while regional comparisons confirm the robustness of the methods used and the importance of the GIA correction model applied.

The contributions of GIA and gravitational fingerprints were estimated using the SELEN⁴ model, integrating both elastic and viscoelastic Earth responses. Two GIA models (ICE-6G_C and ANU)

were used to explore uncertainties related to glacial history and mantle rheology, underscoring their crucial role in correcting altimetric observations and accurately attributing mass changes.

The quantification of individual mass contributions to sea level relies on a combination of satellite observations and global models. Land water storage (LWS) estimates, based on the hydrological model WGHM v22e, highlight persistent uncertainties especially prior to 2000 and emphasize the need to account for both anthropogenic and climate-driven influences. The atmospheric water vapor contribution, derived from ERA5, demonstrates strong consistency with independent datasets (HOAPS, AOD1B) over 2005–2016, although discrepancies after 2016 warrant further investigation.

For the polar ice sheets, consistent mass loss trends were confirmed across datasets from IMBIE-R2, CCI GMB, and GRACE/altimetry-based products. Differences of a few tens of Gt/year are mainly attributed to the treatment of peripheral glaciers and temporal resolution. Mountain glacier (GIC) estimates, validated against GLAMBIE intercomparison results (Zemp et al., 2025), show good global agreement despite regional variability, supporting their inclusion in the budget.

Overall, this work provides a consistent and uncertainty-aware assessment of the global mean sea level budget, reinforcing the value of the SLBC_cci+ approach as a robust framework for component intercomparison and improvement tracking. The integration of updated datasets with improved spatial and temporal resolution represents a notable advance over previous phases.

At the global scale, the mass budget (comparing the GRACE-based barystatic component to the sum of individual mass contributions) closes well over the 2004–2015 period, with only moderate discrepancies emerging after 2016, pointing to potential issues in one or more components.

However, the analysis using the full sea level budget (i.e., altimetry minus steric and barystatic components) reveals larger residuals in SLBC_cci+ Phase 2 compared to Phase 1. These residuals show a distinct low-frequency temporal signal that was not present to the same extent previously. This discrepancy is primarily driven by weaker thermosteric trends in the more recent phase, despite consistent barystatic estimates.

Crucially, the study based on a constraint-based formulation of the sea level budget highlights a previously overlooked contributor to the residuals: an *observability mismatch* between satellite altimetry and in situ observations. This so-called “non-observability” term arises because altimetry provides a globally complete measurement, while the steric component relies on sparse in situ data with limited spatial coverage. This observability mismatch seems to introduce a systematic, non-negligible error, which could significantly impact budget closure, particularly at low frequencies. Further analysis would be necessary to consolidate these results.

This insight repositions the altimetry–steric balance as a central source of discrepancy, where differences in mapping strategies, and unaccounted observational limitations all contribute to budget uncertainty. The formal integration of this non-observability error term may be essential for a more accurate and complete representation of the sea level budget.

Looking forward, key improvements are recommended: adoption of the latest reprocessed GMSL altimetry datasets; incorporation of updated glacier, ice sheet, and land water storage estimates; and exploration of GRACE/GRACE-FO alternatives such as satellite laser ranging or stereodynamic

sea level from reanalyses. Most importantly, refining the steric component and systematically accounting for observational uncertainties will be critical to achieving a fully closed and robust sea level budget.

End of the document